Dissertation

submitted to the

Combined Faculties for the Natural Sciences and for Mathematics

of the Ruperto-Carola University of Heidelberg, Germany

for the degree of

Doctor of Natural Sciences

presented by

M.Sc. Verena Staudacher

born in Ravensburg, Germany

Oral examination: 16.03.2018

Plasmodium falciparum Antioxidant Protein: Kinetic Characterization and Physiological Relevance as a Potential Redox Sensor in Malaria Parasites

Referees: Prof. Dr. Michael Lanzer

PD Dr. Tobias Dick

Table of contents

Acknowledgements

I would like to thank Prof. Dr. Marcel Deponte for giving me the opportunity to work in his lab on this interesting project. Thank you for the good supervision and training on the new methods, especially at the beginning of the project.

Thank you Prof. Dr. Michael Lanzer for giving me the opportunity to write this thesis at the parasitology department. Thank you for being my examiner and thesis advisory committee member. Thank you for the helpful discussion and suggestions on this project.

Thank you PD Dr. Tobias Dick for being my examiner and thesis advisory committee member. Thank you for the helpful discussion and suggestions on this project.

Thank you Dr. Faith Osier for being my examiner.

I also want to thank Carine Djuika, who started this project and did a lot of work on the kinetic characterization of *Pf*AOP and the relevance of *Pf*AOP regarding artemisinin susceptibility. Thank you Joshua Koduka, Sarah Schlossarek, Alissa Beer and Marleen Büchler, who contributed to the kinetic characterization of the *Pf*AOP gatekeeper mutants.

I want to thank my lab mates from the Deponte Lab for their support and the great time we spent together inside and outside of the lab: Linda Liedgens, Sandra Specht, Cletus Wezena, Gino Turra, Kristina Feld and Johannes Krafczyk.

I also would like to thank the members of the Frischknecht and Lanzer lab for their contributions and help during this project.

Thank you Dr. Madia Trujillo and Prof. Dr. Raphael Radi for the collaboration on the stopped-flow kinetic studies, the opportunity to work in your lab in Montevideo and the supervision during my stay in Uruguay.

Thank you Dr. Bruce Morgan for the collaboration and supervision on the roGFP2 studies and the opportunity to work in your lab in Kaiserslautern.

Thank you Marcel Deponte, Linda Liedgens, Catherine Moreau and Henriette Merk for the proofreading of this thesis.

Thank you to my family and friends for their support and help over the course of this time.

Summary

Peroxiredoxins (Prx) are ubiquitous thiol-dependent hydroperoxidases and belong to the most abundant enzymes in a variety of organisms from all kingdoms of life. Furthermore, Prx act as redox sensors in hydrogen peroxide signaling. The Antioxidant Protein (*Pf*AOP), a Prx5-type enzyme from the malaria parasite *Plasmodium falciparum*, was recently shown to belong to a special subclass of Prx using glutaredoxin (Grx) and reduced glutathione (GSH) as electron donors.

In this work, two modulatory residues of *Pf*AOP were characterized that influence the enzyme parameters and the inactivation susceptibility. Gain- and loss-of-function mutants were generated in which the size of residue 109 was altered and the catalytically relevant but nonessential cysteine residue 143 was present or absent. Using steady-state kinetic measurements with recombinant *Pf*AOP, the overall reactivity of these mutant enzymes was analyzed and the mechanism of the reduction of the oxidized enzyme was unraveled. Rate constants for the oxidation and over-oxidation of the peroxidatic cysteine residues were determined by stopped-flow kinetic measurements. A mutant enzyme was identified that is catalytically more active and more durable regarding hydrogen peroxide dependent inactivation compared to the wild-type enzyme. This suggests that *Pf*AOP not only acts as a hydroperoxidase but might also have an additional function as part of a redox relay *in vivo*.

Fusion constructs between redox-sensitive green fluorescent protein 2 (roGFP2) and Prx are valuable tools for redox measurements in living cells. Using the *in vitro* well characterized gain- and loss-of-function mutants of *Pf*AOP, different fusion constructs with roGFP2 were generated and the *in vivo* roGFP2 readouts were analyzed in yeast. We showed that the ratiometrically measured degree of oxidation of the roGFP2 fusion proteins correlates with the corresponding *in vitro* enzyme properties of the attached Prx. Additionally, the roGFP2 signal can be used to map the over-oxidation based inactivation of the Prx. This will allow the assessment of protein structure-function relationships, like post-translational protein modifications, *in vivo*. Further future applications are the estimation of absolute intracellular peroxide concentrations and the improvement of redox sensors.

To gain more insight into the physiological relevance of *Pf*AOP, knockout parasites were generated in the *P. falciparum* strain 3D7 using the CRSIPR/Cas9 system. The 3D7Δ*pfaop*

knockout lines were viable and showed no significant growth phenotype under standard cell culture conditions. Furthermore, the IC_{50} values for external oxidants remained unchanged.
In a previous conducted quantitative trait locus analysis a locus on chromosome 7, encoding 49 genes including *PFAOP*, was associated with altered artemisinin susceptibility in malaria parasites. Here, we showed that the deletion of the gene encoding *Pf*AOP does neither affect IC_{50} values nor ring stage survival rates for artemisinin. Thus, the correlation between chromosome 7 and the artemisinin susceptibility is probably based on one of the other genes within the identified locus.
Western blot analyses of *PFAOP* over-expressing *P. falciparum* strains in combination with peroxide challenges revealed a band corresponding to a probable interaction partner of *Pf*AOP in the cytosol. However, this protein could not be identified so far and it remains to be shown if it is part of a peroxide dependent redox relay involved in redox signaling.
In summary, the findings of this thesis lead to a better understanding of the kinetic mechanism of peroxiredoxins. Furthermore, it could be shown that *in vitro* kinetic properties of peroxidases correlate with the roGFP2 readout of corresponding fusion constructs inside living cells. So far, the physiological relevance of *Pf*AOP remains unknown, but our results suggest that *Pf*AOP might exert an additional function as a redox sensor *in vivo*.

Zusammenfassung

Peroxiredoxine (Prx) sind ubiquitär vorkommende Thiol-abhängige Hydroperoxidasen und gehören zu den häufigsten Enzymen in vielen Prokaryonten, Archaea und Eukaryonten. Prx können außerdem als Redox-Sensoren bei der Signalübertragung durch Wasserstoffperoxid fungieren. Es wurde kürzlich gezeigt, dass das *Antioxidant Protein* (*Pf*AOP), ein Prx5-Typ Enzym des Malariaparasiten, zu einer speziellen Unterklasse von Prx gehört, welche Glutaredoxin (Grx) und reduziertes Glutathion (GSH) als Elektronendonoren nutzt.

In dieser Arbeit wurden zwei regulierende Aminosäurereste von *Pf*AOP charakterisiert, die die Enzymparameter und die Inaktivierungssuszeptibilität beeinflussen. Mutanten, die entweder einen Funktionsgewinn oder -verlust aufweisen, wurden generiert. In ihnen war die Größe des Restes 109 verändert oder der katalytisch relevante, aber nicht essentielle Cysteinrest 143 vorhanden oder abwesend. Die Gesamtreaktivität dieser Mutanten wurde mit *steady-state* Kinetikmessungen mit rekombinanten Enzymen analysiert und der Reduktionsmechanismus des redoxaktiven Cysteinrestes entschlüsselt. Mit *stopped-flow* Messungen wurden Geschwindigkeitskonstanten für die Oxidation und Überoxidation der redoxaktiven Cysteinreste bestimmt. Es konnte eine Mutante identifiziert werden, die im Vergleich zum Wildtypenzym eine höhere katalytische Aktivität aufweist und resistenter gegenüber Wasserstoffperoxid-abhängiger Inaktivierung ist. Das deutet darauf hin, dass *Pf*AOP nicht nur als Hydroperoxidase fungiert, sondern *in vivo* noch eine zusätzliche Funktion als möglicher Redox-Sensor in einer Redox-Kaskade aufweist.

Fusionsproteine zwischen redox-empfindlichem grün fluoreszierendem Protein 2 (roGFP2) und Prx sind nützliche Werkzeuge, um Redox-Messungen in lebenden Zellen durchzuführen. Mit Hilfe der *in vitro* charakterisierten Mutanten von *Pf*AOP, die einen Funktionsgewinn oder -verlust aufweisen, wurden verschiedene Fusionskonstrukte mit roGFP2 generiert und die roGFP2 Signale in Hefe *in vivo* analysiert. Wir konnten zeigen, dass der ratiometrisch gemessene Oxidationsgrad der roGFP2 Fusionsproteine mit den jeweiligen *in vitro* Eigenschaften der korrespondierenden Enzyme korreliert. Das roGFP2-Signal kann auch dazu genutzt werden, die durch Überoxidation bedingte Inaktivierung der gekoppelten Peroxiredoxine zu analysieren. Dies ermöglicht die zukünftige Beurteilung von Struktur-Funktions-Beziehungen wie posttranslationalen Proteinmodifikationen *in vivo*. Des Weiteren

können unsere Erkenntnisse zukünftig dazu dienen, die absolute intrazelluläre Peroxidkonzentration abzuschätzen und Redox-Sensoren zu verbessern.

Um mehr über die physiologische Bedeutung von *Pf*AOP zu erfahren, wurden mit Hilfe des CRISPR/Cas9 Systems Knockout-Parasiten im *P. falciparum* 3D7 Stamm generiert. Die 3D7Δ*pfaop* Knockout-Stämme waren lebensfähig, zeigten unter standardisierten Zellkulturbedingungen keinen signifikanten Wachstumsphänotyp und die IC_{50}-Werte für externe Oxidantien blieben unverändert.

In einer *quantitative trait locus* Analyse, die in einer früheren Studie durchgeführt wurde, konnte ein Abschnitt auf Chromosom 7 identifiziert werden, auf dem 49 Gene, einschließlich *PFAOP*, liegen. Dieser Abschnitt wurde mit einer veränderten Artemisinin-Suszeptibilität von Malariaparasiten assoziiert. Wir konnten hier zeigen, dass der Verlust des *Pf*AOP kodierenden Genes weder die IC_{50} Werte von Artemisinin noch die Ringstadien Überlebensrate der Parasiten verändert. Das deutet darauf hin, dass die Korrelation zwischen Chromosom 7 und der veränderten Suszeptibilität gegenüber Artemisinin wahrscheinlich auf ein anderes Gen im identifizierten Genabschnitt zurückzuführen ist.

In Western-Blot-Analysen von *P. falciparum* Stämmen, die *PFAOP* überexprimieren, konnte nach Peroxid-Behandlung eine Bande identifiziert werden, die einem möglichen Interaktionspartner von *Pf*AOP im Cytosol zuzuordnen ist. Bis jetzt konnte dieses Protein, das Teil einer Peroxid-abhängigen Redox-Kaskade sein könnte, noch nicht identifiziert werden.

Die in dieser Arbeit gewonnenen Erkenntnisse tragen zum besseren Verständnis des katalytischen Mechanismus von Peroxiredoxinen bei. Außerdem konnte gezeigt werden, dass *in vitro* Enzymparameter mit dem roGFP2 Signal von Fusionskonstrukten in lebenden Zellen korrelieren. Obwohl die physiologische Bedeutung von *Pf*AOP bis jetzt unbekannt bleibt, deutet einiges darauf hin, dass *Pf*AOP *in vivo* als Redox-Sensor fungieren könnte.

List of Figures and Tables

Figures

Tables

List of Abbreviations and Symbols

12(S)HpETE	12(S)-hydroperoxy-(5Z,8Z,10E,14Z)-eicosatetraenoic acid
°C	Degree Celsius
α	Anti
Δ	Delta
ε	Extinction coefficient
λ_{em}	Emission wavelength
λ_{ex}	Excitation wavelength
µF	Microfarad
µg	Microgram
µl	Microliter
µM	Micromolar
Å	Ångström
aa	Amino acid(s)
Abs	Absorbance
ACT	Artemisinin-based combination therapy
Amp	Ampicillin
AOP	Antioxidant protein
app	Apparent
approx.	Approximately
AQ	Atovaquone
APS	Ammonium persulfate
ART	Artemisinin
as	Antisense
AUC	Area under the curve
bp	Base pair(s)
BSA	Bovine serum albumin
BTS	Bipartite topogenic signal
C-terminus	Carboxy terminus
cm	Centimeter
CQ	Chloroquine
CRISPR	Clustered Regularly Interspaced Short Palindromic Repeats
Da	Dalton
ddH_2O	Double-distilled water
DHFR	Dihydrofolate reductase
DMSO	Dimethyl sulfoxide
DNA	Deoxyribonucleic acid
DNAse	Deoxyribonuclease
dNTP	Deoxyribonucleoside triphosphate
DTPA	Diethylenetriaminepentaacetic acid
DTT	Dithiothreitol
E. coli	*Escherichia coli*
ECL	Enhanced chemiluminescence
EDTA	Ethylenediaminetetraacetic acid
EGTA	Ethylenebis(oxyethylenenitrilo)tetraacetic acid
ER	Endoplasmic reticulum
et al.	et alii (and others)

FPLC	Fast protein liquid chromatography
FF	Fully folded
g	Gram
gDNA	Genomic DNA
gRNA	Guide RNA
GFP	Green fluorescent protein
GR	Glutathione reductase
Grx	Glutaredoxin
GSH	Glutathione (reduced)
GSSG	Glutathione disulfide
h	Hour(s) or human
HC	Hartwell´s complete (medium)
HEDS	bis-(2-hydroxyethyl)-disulfide
HEPES	4-(2-hydroxylethyl)piperacin-1-(2-ethanesulphonic acid)
HRP	Horseradish peroxidase
HSP	Heat shock protein
IC_{50}	Half maximal inhibitory concentration
IPTG	Isopropyl β-D-1-thiogalactopyranoside
iRBC(s)	Infected red blood cell(s)
kb	Kilobase pair(s)
k_{cat}	Turnover number
kDa	Kilodalton
K_m	Michaelis-Menten constant
k_{obs}	Observed rate constant
KO	Knockout
kV	Kilovolt
l	Liter
LB	Luria Bertani
LU	Locally unfolded
M	Molar
mA	Milliampere
MACS	Magnetic activated cell sorting
MCS	Multiple cloning site
mg	Milligram
min	Minute
ml	Milliliter
mM	Millimolar
mRNA	Messenger ribonucleic acid
ms	Millisecond
MW	Molecular weight
N-terminus	Amino-terminus
NADPH	Nicotinamide adenine dinucleotide phosphate
NEM	N-Ethylmaleimide
Ni-NTA	Nickel-nitrilotriacetic acid
nm	Nanometre
nM	Nanomolar
OD	Optical density
OxD	Degree of oxidation

P. falciparum	*Plasmodium falciparum*
PAGE	Polyacrylamide gel electrophoresis
PBS	Phosphate buffered saline
PCR	Polymerase Chain Reaction
PDB	Protein Data Bank
PEG	Polyethylene glycol
PI	Protease inhibitor
PMSF	Phenylmethylsulphonyl fluoride
Prx	Peroxiredoxin
PVM	Parasitophorous vacuolar membrane
QTL	Quantitative trait locus
RBC	Red blood cell
RIPA	Radioimmunoprecipitation assay
RNA	Ribonucleic acid
RNAse	Ribonuclease
roGFP	Reduction-oxidation sensitive green fluorescent protein
ROS	Reactive oxygen species
rpm	Revolutions per minute
RPMI	Rosewell Park Memorial Institute
RSA	Ring stage survival assay
RT	Room temperature
s	Second
S. cerevisiae	*Saccaromyces cerevisiae*
SD	Standard deviation
SDS	Sodium dodecyl sulfate
SP	Signal peptide
TAE	Tris-acetate-EDTA
Taq	*Thermus aquaticus*
t-BOOH	*tert*-Butyl hydroperoxide
TBS	Tris-buffered saline
TCA	Trichloroacetic acid
TE	Tris-EDTA
TEMED	Tetramethylethylenediamine
TP	Transition peptide
Tris	Tris (hydroxymethyl)-aminomethane
Trx	Thioredoxin
TrxR	Thioredoxin reductase
U	Unit
Ura	Uracil
UTR	Untranslated region
UV	Ultraviolet
V	Volt
v/v	Volume to volume
w/v	Weight to volume
WHO	World Health Organization
WR99210	1,6-Dihydro-6,6-dimethyl-1-(3-(2,4,5trichlorophenoxy) propoxy)-1,3,5-triazine-2,4-diamine
WT	Wild-type

x	Times
x g	Gravitational force
YPD	Yeast extract peptone dextrose

1. Introduction

1.1 Malaria – medical relevance

Malaria, a disease caused by protozoan parasites of the genus *Plasmodium*, belongs to the most important human infectious diseases worldwide. Although cases of malaria incidence were reduced by 41% and malaria mortality rates by 62% between 2000 and 2015, in 2015 about 212 million cases were reported globally, causing 429 000 deaths, most of which were children aged under 5 years in Africa (WHO, 2016). In 2016, 91 countries were considered to be endemic for malaria, including Africa, Southeast Asia, Oceania, the Indian subcontinent, Central and South America (Figure 1.1).

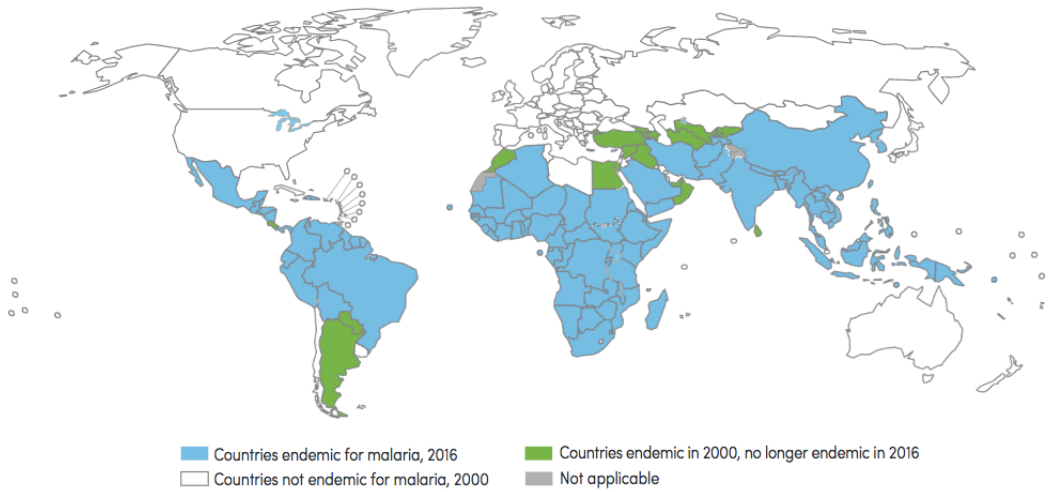

Figure 1.1 Countries endemic for malaria in 2000 and 2016
Source: WHO, 2016.

The symptoms of malaria in humans typically begin after an incubation time of 8-25 days (in some cases several months) and consist of periodic episodes of high fever, occurring every two to three days depending on the *Plasmodium* species, as well as headache, vomiting, feeling tired and muscle pain. In some cases, the disease can progress to severe or complicated malaria, which often results in death. Most deaths occur in African children and are caused by three syndromes that occur separately or in combination: severe anemia, cerebral malaria and respiratory distress (Marsh et al., 1995). Another risk group comprises pregnant women, who also have a high risk to develop severe anemia during infection. Furthermore, fetal complications resulting from placental infection and maternal anemia can

occur and manifest in stillbirth, intrauterine growth restriction or low-weight neonates (Schantz-Dunn and Nour, 2009).

1.2 The malaria parasite

Malaria is caused by protozoan parasites of the genus *Plasmodium*. *Plasmodium* species are eukaryotic single-cell microorganisms belonging to the superphylum Alveolata, phylum Apicomplexa, order Haemosporida and the family of Plasmodiidae (Morrison, 2009). These parasites require two different hosts to complete their life cycle: an invertebrate host, in which the sexual part of the life cycle takes place, and a vertebrate host, in which the asexual phase occurs. Mosquitos, mainly belonging to the genus *Anopheles*, serve as invertebrate hosts (Sinka et al., 2012); vertebrate hosts of *Plasmodium* species include birds, reptiles and mammals. About 200 different *Plasmodium* species are known from which five are responsible for human malaria: *P. falciparum*, *P. vivax*, *P. malariae*, *P. ovale* and *P. knowlesi*. These five species differ in their geographical distribution, pathogenicity, physical appearance and drug susceptibility (Tuteja, 2007). From these species *P. falciparum* is considered as the most virulent, as it is responsible for the majority of severe malaria cases, followed by *P. vivax* (Cowman et al., 2016).

1.3 The life cycle of the human malaria parasite *P. falciparum*

The *P. falciparum* life cycle (Figure 1.2) consists of two major phases taking place in the two different hosts. It starts with the bite of an infected female *Anopheles* mosquito whereupon sporozoites are injected into the human dermis (Figure 1.2A). The sporozoites actively enter the blood vessels and are transported via the blood stream to reach the liver (Yamauchi et al., 2007). Here, they exit the sinusoids via Kupffer or endothelial cells and transmigrate several hepatocytes until they invade a final hepatocyte (Mota and Rodriguez, 2004). In this hepatocyte the parasite forms a parasitophorous vacuole (PV) and starts to replicate, a process called exo-erythrocytic schizogony, until tens of thousands of daughter merozoites are formed and released in packets of merosomes into the vasculature (Figure 1.2B) (Sturm et al., 2006). As soon as merozoites are present in the blood stream, they invade erythrocytes and the 48 h lasting intraerythocytic cycle (schizogony) begins. After invasion, the merozoite develops in a parasitophorous vacuole into the ring stage form. This is

followed by the metabolically very active trophozoite stage, which develops further into the schizont. Inside the erythrocyte, the parasite digests the host hemoglobin to supply itself with amino acids essential for its biosynthetic processes. The toxic free heme is detoxified by crystallization to an insoluble polymer called hemozoin (Gupta et al., 2017). The schizont forms 16-32 merozoites that are released into the bloodstream under rupture of the erythrocyte (Figure 1.2C) (Bannister et al., 2000, Bannister and Mitchell, 2003). The rupture of the infected erythrocytes occurs asynchronously (*P. falciparum*) or respectively synchronously (*P. vivax*) and causes the production of pro-inflammatory proteins, which are responsible for the typical clinical symptoms of the disease. The erythrocytic cycle represents the main target for diagnostics and most of the drugs used to treat malaria target the blood stage forms of *Plasmodium* (Tuteja, 2007).

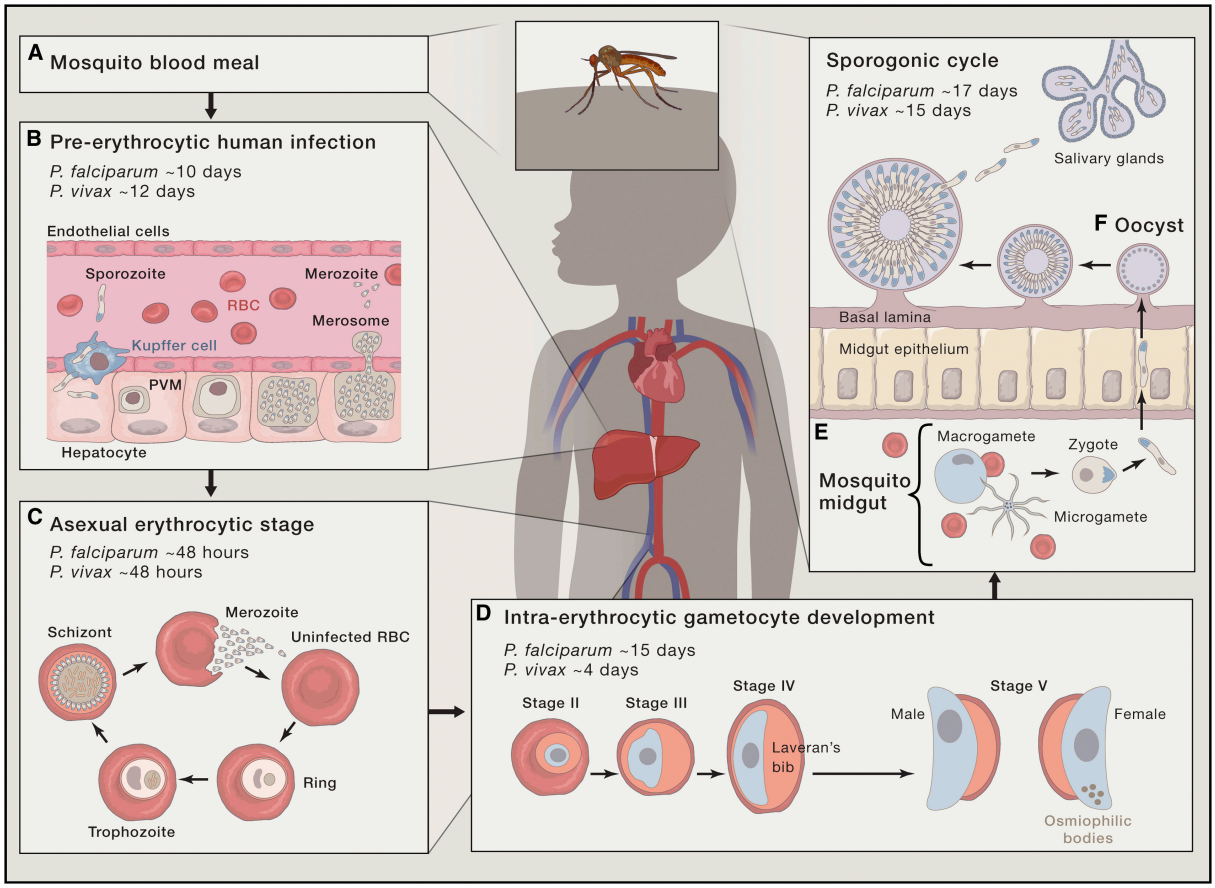

Figure 1.2 Life cycle of *P. falciparum*
Source: Cowman et al., 2016; see text for details (Section 1.3).

During the erythrocytic cycle, a proportion of parasites are reprogrammed to undergo gametocytogenesis. Within about two weeks (*P. falciparum*) or respectively 4 days (*P. vivax*) microgametocytes (male) and macrogametocytes (female) are formed that are essential for

the sexual phase of the life cycle (Figure 1.2D). A female mosquito takes up these gametocytes during its blood meal. In the mosquito midgut, the female gametocyte matures into a macrogamete and the male gametocyte matures into a microgamete in a process called exflagellation (Josling and Llinás, 2015). Haploid male microgametes fertilize the female macrogametes generating a diploid zygote that further develops into an ookinete (Figure 1.2E). The motile ookinete traverses the midgut epithelium and encysts on the other side (underneath the basal membrane) to become an oocyst where asexual sporogenic replication occurs (Sinden and Billingsley, 2001). In the oocyst motile sporozoites are budding within vesicle-like structures and, subsequently, egress the oozyst (Klug and Frischknecht, 2017). These sporozoites are carried via the haemolymph to the salivary glands of the mosquito, which are actively invaded (Figure 1.2F) (Frischknecht et al., 2004, Douglas et al., 2015). The sporozoites can be injected into the next human host to begin a new round of the life cycle (Tuteja, 2007, Cowman et al., 2016).

1.4 The apicoplast: A relict plastid of *P. falciparum*

The protozoan parasites of the genus *Plasmodium* belong to the phylum Apicompexa, which includes a large number of obligate intracellular parasites (Fast et al., 2001, Lim and McFadden, 2010). A common feature of these members is the so-called apical complex that is located at the anterior end of the invasive forms and consists of a set of organelles necessary for the recognition, selection and invasion of the host cell: the rhoptries, the micronemes and the dense granules (Preiser et al., 2000, Blackman and Bannister, 2001).

Another organelle that is found in most Apicomplexa is the apicoplast, a vestigial non-photosynthetic plastid. It was derived via secondary endosymbiosis. This means that in a first step an algal ancestor engulfed a cyanobacterium and in a second step this plastid-containing red alga was engulfed by an auxotrophic protist (Lim and McFadden, 2010, van Dooren and Striepen, 2013). As a result the apicoplast is an organelle with four membranes (Lemgruber et al., 2013). At some point in their evolution, Apicomplexa became parasitic living organisms and lost their ability to photosynthesize. The evolutionary red algal origin of the apicoplast was confirmed by the discovery of *Chromera velia* (Moore et al., 2008) and *Vitrella brassicaformis* (Oborník et al., 2012) that retain a photosynthetic plastid and are

closely related to apicomplexan parasites (Janouškovec et al., 2010, Arisue and Hashimoto, 2015).

The apicoplast has its own 35 kb circular genome that encodes less than 50 proteins (Wilson et al., 1996) which represent only a fraction of the apicoplast proteome that consists of approximately 500 predicted proteins (Foth and McFadden, 2003). This means that most of the apicoplast proteins are transported from the cytosol into the apicoplast. This traffic is mediated by an N-terminal sequence, the bipartite topogenic signal (BTS). The BTS consists of a signal peptide (SP) that directs the proteins to the endoplasmic reticulum (ER) and a transit peptide (TP) that is responsible for the further transport from the ER to the apicoplast (Waller et al., 1998, Waller et al., 2000, Kalanon and McFadden, 2010). The SP is cleaved after co-translational import into the ER and the TP cleavage occurs after protein import into the apicoplast (van Dooren et al., 2002).

In the apicoplast many biosynthetic pathways take place such as the synthesis of fatty acids, isoprenoids, iron-sulfur clusters and heme (Ralph et al., 2004, Lim and McFadden, 2010, van Dooren and Striepen, 2013). In both, blood and liver stages, the apicoplast was shown to be essential for parasite survival (Kalanon and McFadden, 2010, Yeh and DeRisi, 2011) and therefore represents an interesting target for the development of antiplasmodial drugs.

1.5 Treatment and resistances

Since there is still no licensed malaria vaccine available, malaria treatment focuses mainly on vector control, chemoprophylaxis and chemotherapeutical treatment. Vector control includes the use of insecticides, insecticide-treated mosquito nets and indoor residual spraying (WHO, 2015). Due to emerging drug resistance and high treatment costs, chemoprophylaxis is restricted to specific groups: travellers from non-endemic countries, pregnant women and children (Schwartz, 2012).

For chemotherapeutical treatment several drugs are available. Most of these drugs target the asexual blood stages of the parasite. Only a few are known to possess an additional gametocytocidal activity and an activity against hypnozoites (dormant stage of the *P. vivax* parasite) in the liver (e.g. primaquine). The following overview gives a summary of the currently known antimalarial drugs, known modes of action and the corresponding identified genetic markers for drug resistance (Petersen et al., 2011, Antony and Parija, 2016):

- **Quinoline derivatives:** Aminoquinolines (chloroquine, amodiaquine, primaquine) and amino alcohols (quinine, mefloquine, halofatrine, lumefatrine). These drugs accumulate in the digestive vacuole of the parasite and inhibit the heme detoxification. For all of these drugs resistances were identified. For example, chloroquine resistance was correlated with mutations in the chloroquine resistance transporter (*Pf*CRT) (Sidhu et al., 2002, Petersen et al., 2015). Furthermore, resistances to all quinoline derivatives were correlated with point mutations in *Pf*MDR1 (Barnes et al., 1992).
- **Naphoquinon:** Atovaquone targets the cytochrome *bc1* complex that is located in the inner mitochondrial membrane of the parasite and therefore inhibits the respiratory chain of the parasite. Resistance to atovaquone was associated with a point mutation in the cytochrome *b* gene (Korsinczky et al., 2000).
- **Antifolate derivatives:** Sulfa drugs (sulfadoxine, sulfene), pyrimethamine and proguanil. These drugs interfere with the biosynthesis of folate that is essential for parasite survival by inhibiting either the dihydropteroate synthetase (*Pf*DHPS) or the dihydrofolate reductase (*Pf*DHFR) of the parasite. Point mutations in these enzyme lead to resistances against the antifolate derivatives (Gregson and Plowe, 2005).
- **Artemisinin derivatives:** Endoperoxides artesunate, artemisinin and artemeter. The mode of action of these drugs is not precisely known. Early stage resistances against artemisinin derivatives were associated with polymorphisms in the gene that encodes the *P. falciparum* kelch protein K13 (Ariey et al., 2014, Ashley et al., 2014, Straimer et al., 2015).
- **Antibiotics:** Tetracycline and clindamycin inhibit the protein biosynthesis pathway of the parasite in the apicoplast (Ramya et al., 2007). Doxycycline inhibits gene expression in the apicoplast (Dahl et al., 2006). No genetic markers for resistances against these antibiotics were identified so far.

To limit the spread of resistances, provide safe and effective malaria treatment and design effective treatment protocols, the WHO has established a guideline for malaria treatment that is updated every two years or more frequently. The current mainstays are artemisinin-based combination therapies (ACT). An ACT consists of the combination of a rapidly acting artemisinin derivative with a longer-acting (more slowly eliminated) partner drug (WHO, 2015).

1.6 *P. falciparum* and the oxidative stress hypothesis

It has been postulated that all organisms living under aerobic conditions are exposed to so-called 'oxidative stress' and depend on defense mechanisms to deal with oxidative challenges that can damage nucleic acids, protein, lipids and membranes (Imlay, 2003). 'Oxidative stress' is defined as a prolonged redox imbalance with the accumulation of oxidized and damaged molecules (Sies, 1986). Metabolites that result from the incomplete reduction of molecular oxygen can be free radicals acting as one-electron oxidants such as the superoxide anion ($O_2^{\bullet -}$) or the hydroxyl radical ($OH^{\bullet}$) or non-radical species acting as two-electron oxidants such as hydrogen peroxide (H_2O_2) or peroxynitrite ($ONOO^-$) (Winterbourn, 2008, Imlay, 2013).

During the erythrocytic cycle, parasite survival and parasite clearance by the host immune system have been hypothesized to depend on oxidative stress generated by the host immune system and by the parasite itself (Becker et al., 2004, Jortzik and Becker, 2012). According to this theory, the high metabolic rate of the rapidly growing parasites is responsible for the generation of several redox metabolites, such as $O_2^{\bullet -}$, $OH^{\bullet}$ and H_2O_2 (Figure 1.3) (Müller, 2004).

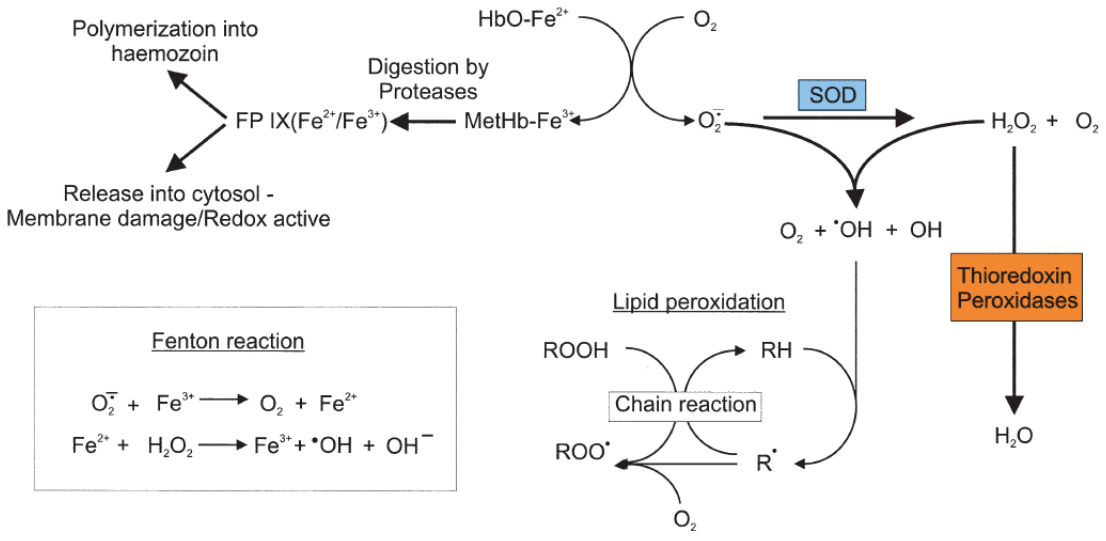

Figure 1.3 Potential sources of reactive oxygen species in *P. falciparum*
See text for details (Section 1.6). FP IX, ferri/ferroprotoporphyrin IX; HbO-Fe^{2+}, oxy-hemoglobin containing ferriprotoporphyrin IX; MetHb-Fe^{3+}, methemoglobin containing ferroprotoporhpyrin IX; SOD, superoxide dismutase.
Source: Müller et al., 2004.

The parasite digests the host hemoglobin to assure the supply with amino acids that are essential for its biosynthetic processes. During this process toxic free heme (ferri/ferroprotoporphyrin IX) is released, which the parasite detoxifies by the conversion into non-toxic insoluble hemozoin crystals (malaria pigment) (Becker et al., 2004). However, a certain amount of toxic free heme is supposed to escape the bio-mineralization and, subsequently, to undergo redox reactions. Oxidation of heme iron can generate $O_2^{\bullet-}$. Furthermore, hydroxyl radicals can be generated via the Fenton reaction. These species are highly reactive and are hypothesized to cause, for instance, membrane damage by lipid peroxidation in the parasite (Figure 1.3) (Müller, 2004).

However, these processes take place in the food vacuole that has a low pH value (Biagini et al., 2003). This would lead to the spontaneous disproportionation of $O_2^{\bullet-}$ and, furthermore, it seems quite unlikely that highly reactive radicals are able to cross the food vacuole membrane. In addition, the host-parasite unit is packed with numerous hydroperoxidases that can efficiently reduce several peroxides, such as H_2O_2, *t*-BOOH and peroxynitrite and it was shown that *P. falciparum* parasites are extremely robust towards challenges with external oxidizing agents in cell culture (Wezena et al., 2017).

Although several studies point to a physiological relevance of 'oxidative stress' regarding parasite survival and clearance by the immune system, it remains to be shown how the redox-state really affects the host-parasite unit.

1.7 The antioxidant defense of *P. falciparum*

Aerobic living organisms have evolved a complex network of antioxidant proteins to detoxify free radicals and other oxidant species. In mammals the major antioxidant enzymes are superoxide dismutases (SODs), peroxiredoxins (Prx), catalase and glutathione peroxidases (Sies, 1993, Birben et al., 2012, Espinosa-Diez et al., 2015). Interestingly, the antioxidant network of *P. falciparum* lacks two of these powerful enzymes, catalase and canonical glutathione peroxidase, and consists of two superoxide dismutases (*Pf*SOD1 and *Pf*SOD2), a thioredoxin-dependent gluthatione peroxidase and several Prx (Müller, 2004, Sienkiewicz et al., 2004, Deponte et al., 2007). These enzymes function in connection with the NADPH-dependent glutathione and thioredoxin systems.

The glutathione system of *P. falciparum* consists mainly of glutathione (GSH), two glutathione synthetases, glutathione reductase, glutathione transferase and glutaredoxin or glutaredoxin-like-proteins. The thioredoxin system of *P. falciparum* consists mainly of thioredoxins of thioredoxin-like proteins, thioredoxin reductase, thioredoxin-dependent peroxidases and plasmoredoxin (Krauth-Siegel et al., 2005, Jortzik and Becker, 2012, Chaudhari et al., 2017).

GSH is the most abundant low molecular weight thiol in the cells (≈2 mM in trophozoites) (Becker et al., 2003). It is synthesized from the three amino acids L-glutamic acid, L-cysteine and glycine by two cytosolic synthetases (γ-glutamyl-cysteine synthetase and glutathione synthetase). Oxidized GSH, glutathione disulfide (GSSG), is the substrate of glutathione reductase (GR) that catalyzes the NADPH-dependent reduction of GSSG to 2 GSH. The maintenance of a high GSH/GSSG ratio by GSH *de novo* synthesis and GSSG reduction is mandatory for intracellular redox homeostasis (Atamna and Ginsburg, 1997, Morgan et al., 2013). The glutathione and the thioredoxin system are involved in a variety of thiol-based detoxification processes, thiol/disulfide exchange reactions and redox regulation processes with NADPH as the main electron source (Krauth-Siegel et al., 2005, Deponte, 2013, Deponte, 2017).

1.8 Peroxiredoxins – an overview

Peroxiredoxins (Prx) are ubiquitous enzymes and belong to the most abundant proteins in a cell representing ≈1% of the total cellular protein concentration. Their catalytic efficiencies are in the range of 10^3-10^7 (Winterbourn and Hampton, 2008, Perkins et al., 2016). The main substrates of Prx are H_2O_2, organic hydroperoxides and peroxynitrite, which are by-products of cellular catabolism and can damage biomembranes and proteins.

In addition to their contribution in antioxidant protection, they take part in cellular signaling pathways using H_2O_2 as a second messenger. For example, human Prx2 was shown to take part in the redox regulation of the transcription factor STAT3 (Sobotta et al., 2015) and yeast Gpx3 was shown to act as a signal transducer in the hydroperoxide-dependent activation of the transcription factor Yap1 (Delaunay et al., 2002).

Another model of peroxide-mediated redox regulation of proteins, the so-called 'floodgate-theory', considers the susceptibility of Prx to peroxide-mediated inactivation (Wood et al.,

2003a, Karplus and Poole, 2012, Perkins et al., 2014). Prx are to different extends (reversibly) over-oxidized and inactivated. Thus, high peroxide concentrations may locally accumulate and are hypothesized to modify proteins directly. But there is currently little experimental evidence to support the floodgate model and it exhibits some problems. For instance, it is unknown how the signal specificity is achieved and it is questionable whether most of the proteins are sufficiently reactive towards peroxides to become modified directly (Winterbourn, 2008, Winterbourn and Hampton, 2008, Brigelius-Flohé and Flohé, 2011, Deponte and Lillig, 2015).

Furthermore, Prx possess molecular chaperone activities. To execute this function, the enzymes have to undergo a structural shift from low molecular weight species to high molecular weight complexes (Jang et al., 2004, Chuang et al., 2006).

1.9 Structure, catalytic mechanism and classification of peroxiredoxins

The members of the Prx family are either grouped according to their primary sequence or their catalytic mechanism. Based on the sequence, they are divided into six different subfamilies: Prx1/AhpC, Prx6, Prx5, Tpx (thiol peroxidase), PrxQ/BCP (bacterioferritin comigratory protein) and AhpE. The Prx1/AhpC and Prx6 subfamilies include members from archaea, bacteria, as well as uni- and multicellular eukaryotes. The BCP/PrxQ family includes mostly Prx from bacteria and plants, while the Tpx and AhpE families are all bacterial Prx. The Prx5 subfamily includes Prx from bacteria and eukaryotes (Soito et al., 2011, Poole et al., 2011, Nelson et al., 2011).

According to the other classification system, Prx are categorized based on the catalytic mechanism into three classes: 1-Cys, typical 2-Cys and atypical 2-Cys Prx. The differences of the three groups are based on the number and position of the redox active cysteine residues involved in the catalytic cycle (Rhee et al., 2001, Rhee, 2016).

All Prx have a common catalytic cycle and most Prx are active as homodimers. The first step of the cycle, the peroxidation, takes place in the fully folded conformation (FF) and involves a nucleophilic attack of the peroxidatic cysteine (C_P) thiolate on a peroxide substrate. The corresponding alcohol (or water) is released and the C_P is oxidized to sulfenic acid (S_pOH) (Figure 1.4 step 1).

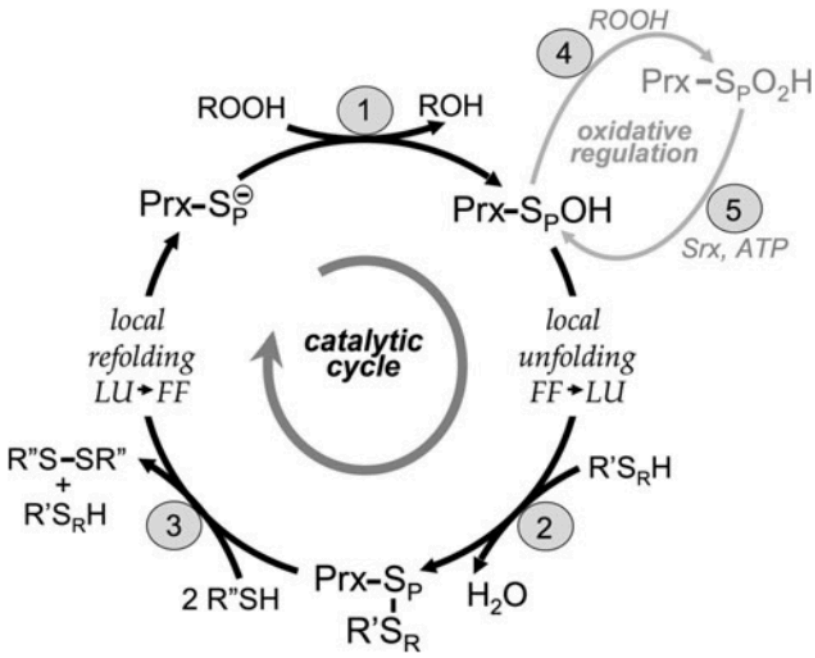

Figure 1.4 The peroxiredoxin catalytic cycle
(1) peroxidation (2) resolution and (3) recycling of the peroxidatic cysteine residue (C_P). Protein conformations in the cycle: FF (fully folded) and LU (locally unfolded). The local unfolding is required for disulfide bond formation in step 2, the local refolding to reform the peroxide-binding active site after the disulfide is reduced in step 3. Oxidative regulation (gray, steps 4 and 5) is seen in some 2-Cys Prxs. Inactivation of the Prx by over-oxidation of the C_P (step 4) is peroxide-dependent. The inactivated form can be rescued by sulfiredoxin (Srx) (step 5). See text for more details (Section 1.9)
Source: Hall et al., 2011.

Following peroxidation a local unfolding event of helix α2 (containing C_P) takes place that is mandatory for disulfide formation. In this locally unfolded (LU) conformation a resolving thiol (S_RH) attacks the sulfenic acid, releases water and forms a disulfide bridge (Prx-S_P-S_RR') (Figure 1.4 step 2). The resolving thiol can be either present on the Prx itself on the opposite subunit (typical 2-Cys Prx), the same subunit (atypical 2-Cys Prx) or on another protein or small molecule (1-Cys Prx).

In the next step, the recycling, the disulfide is reduced by another protein or small molecule regenerating the free Prx-S_P^-. Following reduction, a local refolding of the active site takes place and the enzyme can enter a new round of catalysis (Figure 1.4 step 3) (Hall et al., 2011, Deponte, 2013, Perkins et al., 2016).

In competition to the resolution (step 2) the sulfenic acid can be attacked by another peroxide in the FF conformation to form a sulfinic acid (S_pO_2H) or sulfonic acid (S_pO_3H) that represent inactive forms of the enzyme (Figure 1.4 step 4). The susceptibility to be converted into this over-oxidized form varies among different Prx and is thought to be important for the oxidative regulation of peroxide signaling (Wood et al., 2003b, Hall et al.,

2009, Hall et al., 2011). In some cases, the over-oxidation is reversible and the sulfinic acid can be reduced to sulfenic acid by sulfiredoxin (Srx) to reactivate the Prx for catalysis (Figure 1.4 step 5) (Jönsson and Lowther, 2007).

1.10 *P. falciparum* peroxiredoxins

In *P. falciparum* five different Prx have been identified (Gretes, 2012, Jortzik and Becker, 2012). Furthermore, it was reported that *P. falciparum* imports the human Prx2 from the erythrocytes into its cytosol during blood-stage development (Koncarevic et al., 2009). The nomenclature of the *Pf*Prx is inconsistent in the literature. In this work, I will use the nomenclature according to Gretes and colleagues. The five enzymes belong to four subfamilies of Prx: two from the Prx1 subfamily (*Pf*Prx1a and *Pf*Prx1m), one PrxQ (*Pf*PrxQ), one Prx5 (*Pf*Prx5/*Pf*AOP) and one Prx6 (*Pf*Prx6) (Gretes, 2012).

***Pf*Prx1a** (*Pf*TPx1) is a typical 2-Cys peroxiredoxin (Kawazu et al., 2008) that is located to the cytosol (Kehr et al., 2010). It forms decamers in its reduced state (Akerman and Müller, 2003, Kawazu et al., 2008) and is constitutively expressed in all erythrocytic stages (Yano et al., 2005). *Pf*Prx1a reduces H_2O_2, *t*-BOOH, cumene hydroperoxide and peroxynitrite by accepting *Pf*Trx and plasmoredoxin as electron donors *in vitro* (Nickel et al., 2005, Jortzik and Becker, 2012). Under standard culture conditions *Pf*Prx1a is dispensable for blood-stage development, as knockout parasites showed no difference to the wild-type strain in growth rates or morphology (Komaki-Yasuda et al., 2003).

***Pf*Prx1m** (*Pf*TPx2), the second typical 2-Cys Prx, is located in the mitochondrion (Boucher et al., 2006, Kehr et al., 2010). It forms decamers and a small proportion of dimers (Boucher et al., 2006) and is expressed during the trophozoite and schizont stages (Yano et al., 2005). *Pf*Prx1m is a thioredoxin-dependent peroxidase that reduces H_2O_2 and *t*-BOOH but was inactive with cumene hydroperoxide as a substrate *in vitro* (Boucher et al., 2006). Knockout of Prx1m in the rodent malaria parasite *P. berghei* showed that Prx1m is not essential for the blood- and mosquito-stages of the parasite (Masuda-Suganuma et al., 2012).

***Pf*PrxQ** (*Pf*nPrx) is located in the nucleus of the parasite (Richard et al., 2011). A thioredoxin- and glutaredoxin-dependent peroxidase activity was shown for different peroxides such as H_2O_2 and cumene hydroperoxide *in vitro*. Attempts to disrupt the gene in both *P. falciparum*

and *P. berghei* were unsuccessful so far pointing to an essential role of the protein for parasite survival (Richard et al., 2011).

***Pf*Prx6** (*Pf*1-Cys-Prx) is a 1-Cys peroxiredoxin and located in the cytosol (Kehr et al., 2010). Its expression levels are elevated in the trophozoite stage (Yano et al., 2005). Kinetic studies on recombinant *Pf*Prx6 revealed contradictory results. One study showed a glutathione-dependent reduction of H_2O_2 (Kawazu et al., 2000) whereas another study showed that H_2O_2 is reduced using the thioredoxin system as electron donor (Krnajski et al., 2001). A third group could not reproduce a significant GSH-dependent activity with H_2O_2 or *t*-BOOH and detected just a slight activity with *Pf*Trx1 and *Pf*Grx (Nickel et al., 2006). As the activity of *Pf*Prx6 was quite low with both systems, the physiological reductant remains unknown.

***Pf*Prx5/*Pf*AOP** mechanistically belongs to the 1-Cys peroxiredoxins and appears in the crystal structure and in solution as a homodimer consisting of two 21 kDa monomers (Sarma et al., 2005, Nickel et al., 2006, Djuika et al., 2013). It is expressed in all erythocytic stages with elevated expression levels in the trophozoite stage (Nickel et al., 2006). *Pf*AOP was predicted to localize to the apicoplast (Nickel et al., 2006, Deponte et al., 2007) and a GFP-fusion protein with the N-terminus of *Pf*AOP was shown to localize to the apicoplast (Kehr et al., 2010). However, a recent study of our group showed that *Pf*AOP is dually localized to the apicoplast and cytosol using subcellular fractionation and co-localization experiments with transgenic parasites (Djuika et al., 2015).

The coding sequence of *PFAOP* includes two exons separated by one intron. It consists of 723 base pairs that translate into 240 amino acids. The first exon encodes the bipartite topogenic signal (BTS) that is responsible for targeting to the apicoplast and is usually processed upon protein import (Waller et al., 2000, van Dooren et al., 2002, Djuika et al., 2015). The second exon encodes the Prx5 domain. The full-length protein includes three cysteine residues at positions 20, 117 and 143. Cys20 is part of the BTS sequence and therefore not involved in protein catalysis. Based on the crystal structure and *in vitro* peroxidase assays Cys117 was identified as the peroxidatic cysteine (Sarma et al., 2005, Djuika et al., 2013). The role of Cys143 could not be defined yet. It is conserved in a variety of Prx5-type homologues from bacteria, plants and animals (Figure 1.5a). The mutant *Pf*AOP^{C143S} is still catalytically active albeit to a lesser extent. Cys143 was found buried in the crystal structure (Sarma et al., 2005) but surprisingly its gluthationylation was detected *in vitro* and in *Escherichia coli* (Djuika et al., 2013). SDS-PAGE redox mobility shift assays

revealed that Cys143 is able to form a reversible disulfide bond with Cys117 depending on the hydroperoxide- and GSH-concentration (Djuika et al., 2013). Furthermore, the crystal structure revealed that residues Cys117 and Cys143 are separated by the side chain of Leu109 at the bottom of the active side pocket, which adopts different conformations in both subunits of the crystallized homodimer (Sarma et al., 2005) (Figure 1.5b,c,d). It was therefore hypothesized by our group that Leu109 might play a regulatory role and act as a gatekeeper controlling the accessibility of Cys143 (Djuika et al., 2013).

Recombinant *Pf*AOP was shown to reduce different peroxides *in vitro*. The highest activities were measured with *t*-BOOH as electron acceptor whereas the reduction of H_2O_2 and cumene hydroperoxide led to lower activities under the chosen assay conditions (Nickel et al., 2006). The same study showed that *Pf*AOP accepts both *Pf*Grx and *Pf*Trx1 as electron donor whereas higher peroxidase activity was measured with the glutaredoxin system (Nickel et al., 2006).

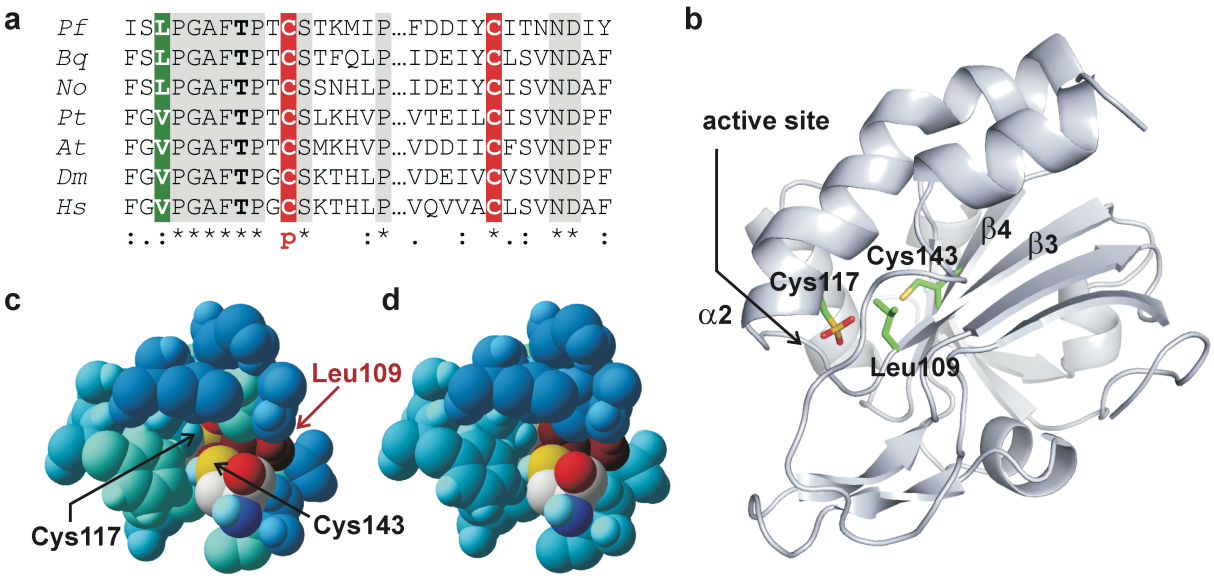

Figure 1.5 The second cysteine residue and a potential gatekeeper of *Pf*AOP and Prx5 homologues
(a) Sequence alignment of Prx5 stretches comprising the peroxidatic cysteine residue, which is labeled with a "p," and the second cysteine residue, which is found in many bacterial and eukaryotic homologues. The potential gatekeeper residue is shaded in green. *Pf*, *P. falciparum*; *Bq*, *Bartonella quintana*; *No*, *Nitrosococcus oceani*; *Pt*, *Populus tremula*; *At*, *Arabidopsis thaliana*; *Dm*, *Drosophila melanogaster*; *Hs*, *Homo sapiens*. (b) Structure of *Pf*AOP chain A as ribbon diagram with the peroxidatic Cys117 at the beginning of helix α2, Leu109 at the end of β-strand 3, and Cys143 in β-strand 4 highlighted. (c) View along the two cysteine residues of *Pf*AOP toward the bottom of the active site pocket. Only selected residues of the crystal structure PDB entry 1XIY are shown for clarity. The entry side for the hydroperoxide substrate is behind oxidized Cys117 and cannot be seen from the chosen perspective. Subunit A reveals a potential gate between both cysteines with the sulfur atom of Cys117 at the back pointing toward the sulfur atom of Cys143 at the front. The side chain of the potential gatekeeper Leu109 is depicted in dark red and adopts a partially "open" conformation. (d) Same view along the cysteine residues of subunit B with residue Leu109 adopting a rather "closed" conformation.
Source: Staudacher et al., 2015.

Our group showed that *Pf*AOP is a model enzyme for Grx/GSH-dependent Prx-isoforms but the exact mechanism could not be identified so far. Two mechanisms of the reductive half-reaction are possible: The sulfenic acid could react with *Pf*Grx resulting in a mixed disulfide that is subsequently cleaved by GSH. The second possibility is the direct reaction of the sulfenic acid of *Pf*AOP with GSH followed by degluthationylation by *Pf*Grx (Djuika et al., 2013).

PFAOP is part of a genetic locus on chromosome 7 that is associated with altered artemisinin susceptibility. This locus was identified in a quantitative trait locus (QTL) analysis, conducted by our cooperation partners from the Lanzer group, using a genetic cross between the *P. falciparum* strains 7G8 (Latin America) and GB4 (Africa) (Djuika et al., 2017). Nevertheless, in a subsequent study by Carine Djuika, it was shown that artemisinin is neither a substrate nor an inhibitor of *Pf*AOP. Furthermore, 3D7 strains over-expressing GFP fusion constructs of *Pf*AOP did not show altered susceptibility to artemisinin in standard IC_{50} measurement assays (Djuika et al., 2017).

1.11 Peroxiredoxin-based roGFP fusion constructs as redox sensors

The visualization of disulfide bond formation in living cells is essential to gain information about redox-regulated metabolic processes. Therefore, redox-sensitive green fluorescent proteins (roGFP) were engineered that can be used as genetically encoded sensors for monitoring intracellular redox changes. These sensors can form a reversible disulfide bond between two cysteine residues (Østergaard et al., 2001) and change their fluorescence excitation spectra depending on the redox state in a ratiometric manner (Zhang et al., 2002, Griesbeck, 2004). Disadvantages of these proteins are their slow responses to changes in the cellular redox potential and their low selectivity regarding the redox system they interact with or the cellular compartment. To overcome these limitations different genetically encoded fusion constructs of redox enzymes and roGFP or other redox-sensitive fluorescent proteins were developed (Belousov et al., 2006, Gutscher et al., 2008, Schwarzlander et al., 2016). Fusion constructs between human glutaredoxin 1 and roGFP2 (Grx1-roGFP2) allowed real-time imaging of the intracellular glutathione potential (Gutscher et al., 2008, Kasozi et al., 2013). Intracellular H_2O_2 levels were measured with a probe consisting of roGFP2 and Orp1, a glutathione peroxidase found in *Saccaromyces cerevisiae*, which forms a redox relay

with the transcription factor Yap1. With this probe it was shown that a peroxidase can transfer oxidizing equivalents to roGFP2, replacing Yap1, on the basis of a thiol-disulfide exchange (Gutscher et al., 2009). Other peroxiredoxins show much higher second-order rate constants for H_2O_2 and can also form redox relays with different proteins. Based on this, further peroxiredoxin-based roGFP fusion constructs were developed that are sensitive to endogenous H_2O_2 levels (Morgan et al., 2016, Van Laer and Dick, 2016). However, so far it was not really understood how the roGFP readout is affected by the kinetic parameters of the coupled peroxiredoxin and it remains unknown how inactivation kinetics due to over-oxidation of the active site cysteine residue are translated to the roGFP.

1.12 Aim of this thesis

This PhD project was mainly based on the previous work on *Pf*AOP by Carine Djuika and other members of the Department, who kinetically characterized *Pf*AOP^{wt} and identified the *Pf*AOP^{L109M} mutant as a more active enzyme compared to *Pf*AOP^{wt}. Moreover, the contribution of *Pf*AOP to the artemisinin susceptibility of *P. falciparum* was previously investigated using *PFAOP-GFP* over-expressing parasite strains and steady-state kinetic analysis with the recombinant enzyme and artemisinin (Djuika et al., 2013, Djuika et al., 2015, Staudacher et al., 2015, Djuika et al., 2017).

Prx are known to play central roles in redox signaling, thus, a deeper understanding about the redox regulation and inactivation properties is essential to understand what makes Prx good enzymes or redox sensors. As the role of the second cysteine residue Cys143 and the potential gatekeeper residue Leu109 in the *Pf*AOP structure could not be identified so far, the first aim of this work was to further characterize the catalytic mechanism, especially the reductive half-reaction, using recombinant wild-type and Leu109X and Cys143Ser mutant enzymes. Therefore, different *in vitro* methods, such as steady-state and stopped-flow kinetic measurements, were used.

To translate these *in vitro* results to an *in vivo* system, different roGFP2-*Pf*AOP fusion constructs were generated and characterized in yeast. So far, it was unknown how and to which extend classic enzyme parameters of Prx affect the roGFP2 readout. Thus, it was investigated if fusion constructs of roGFP2 and Prx can be used to monitor kinetic properties of Prx in living cells. Furthermore, the aim was to gain more insights into the mechanism

how Prx, which act as the peroxide sensor moiety, transfer their redox state to roGFP2, which acts as the reporter moiety of the roGFP2 fusion construct. These findings will contribute to the optimization of redox sensors and allow potential future applications such as the noninvasive characterization of peroxidases, the evaluation of post-translational protein modifications and the estimation of intracellular hydroperoxide concentrations.

So far, several Prx were identified as parts of redox-relays in different organisms. Thus, the second aim of this thesis was to unravel the physiological relevance of *Pf*AOP. The following questions were addressed: (i) is the protein essential and (ii) which are its interaction partners. To answer the first question, the *PFAOP* gene was knocked-out by double-crossover using the CRISPR/Cas9 system to investigate whether the encoded protein has an essential function for asexual blood-stage development of the malaria parasite. Parasite growth was monitored under standard growth conditions and under elevated levels of oxidizing agents. Furthermore, the artemisinin susceptibility of the 3D7Δ*pfaop* knockout parasites was tested. To answer the second question non-reducing SDS-PAGE and western blot analyses of parasite extracts of challenged and unchallenged *P. falciparum* strains with wild-type *Pf*AOP or different *Pf*AOP-GFP fusion proteins were conducted and evaluated.

2 Materials and Methods

2.1 Materials

2.1.1 Equipment

Table 2.1 Equipment list

Equipment	***Manufacturer***
Äkta FPLC system	GE Healthcare
Analytical balance	Sartorius
Autoclave	Systec
Centrifuges (J-6B; J2-21M/E, Rotor JA-17, JA-10)	Beckman Coulter
DNA electrophoresis apparatus	Bio-Rad
Electrophoresis power supply (EPS 601)	GE Healthcare
Electroporator (Gene Pulser®)	Bio-Rad
Film developer (Curix 60)	Agfa
Gel documentation system (E.A.S.Y 440K, UVT-28L)	Herolab
Heating block (MBT 250)	Kleinfeld Labortechnik
Incubator for bacteria, solid culture	Heraeus
Incubator for *P. falciparum* culture	Mytron
Incubator for yeast, solid culture	Heraeus
Incubator with shaker for bacteria and yeast, liquid culture	Infors AG
Laminar flow hood for *E. coli* culture (gelaire® BSB 3A)	Flow Laboratories
Laminar flow hood for *P. falciparum* culture	Thermo Scientific
Light microscope	Zeiss
Magnetic stirrer (MR-Hei Standard)	Heidolph
Microcentrifuge 5417R	Eppendorf
Microcentrifuge SU1550	Sunlab
Microplate reader (FLUOstar OPTIMA)	BMG Labtech
Microplate reader (CLARIOstar)	BMG Labtech
Microwave	AEG
Multifuge 1 S-R	Heraeus
Multi-function rotator (PTR-30)	Grant-bio
Neubauer chamber (hemocytometer)	Marienfeld
PCR machine (Mastercycler gradient)	Eppendorf
Peristaltic Pump P-1	GE Healthcare
pH meter (Basic Meter PB-11)	Sartorius
pH electrode (Blueline 56 Electrode)	SI Analytics
PIPETMAN® P (P10, P20, P100, P200, P1000)	Gilson
Pipette Controller (Accu-jet® pro)	Brand

Portable spectrophotometer (Ultrospec 10)	Amersham Biosciences
Power supply (PowerPac Basic)	Bio-Rad
Power supply (E831 or EV231)	Consort
Red light lamp	Electric Petra
Rocking platform shaker (Duomax 1030)	Heidolph
SDS-PAGE electrophoresis system (Mini-PROTEAN Tetra Electrophoresis Cell)	Bio-Rad
Stopped-flow spectrofluorometer SX-20	Applied Photophysics
Thermoblock (Thermomixer® comfort)	Eppendorf
Ultrasonic laboratory homogenizer (Sonopuls HD 2070)	Bandelin electronic
UV/Vis-Photometer (V-650 spectrophotometer)	JASCO
VarioMACS magnetic separator	Miltenyi Biotec
Vortex-Mixer	Heidolph
Water bath Isotemp 210	Fisher Scientific
Western blot apparatus (PerfectBlue Semi-Dry Electro Blotter)	peqlab

2.1.2 Disposables

Table 2.2 List of disposables

Disposable	***Source***
6 and 48 well plates (cell culture)	Greiner bio-one
96 well plates black, F-bottom	Greiner bio-one
96 well plates black, F-bottom, transparent bottom	BD Falcon
Cell culture flasks	Greiner bio-one
Cryovials	Greiner bio-one
Disposable cuvettes	Sarstedt
Electroporation cuvettes Gene Pulser /Micro Pulser, 0,2 cm gap	Bio-Rad
HiTrap desalting columns	Amersham Biosciences
MACS separation CS columns	Miltenyi Biotec
Microscope Slides (SuperFrost®)	Buddeberg
Nitrocellulose membrane	GE Healthcare
Parafilm	Sigma Aldrich
PCR reaction tubes	Kisker Biotech
Petri dishes	Greiner bio-one
Pipette tips	Steinbrenner
Poly-Prep chromatography columns	Bio-Rad
Quartz cuvettes (104B-OS)	Hellma
Reaction tubes (1,5 & 2 ml, safe seal)	Sarstedt
Reaction tubes (15 & 50 ml)	Greiner bio-one
Scalpel	Braun
Serological pipettes (1, 5, 10 & 25 ml)	Sarstedt

Sterile syringe filters (0.2 µM)	Millipore
Sterile syringes	BD Plastipak
Sterile Vacuum filter (0.22 µM, Stericup®)	Millipore
Whatmann paper	GE Healthcare
X-ray films (Super RX-N)	Fujifilm

2.1.3 Chemicals

Table 2.3 List of chemicals

Chemical	*Source*
12(S)-hydroperoxy-5Z ,8Z,10E,14Z-eicosatetraenoic acid	Cayman Chemicals
Acetic acid	Sigma Aldrich
Acetone	Honeywell
Acrylamide/Bis Solution, 37.5:1 (30 % w/v)	Serva
Adenine	Sigma Aldrich
Agarose	Serva
Albumax II	Life Technologies
Ammonium sulfate	Sigma Aldrich
Ampicillin	AppliChem
APS	Bio-Rad
Artemisinin	Sigma Aldrich
Atovaquone	Sigma Aldrich
Bradford reagent (Protein assay Dye Reagent Concentrate)	Bio-Rad
Bromophenol blue	Waldeck
BSA (Albumin bovine Fraction V, Fatty acid free)	Serva
Calciumchlorid dihydrate	Merck
Chloroform	Sigma Aldrich
Complete protease inhibitor cocktail tablet	Roche
Coomassie® Brilliant Blue G 250	AppliChem
Cumene hydroperoxide	Sigma Aldrich
D-Glucose	Merck
D-Sorbitol	Sigma Aldrich
Diamide	Sigma Aldrich
DMSO	Sigma Aldrich
DNA ladder (100bp, 1kb)	New England Biolabs
DNase I	Roche
dNTPs	Thermo Scientific
DTPA	Sigma Aldrich
DTT	Sigma Aldrich
EDTA	Sigma Aldrich
EGTA	AppliChem

Ethanol (absolute)	VWR
Gel loading Dye, Purple 6x	New England Biolabs
Gentamicin	Life Technologies
Giemsa stock solution	Carl Roth
Glass beads 425-600µm	Sigma Aldrich
Glycerol	AppliChem
Glycin	Merck
GSH	Sigma Aldrich
GSSG	Sigma Aldrich
HCl	VWR
HEDS	Alfa Aesar
HEPES	Merck
Horseradish peroxidase	Sigma Aldrich
Hydrogen peroxide (30%)	Merck, Sigma Aldrich, Mallinckrodt Chemicals
Hypoxanthine	c.c.pro
Imidazole	Merck
IPTG	Serva
Isopropanol	Sigma Aldrich
Kanamycin	AppliChem
L-Arginine	Sigma Aldrich
L-Aspartic acid	Sigma Aldrich
LB-agar	Carl Roth
LB-medium	Carl Roth
L-Glutamic acid	Sigma Aldrich
L-Histidine	Sigma Aldrich
L-Isoleucine	Sigma Aldrich
Lithium acetate	Sigma Aldrich
L-Leucine	Sigma Aldrich
L-Lysine	Sigma Aldrich
L-Methionine	Sigma Aldrich
L-Phenylalanine	Sigma Aldrich
L-Serine	Sigma Aldrich
L-Threonine	Sigma Aldrich
L-Tryptophan	Sigma Aldrich
L-Tyrosine	Sigma Aldrich
L-Valine	Sigma Aldrich
Lysozyme	Serva
Magnesium chloride hexahydrate	Merck
β-Mercaptoethanol	Sigma Aldrich
Methanol	Honeywell

Midori Green Advance	Nippon Genetics
Milk (lowfat powdered)	Carl Roth
NADPH	Gerbu
NEM	Sigma Aldrich
Ni-NTA-Agarose	Qiagen
Nonidet P-40	AppliChem
PEG 3350	Sigma Aldrich
Peptone	Fluka Analytical
PMSF	Serva
Ponceau S	Serva
Potassium acetate	Sigma Aldrich
Potassium chloride	AppliChem
Potassium dihydrogen phosphate	Merck
Potassium monohydrogen phosphate	Merck
Prestained protein ladder	Thermo Scientific
Proteinase K	Roche
RNase A	Sigma Aldrich
Roti Phenol/Chloroform/Isoamylalcohol	Carl Roth
RPMI 1640, HEPES	Life Technologies
Saponin	Sigma Aldrich
SDS	Serva
Sodium acetate	Sigma Aldrich
Sodium chloride	Sigma Aldrich
Sodium deoxycholate	AppliChem
Sodium dihydrogen phosphate	Merck
Sodium hydrogen phosphate	Merck
Sodium hydroxide	Sigma Aldrich
SYBR Green I nucleic acid gel stain	Sigma Aldrich
TEMED	Serva
tert-Butyl hydroperoxide	Sigma Aldrich
Trichloroacetic acid	Merck
Tris	Carl Roth
TritonX-100	Merck
Tryptone	BD
Tween-20	Sigma Aldrich
UltraPure Salmon Sperm DNA Solution	Invitrogen
Unstained protein ladder	Thermo Scientific
WR 99210	Jacobus Pharmaceutical
Yeast extract	BD
Yeast nitrogen base without amino acids	Sigma Aldrich

2.1.4 Software/Bioinformatic tools

Table 2.4 List of software and bioinformatics tools

Software/Bioinformatic tool	*Source*
BioEdit	http://bioedit.software.informer.com/7.2/
CorelDraw X7	Corel Corporation
EndNote X7	Thomson Reuters
ExPASy	https://www.expasy.org/
JustBio	http://www.justbio.com
MARS	BMG Labtech
MS Office	Microsoft
NCBI (Database)	http://www.ncbi.nlm.nih.gov
NEBcutter V2.0	http://nc2.neb.com/NEBcutter2/
PlasmoDB	http://plasmodb.org/plasmo/
Pro-data SX	Applied Photophysics
Protospacer	http://www.protospacer.com/
SigmaPlot 13.0	Systat Software, Inc.
Spectra manager	JASCO

2.1.5 Kits

Table 2.5 List of Kits

Kit	*Source*
Amersham ECL Western Blotting Detection Reagents	GE Healthcare
In Fusion HD cloning Kit	Clontech
Plasmid Maxi Kit	Qiagen
Plasmid Mini Kit	Qiagen
SuperSignal West Femto	Thermo Scientific
Topo TA – Cloning Kit	Invitrogen
Wizard® SV Gel and PCR Clean-Up System	Promega

2.1.6 Enzymes

Table 2.6 List of enzymes

Enzyme	*Source*
Restriction enzymes	New England Biolabs
T4 DNA ligase	Fermentas
Taq DNA polymerase	New England Biolabs

2.1.7 Antibodies

All antibodies were diluted in blocking buffer (5 % milk in TBST).

TBS 10 mM Tris/HCl, 0.9% (w/v) NaCl, pH 7.4

TBST TBS, 0.1% (v/v) Tween 20

Table 2.7 List of antibodies

Name	*Origin*	*Source/Reference*	*Dilution*
Primary antibodies			
α*Pf*AOP-2	Rabbit	(Djuika et al., 2015)	1:100
α*Pf*AOP-5	Rabbit	(Djuika et al., 2015)	1:200
αGFP	Rabbit	Prof. Dr. A. Reichert*	1:500
αHSP70	Mouse	(Tsuji et al., 1994)	1:200
Secondary antibodies			
Goat Anti-rabbit IgG (H+L)-HRP Conjugate	Goat	Bio-Rad	1:10000
Goat Anti-rabbit IgG (H+L)-HRP Conjugate	Goat	Bio-Rad	1:10000

* Buchmann Institute for Molecular Life Sciences, Goethe University Frankfurt

2.1.8 Oligonucleotide primers

All oligonucleotide primers were purchased from Metabion. Restriction sites are underlined in the sequence and named in brackets.

Table 2.8 List of oligonucleotide primers

Primer	*Sequence 5' → 3'*
Cloning of pL7/*PFAOP*	
PFAOP/3'MCS/pL6/KO/s (EcoRI)	GATCGAATTCCAAACGATTTTACTTCAATAGATAC
PFAOP/3'MCS/pL6/KO/as (NcoI)	GATCCCATGGCTGATTATTTTTTAAAAACTCTTTTAC
PFAOP/5'MCS/KO/s (SacII)	GATCCCGCGGCTGTTCTTTTTATTATATGAATGAAGAG
PFAOP/5'MCS/KO/as (XbaI)	GATCTCTAGAGGATTCATAAACTTTTTGGGAAAACC
pL6/gRNA/*PFAOP*/s	TAAGTATATAATATTACAACATATCTGATACCGATGTTTTAG AGCTAGAA
pL6/gRNA/*PFAOP*/as	TTCTAGCTCTAAAACATCGGTATCAGATATGTTGTAATATTA TATACTTA

Analytical PCR reactions	
3D7/P1/*PFAOP*/s	ATATGATATATCTTATCGGTCCC
probe/hDHFR/s	CATGGTTCGCTAAACTGCATC
probe/hDHFR/as	CCTTTCTCCTCCTGGACATC
3D7/P4/*PFAOP*/as	TGGTATTACAAATAAGGGAAGAC

2.1.9 Plasmids/constructs

Table 2.9 List of plasmids and constructs

Plasmid/construct	***Characteristics/Applications***	***Reference***
Vectors		
pL6	Guide RNA expression and homologous recombination in *P. falciparum*	PhD J.J. Lopez-Rubio*
pUF1-Cas9	Expression of Cas9 in *P. falciparum*	PhD J.J. Lopez-Rubio*
p416TEF	Expression of roGFP2 and fusion constructs in *S. cerevisiae*	Prof. PhD B. Morgan**
His_6-tagged fusion constructs		
pQE30/*PFGR*	Expression of *Pf*GR in *E. coli*, N-terminal His_6 tag; kinetic assays	(Urscher et al., 2012)
pQE30/*PFGRX*$^{C32S/C88S}$	Expression of *Pf*Grx$^{C32S/C88S}$ in *E. coli*, N-terminal His_6 tag; kinetic assays	(Djuika et al., 2013)
pQE30/*PFAOP*	Expression of *Pf*AOP^{wt} in *E. coli*, N-terminal His_6 tag; kinetic assays	(Djuika et al., 2013)
pQE30/*PFAOP*^{C117S}	Expression of *Pf*AOP^{C117S} in *E. coli*, N-terminal His_6 tag; kinetic assays	(Djuika et al., 2013)
pQE30/*PFAOP*^{C143S}	Expression of *Pf*AOP^{C143S} in *E. coli*, N-terminal His_6 tag; kinetic assays	(Djuika et al., 2013)
pQE30/*PFAOP*^{L109M}	Expression of *Pf*AOP^{L109M} in *E. coli*, N-terminal His_6 tag; kinetic assays	(Staudacher et al., 2015)
pQE30/*PFAOP*^{L109A}	Expression of *Pf*AOP^{L109A} in *E. coli*, N-terminal His_6 tag; kinetic assays	(Staudacher et al., 2015)
***PFAOP* knockout construct**		
pL7/*PFAOP*	Knockout of *PFAOP* via the CRISPR-Cas9 system in *P. falciparum*	This work
roGFP2-*Pf*AOP fusion constructs		
p416TEF/*roGFP2*	Expression of roGFP2 in *S. cerevisiae*; kinetic assays	Prof. PhD B. Morgan**
p416TEF/*roGFP2-PFAOP*	Expression of roGFP2-*Pf*AOP^{wt} in *S. cerevisiae*; kinetic assays	Prof. PhD B. Morgan**
p416TEF/*roGFP2-PFAOP*^{C143S}	Expression of roGFP2-*Pf*AOP^{C143S} in *S. cerevisiae*; kinetic assays	Prof. PhD B. Morgan**

p416TEF/*roGFP2-PFAOP*^{L109M}	Expression of roGFP2-*Pf*AOP^{L109M} in *S. cerevisiae*; kinetic assays	Prof. PhD B. Morgan**
p416TEF/*roGFP2-PFAOP*^{L109A}	Expression of roGFP2-*Pf*AOP^{L109A} in *S. cerevisiae*; kinetic assays	Prof. PhD B. Morgan**

*Laboratoire de Parasitologie - Mycologie, Montpellier, France
**Zelluläre Biochemie, Technische Universität Kaiserslautern

2.1.10 Bacterial strains

Table 2.10 Bacterial strains

E. coli strain	*Genotype*	*Application*	*Source*
XL1-blue	recA1 endA1 hsdR17 supE44 thi-1 recA1 gyrA96 relA1 lac (F' proAB lacIqZ¢M15 Tn10) (TetR)	Cloning; Expression of recombinant proteins	Qiagen
NovaBlue Singles™ Competent Cells	endA1 hsdR17 (r_{K12}^{-} m_{K12}^{+}) supE44 thi-1 recA1 gyrA96 relA1 lac F'(proA^{+}B^{+} lacI^{q}ZΔM15::Tn10) (Tet^{R})	Cloning	Merck

2.1.11 Yeast strains

Table 2.11 Yeast strains

S. cerevisiae strain	*Genotype*	*Application*	*Source*
BY4742	MATα his3Δ1 leu2Δ0 lys2Δ0 ura3Δ0	Expression of roGFP2-AOP	Prof. PhD B. Morgan*

*Zelluläre Biochemie, Technische Universität Kaiserslautern

2.1.12 *P. falciparum* strains

Table 2.12 *P. falciparum* strains

P. falciparum strain	*Characteristics*	*Source / Reference*
Lab strain		
3D7	Origin: derived from NF54	Prof. Dr. M. Lanzer*
Transgenic parasites		
3D7pUF1-Cas9	Transfectant expressing Cas9	This work
3D7Δ*pfaop*	Δ*pfaop* knockout strain	This work
3D7Fl-AOP	Transfectant harboring an episomally encoded GFP fusion of *Pf*AOP	(Djuika et al., 2015)
3D7AOP-ΔN-term	Transfectant harboring an episomally encoded GFP fusion of *Pf*AOP-Δ-Nterm	(Djuika et al., 2015)
3D7AOP-ΔN-term, C117S	Transfectant harboring an episomally encoded GFP fusion of *Pf*AOP-Δ-Nterm, C117S	(Djuika et al., 2015)

NF54K13^{C580Y}	Artemisinin resistant transgenic parasites harboring *Pf*K13^{C580Y}	Prof. Dr. M. Lanzer*

* Centre for Infectious Diseases, Parasitology, Uniklinik Heidelberg

2.1.13 Selection drugs

Drug solutions were filter-sterilized using a 0.2 µm filter unit. Antimalarial drugs were diluted in DMSO, further diluted with RPMI1640 and stored under light protection. All stock solutions were stored at -20°C.

Table 2.13 List of antimalarials and antibiotics

Drug	*Stock solution*	*Working concentration*
Antimalarials		
WR99210	20 µM in RPMI1640	5 nM
Atovaquone	200 µM in RPMI1640	100 nM
Artemisinin	1.8 µM or 100 µM in RPMI1640	variable
Antibiotics		
Ampicillin	100 mg/ml in 50% ethanol	100 µg/ml
Kanamycin	25 mg/ml in ddH_2O	25 µg/ml

2.2 Molecular biology methods

2.2.1 Cloning of pL7/*PFAOP*

The pL7/*PFAOP* construct was generated in multiple cloning steps. A suitable guide sequence was identified in *PFAOP* using the protospacer software. The specific DNA fragments for homologous recombination were amplified by polymerase chain reaction (PCR). PCR conditions were adapted to the fragment size and the melting temperature of the primers. All PCR reactions were conducted with *Taq* polymerase.

The *PFAOP* 3'- homology region was amplified from plasmid pQE30/*PFAOP*^{C117S} with the primers *PFAOP*/3'MCS/pL6/KO/s and *PFAOP*/3'MCS/pL6/KO/as. The PCR fragments were subcloned using the TopoTA cloning kit according to the manufacturer's protocol and, subsequently, cloned into pL6 using the restriction sites EcoRI and NcoI.

The *PFAOP* 5'-homology region was amplified from genomic DNA of strain 3D7 with the primers *PFAOP*/5'MCS/KO/s and *PFAOP*/5'MCS/KO/as. The PCR fragments were subcloned

using the TopoTA cloning kit and, subsequently, cloned using the restriction site SacII and the compatible restriction sites generated by XbaI (insert) and SpeI (pL6).

For cloning of the guide-RNA, the pL6 plasmid bearing the 3'- and 5'-homology regions of *PFAOP* was consecutively digested by the restriction enzymes AvrII (2 h, 37°C) and BtgZI (2 h, 60°C). The insert was generated by annealing the oligonucleotide pL6/gRNA/*PFAOP*/s to the complementary reverse oligonucleotide pL6/gRNA/*PFAOP*/as. Therefore, the oligonucleotides were incubated at 94°C for 2 min and slowly cooled to room temperature. The resulting insert was mixed with digested pL6 and fused using the In-Fusion HD Cloning Kit according to the manufacturer´s protocol.

2.2.2 Restriction digest of DNA

For cloning or plasmid analysis, PCR products and plasmid DNA were cleaved with restriction endonucleases. All restriction enzymes were used according to the manufacturer´s recommendations. Typically 2-5 µl plasmid from a standard miniprep or 10-15 µl PCR product were digested with 0.5-1 µl of each restriction enzyme at 37°C for 2-3 h. The final reaction volume was 25 µl for analytical digestions and 50 µl for preparative digestions. When double-digestions were performed the compatibility of the enzymes was verified and the appropriate buffer was chosen using the double digest finder (NEB). Restriction digests were always controlled by agarose-gel electrophoresis.

2.2.3 Analysis of DNA by agarose-gel electrophoresis

Size and purity of DNA fragments or plasmids were analyzed using agarose-gel electrophoresis. A 0.8-1.5 % agarose-gel was prepared and installed in an electrophoresis tank containing 1x TAE buffer. The samples and an appropriate DNA ladder were mixed with 6x gel loading dye purple containing 1 µl/ml Midori Green Advance and loaded onto the gel. Gels were run for 30 min to 1 h at 80-120 V. Subsequently, the DNA was visualized under an UV transilluminator connected to a camera to capture gel images.

To extract DNA from the gel, the fragments were excised with a scalpel after quick visualization under low UV intensity to avoid UV-induced DNA damage.

Additionally, agarose-gel electrophoresis was used to quantify the DNA concentration. Therefore, a known amount of DNA ladder was loaded together with the DNA sample. As

the mass that corresponds to the single bands of the ladder is indicated by the manufacturer, the mass of the DNA sample loaded was calculated by comparing the band intensities of the marker vs. the sample.

1x TAE buffer 40 mM Tris/HAc, 1 mM EDTA, pH 7.6

2.2.4 Purification of DNA fragments

DNA fragments were purified directly following PCR or after separation by agarose-gel electrophoresis to remove salts, primers, enzymes, agarose-gel residues etc. Therefore, the kit Wizard® SV Gel and PCR Clean-Up System was used according to the manufacturer´s protocol.

2.2.5 Ligation of DNA fragments

To generate recombinant plasmid constructs, DNA fragments and plasmids were digested with appropriate restriction enzymes to generate cohesive ends and, subsequently, ligated using T4 ligase. Usually 20 µl of reaction mixture was prepared containing 1 µl of purified vector, 2 µl of insert and 1 µl of T4 ligase. The mixture was incubated at 16°C over night and, subsequently, 10 µl of the mixture were transformed into competent *E. coli* cells.

2.2.6 Transformation of chemically-competent *E. coli* cells

Chemically competent *E. coli* XL1-blue cells (50 µl, stored at -80°C) were thawed on ice and 0.5-10 µl plasmid DNA or ligation mixture were added and mixed by gently flicking the tube with the finger. The mixture was incubated on ice for 30 min, followed by a heat shock at 42°C for exactly 90 s. The cells were incubated for another 5 min on ice, 500 µl pre-warmed SOC-medium was added and the cells were incubated in a thermo mixer at 37°C and 500rpm for 30 min (ampicillin resistance) or 1 h (kanamycin resistance). Afterwards, the cells were spread on LB-agar-plates containing the appropriate antibiotic and incubated at 37°C over night.

Transformation of NovaBlue Singles™ Competent Cells was conducted according to the manufacturer´s protocol.

SOC-medium	2% (w/v) tryptone, 0.5% (w/v) yeast extract, 10 mM NaCl, 2.5 mM KCl, autoclaved 10 mM $MgCl_2$, 20 mM glucose, sterile filtered

2.2.7 Culture of *E. coli*

Depending on the application *E. coli* cells were cultured on solid or in liquid growth medium. Liquid growth medium was prepared by dissolving 25 g LB medium in 1 l H_2O. The medium was autoclaved, stored at 4°C and supplemented with the appropriate antibiotic immediately before use. For the preparation of solid growth medium 40 g of LB agar were dissolved in 1 l H_2O, autoclaved and cooled down to approx. 50°C. The appropriate antibiotic was added and the medium was poured into petri dishes. The plates were left uncovered in the laminar flow cabinet until the agar was solidified, packed in plastic bags and stored at 4°C.

For propagation of plasmid DNA, freshly transformed cells were spread on LB agar plates containing the appropriate antibiotic and incubated over night at 37°C. Afterwards the plates were sealed with Parafilm and stored at 4°C for up to one week.

For isolation of plasmid DNA (section 2.2.8) or expression of recombinant proteins (section 2.4.1) a single *E. coli* colony was picked from a LB agar plate and inoculated in the required volume of liquid LB medium containing the appropriate antibiotic. The cultures were grown at 37°C in a shaking incubator (135 rpm) over night or until the required bacterial density was reached.

2.2.8 Isolation of plasmid-DNA from *E. coli* cells

Plasmid DNA was isolated from *E. coli* cells using the alkaline lysis method (Birnboim and Doly, 1979). For large-scale isolation (maxiprep) the Plasmid Maxi Kit was used according to the manufacturer´s recommendations.

For small-scale isolation (miniprep) 2 ml cells from a liquid over night culture were harvested by centrifugation (13000 x g, 1 min, 4°C) and the pellet was resuspended in 100 µl ice-cold buffer P1. For cell lysis 200 µl buffer P2 were added, gently mixed and incubated at room temperature for 5 min. To neutralize the pH and precipitate genomic DNA and proteins 150 µl ice-cold buffer P3 were added, gently mixed and centrifuged (13000 x g, 10 min, 4°C).

The clear supernatant was transferred to a fresh reaction tube and 600 µl isopropanol were added to precipitate the plasmid DNA. After centrifugation (13000 x g, 5 min, 4°C), the DNA pellet was washed with 600 µl ice-cold 70% ethanol, centrifuged again and the supernatant was completely removed by aspiration. The pellet was dried under red light for 15-30 min, dissolved in 30 µl ddH_2O or TE buffer and stored at -20°C.

If problems occurred during sequencing, PCR or restriction digest, the DNA was further purified using the Plasmid Mini Kit according to the manufacturer´s recommendations.

Buffer P1	50 mM Tris, 10 mM EDTA, pH 8.0, 0.1 mg/ml RNase A
Buffer P2	0.2 M NaOH, 1% (w/v) SDS
Buffer P3	1.8 M KAc/HAc, pH 5.2

2.2.9 Ethanol precipitation of plasmid DNA

Sterile plasmid aliquots for *P. falciparum* transfection were obtained by ethanol precipitation. The plasmid DNA (100 µg) was mixed with 20 µl of 3 M sodium acetate solution at pH 5.0 and filled up to 200 µl with ddH_2O. Ice-cold absolute ethanol (500 µl) was added, the samples were vortexed and incubated for 30 min at -20°C. The precipitated plasmid DNA was pelleted by centrifugation (20800 x g, 30 min, 4°C). The pellet was rinsed with 500 µl 70% ethanol and centrifuged again (20800 x g, 15 min, 4°C). The supernatant was removed, the pellet was air-dried under sterile conditions (laminar flow) and resuspended in 30 µl of sterile TE buffer. The plasmid DNA was stored at -20°C until use.

TE buffer	10 mM Tris/HCl, 1 mM EDTA, pH 7.5

2.2.10 Sequencing

To verify the DNA sequence, plasmids were sent for sequencing to GATC Biotech (Konstanz, Germany). Typically, plasmids from standard minipreps were diluted 1:4 with ddH_2O and 20 µl were sent. If necessary, 20 µl of sequencing or cloning primers were sent in a concentration of 10 pmol/µl. Otherwise, GATC universal primers were selected. Sequencing results were analyzed using the program BioEdit and the online tool JustBio.

2.3 Yeast methods

2.3.1 Yeast culture

Depending on the application *S. cerevisiae* BY4742 cells were cultured on solid or in liquid growth medium. Liquid YPD medium was prepared by dissolving 10 g bacto yeast extract and 20 g peptone in 900 ml ddH_2O. The medium was autoclaved and 100 ml of a sterile filtered 20% glucose solution were added. The medium was stored at 4°C. Liquid HC-Ura medium was prepared according to the scheme indicated below and sterile filtered. For solid HC-Ura agar plates, agar was dissolved in ddH_2O, autoclaved and the remaining components were added. The medium was poured into petri dishes, the plates were left uncovered in the laminar flow cabinet until the agar was solidified, packed in plastic bags and stored at 4°C.
Wild-type cells were inoculated in liquid YPD medium and incubated in a shaking incubator at 30°C until the required cell density was reached. For the expression of roGFP2 fusion constructs, freshly transformed cells (section 2.3.2) were spread on HC-Ura agar plates and incubated at 30°C. After 2-3 days several colonies were picked, inoculated in liquid HC-Ura medium and incubated in a shaking incubator at 30°C until the required cell density was reached.

10x HC 0.6 g/l tyrosine, 0.8 g/l isoleucine, 0.5 g/l phenylalanine, 1 g/l glutamic acid, 2 g/l threonine, 1 g/l aspartic acid, 1.5 g/l valine, 4 g/l serine, 0.2 g/l arginine

10x YNB 14.5 g/l yeast nitrogen base w/o amino acids, 50 g/l ammonium sulfate

HC-Ura medium (Composition for 1 l):

Table 2.14 Composition of HC-Ura medium

	Liquid medium	***Agar plates***
20% glucose	100 ml	100 ml
10x YNB	100 ml	100 ml
10x HC	100 ml	100 ml
1 mg/ml adenine	20 ml	20 ml
10 mg/ml lysine	12 ml	12 ml
2 mg/ml methionine	10 ml	10 ml
10 mg/ml tryptophan	8 ml	8 ml
20 mg/ml leucine	4 ml	4 ml

10 mg/ml histidine	2 ml	2 ml
ddH_2O	644 ml	144 ml
40 g/l agar	-	500 ml

HC, YNB and agar were autoclaved, glucose and amino acids were sterile filtered

2.3.2 Transformation of yeast cells

A colony of *S. cerevisiae* BY4742 wild-type cells was inoculated in 5 ml YPD medium and grown over night until midlogarithmic phase. Aliquots of the cell suspension (500 µl) were centrifuged (10000 x g, 1 min), washed with 1 ml H_2O and centrifuged again. The cell pellets were resuspended in 100 µl One-Step-Transformation buffer and thoroughly vortexed. Salmon sperm carrier DNA (5 µl of 10 mg/ml, freshly denatured at 95°C for 5 min and chilled for at least 1 min on ice) and 1 µl plasmid DNA were added to each transformation mix. The mixtures were vortexed and incubated at 45°C for 30 min in a thermomixer at 650 rpm. Cells were centrifuged (10000 x g, 1 min) and the resulting pellets were resuspended in 100 µl H_2O. The transformed cells were plated on HC-Ura plates and incubated at 30°C for 2-3 days.

One-Step-Transformation buffer 0.2 M lithium acetate, pH 5.0, 40% (w/v) PEG 3350, 100 mM DTT

2.3.3 Protein extraction from yeast cells

Yeast cells from a liquid culture equivalent to 2.5 OD_{600} units were harvested by centrifugation (13000 x g, 1 min) washed once with 500 µl PBS and resuspended in 50 µl ice-cold RIPA buffer complemented with 1 mM PMSF. Chilled glass beads (50 µl) were added and the mixture was vortexed for 30 s followed by 30 s incubation on ice. This step was repeated three times and, subsequently, the cells were centrifuged (13000 x g, 1 min) and the supernatant was transferred to a fresh tube on ice. The samples were mixed with 20 µl Lämmli buffer containing 15% β-mercaptoethanol, boiled for 5 min at 95°C and proteins were separated by SDS-PAGE according to section 2.4.5.

PBS 1.84 mM KH_2PO_4, 10 mM Na_2HPO_4, 137 mM NaCl, 2.7 mM KCl, pH 7.4

RIPA buffer	150 mM NaCl, 1% (v/v) Nonidet P-40, 0.5% (w/v) sodium deoxycholate, 0.1% (w/v) SDS, 50 mM Tris/HCl, pH 7.2
5x Lämmli buffer	50 mM Tris/HCl pH 6.8, 10% (w/v) SDS, 25% (v/v) glycerol, 0.1% (w/v) bromophonol blue

2.4 Biochemistry methods

2.4.1 Expression of recombinant His_6-tagged proteins in *E. coli*

The respective plasmids (pQE30/*PFGR*, pQE30/*PFGRX*$^{C32S/C88S}$, pQE30/*PFAO*P, pQE30/*PFAOP*^{C117S}, pQE30/*PFAOP*^{C143S}, pQE30/*PFAOP*^{L109M}, pQE30/*PFAOP*^{L109A}) were transformed into XL1-blue cells (section 2.2.6) and clones were selected on LB_{Amp} plates over night. Colonies were picked and inoculated under sterile conditions in 100 ml flasks containing 25 ml LB_{Amp} liquid medium and incubated for approximately 14 h at 37°C and 135 rpm. After incubation, the OD_{600nm} was determined and 2 l flasks, containing 1 l LB_{Amp} liquid medium, were inoculated under sterile conditions with the pre-cultures to an initial OD_{600nm} of 0.04. The cultures were incubated at 37°C and 135 rpm. At an OD_{600nm} of 0.5-0.6 protein expression was induced by adding IPTG to a final concentration of 0.5 mM. For the expression of *Pf*GR, cultures were cooled to 16°C and protein expression was induced with 0.3 mM IPTG. After 4 h incubation at 37°C (14 h at 16°C in the case of *Pf*GR) the bacterial cultures were transferred to 1 l centrifugation buckets, incubated in an ice-water bath for 10 min and collected by centrifugation (4000 x g, 15 min, 4°C). The resulting bacterial pellets were rapidly resuspended on ice in 15 ml ice-cold purification buffer, split into suitable aliquots and stored at -20°C until use.

Purification buffer	20 mM imidazole, 50 mM $Na_xH_yPO_4$, 300 mM NaCl, pH 8.0 at 4°C

2.4.2 Extraction and affinity purification of recombinant His_6-tagged proteins

For protein purification the bacterial suspensions (section 2.4.1) were thawed, supplemented with approx. 20 mg lysozyme + DNase I and thoroughly stirred on ice for 1 h. The suspensions were transferred into pre-chilled centrifugation tubes and sonicated on ice (5 x 10 s, cycle 5, 50-60% power, 10 s break between each pulse sequence). Subsequently, the lysates were centrifuged (10000 x g, 30 min, 4°C) and the supernatants were collected in pre-chilled falcon tubes on ice.

For affinity chromatography Poly-Prep chromatography columns were loaded with 1 ml of a 50% nickel-nitriloacetic acid (Ni-NTA) agarose slurry, connected vertically to a peristaltic pump and equilibrated with 15 column volumes of purification buffer. The supernatant of the cleared *E. coli* lysate was loaded onto the column at a flow rate of approx. 1-2 ml/min. The column was subsequently washed with 15 column volumes of purification buffer (flow rate 1-2 ml/min).

For protein elution, one column volume of elution buffer was added at a flow rate of 0.5 ml/min. As soon as the column was completely loaded with elution buffer, the column was disconnected from the pump and the bottom outlet was closed. After 3 min incubation, another 1.5 column volumes of elution buffer were added to the column, the outlet was opened and the protein was collected on ice by gravity-flow in a single 1.5 column volume fraction. The column was washed slowly with two column volumes elution buffer, re-equilibrated with 10 column volumes purification buffer and stored at 4°C.

All buffers were stored at 4°C and kept on ice during the purification procedure.

Purification buffer	20 mM imidazole, 50 mM $Na_xH_yPO_4$, 300 mM NaCl, pH 8.0 at 4°C
Elution buffer	200 mM imidazole, 50 mM $Na_xH_yPO_4$, 300 mM NaCl, pH 8.0 at 4°C

2.4.3 Estimation of the protein concentration

The protein concentration was estimated according to the Bradford method (Bradford, 1976) with slight variations. In this assay the protein concentration is measured spectrophotometrically by adding a particular dye, Coomassie Brilliant Blue G-250 (Bradford

reagent) that changes its absorption maximum upon protein binding directly proportional to the protein concentration from 465 nm to 595 nm.

For the standard curve eight different samples with 0-14 µg BSA (from a 1 mg/ml stock solution), diluted in 800 µl ddH_2O, were prepared. Analogously, a suitable amount (V_p, typically 2-10 µl) of the protein sample was diluted in triplicate in 800 µl ddH_2O each. Then, 200 µl Bradford reagent was added to the cuvettes in a 20 s interval and the samples were mixed thoroughly by pipetting up and down. The samples were incubated for 15 min and, subsequently, the absorbance was measured at 595 nm (Abs_{595}) in the same 20 s interval as the reagent was added. The absorbance of the blank (BSA free cuvette) was subtracted from all measurements and the corrected absorbance values for the standard curve samples were plotted against the corresponding BSA concentration using the SigmaPlot software. The data were fitted to a rectangular hyperbola according to the equation: $y = \frac{a \cdot x}{b+x}$. With this equation the protein concentration of the sample (C_p) could be calculated by taking the molecular weight (MW_p) and the dilution factor into account (see equations below).

$$x(\mu g) = \frac{y \cdot b}{a-y}; \; C_p = \frac{DF \cdot x}{V_p \cdot MW_p}$$

Alternatively the protein concentration was measured directly using the molar extinction coefficient of the protein. For stopped-flow kinetic measurements (section 2.5.2) the molar extinction coefficient of *Pf*AOP wild-type and mutants was calculated according to the amino acid sequence of the protein using ExPASy ProtParam (http://web.expasy.org/protparam) (ε_{280nm} = 21430 $M^{-1}cm^{-1}$). The absorbance of the protein solution at 280 nm (Abs_{280}) was corrected for the absorbance of the blank (buffer without protein) and the dilution factor, and the protein concentration (C_p) was calculated using the following equation: $C_p = \frac{Abs_{280}}{\varepsilon \cdot d}$.

2.4.4 Preparation of polyacrylamide gels for electrophoresis

For the separation of recombinant or native proteins 10-12% polyacrylamide gels were used. Gels for up to ten samples were cast using the Mini-PROTEAN system from BioRad. The glass plates were thoroughly cleaned using detergent and 70% ethanol and assembled according to the manufacturer´s instructions. The resolving gel (approx. 10 ml per gel) and the stacking gel (approx. 2 ml per gel) were prepared as indicated below. The resolving gel was cast between the plates and overlayed with isopropanol. After the gel was completely polymerized the isopropanol was discarded, the stacking gel was cast on top and the 10-well

comp was inserted immediately. After polymerization the gel was directly used or stored at 4°C for up to 3 days.

Resolving gel buffer 1.5 M Tris, pH 8.8

Stacking gel buffer 1 M Tris, pH 6.8

Pipetting scheme:

Table 2.15 Pipetting scheme for resolving and stacking gels

Resolving gel (10 ml)	***10%***	***12%***
ddH_2O	4.0 ml	3.3 ml
30% Acrylamide mix	3.3 ml	4.0 ml
Resolving gel buffer	2.5 ml	2.5 ml
10% SDS	0.1 ml	0.1 ml
10% APS	0.1 ml	0.1 ml
TEMED	0.004 ml	0.004 ml
Stacking gel (2 ml)	***5%***	
ddH_2O	1.4 ml	
30% Acrylamide mix	0.33 ml	
Stacking gel buffer	0.25 ml	
10% SDS	0.02 ml	
10% APS	0.02 ml	
TEMED	0.002 ml	

2.4.5 Separation of proteins by one-dimensional SDS-PAGE

Using sodium dodecyl sulfate polyacrylamide gel electrophoresis (SDS-PAGE) proteins were separated under denaturing conditions with a discontinuous buffer system (Laemmli, 1970). Casted polyacrylamide gels (section 2.4.4) were placed into an electrophoresis tank that was filled with SDS-PAGE running buffer according to the manufacturer´s instructions. Protein samples were mixed with 5x Lämmli buffer (with or without 30% β-mercaptoethanol), heated to 95°C for 10 min, centrifuged (20800 x g, 1 min) to precipitate insoluble materials and loaded (5-20 µl) into the wells of the gel alongside with a protein marker (5 µl). Samples were run at 12 mA per gel until the dye front reached the bottom of the gel (approx. 1.5 h). Gels were subsequently either stained with Coomassie® blue (section 2.4.6) or blotted on nitrocellulose membranes (section 2.4.7).

SDS-PAGE running buffer	25 mM Tris/HCl, 250 mM glycin, 0.1% (w/v) SDS, pH 8.3
5x Lämmli buffer	50 mM Tris/HCl pH 6.8, 10% (w/v) SDS, 25% (v/v) glycerol, 0.1% (w/v) bromophonol blue

2.4.6 In-gel detection of proteins with Coomassie® blue

To visualize all proteins that where separated via SDS-PAGE (section 2.4.5), the gel was stained with the dye Coomassie Brilliant Blue. Following electrophoresis, the stacking gel was removed and discarded. The resolving gel was carefully transferred to a plastic box containing staining solution and incubated for 1 h to over night at room temperature on a rocking platform shaker. Subsequently, the staining solution was removed, the gel was rinsed once with destaining solution and incubated in destaining solution on the rocking platform shaker for at least 30 min until the background of the gel became clear and the blue protein bands were clearly visible. The gel was then transferred into ddH_2O, incubated over night to improve the contrast of the bands and photographed.

Staining solution	25% (v/v) isopropanol, 10% (v/v) acetic acid, 0.05% (w/v) Coomassie Blue G250
Destaining solution	25% (v/v) isopropanol, 10% (v/v) acetic acid

2.4.7 Western blot analysis

For immunodetection of proteins that were separated via SDS-PAGE (section 2.4.5), the proteins were transferred from the gel to a nitrocellulose membrane using the semi-dry electrotransfer system. For each gel, one piece of nitrocellulose membrane and ten sheets of Whatmann paper with the same size as the gel were prepared and incubated in blotting buffer for 5-10 min. On the anode part of the PerfectBlue Semi-Dry Electro Blotter the blot sandwich was assembled in the following order: 5 sheets Whatmann paper – nitrocellulose membrane – resolving gel – 5 sheets Whatmann paper. The proteins were transferred at 100 mA for 1 h. Afterwards, the membrane was rinsed with TBS and further handled as described in section 2.4.8 and 2.4.9.

Blotting buffer	20 mM Tris, 150 mM glycin, 20% (v/v) methanol, 0.02% (w/v) SDS
TBS	10 mM Tris/HCl, 0.9% (w/v) NaCl, pH 7.4

2.4.8 Staining of proteins with Ponceau S

Following proteintransfer (section 2.4.7), proteins were reversibly visualized on the nitrocellulose membrane using the dye Ponceau S. Thus, the transfer efficiency was checked and the amount of protein loaded into the different wells was compared. Furthermore, the localization of the proteins on the membrane was visualized for optional cutting of the membrane. The TBS rinsed membrane was put into a plastic box containing Ponceau S solution and incubated on the rocking platform shaker for 2-5 min. Afterwards, the membrane was rinsed with ddH_2O until the background of the membrane became white and the proteins bands were clearly visible in red. The membrane was scanned and completely destained with TBS.

Ponceau S solution	3% (w/v) Ponceau S, 3% (w/v) trichloroacetic acid

2.4.9 Immunodetection of proteins

Following Ponceau S staining (section 2.4.8), proteins transferred to a nitrocellulose membrane (section 2.4.7) were detected with specific antibodies. The completely destained membrane was incubated in blocking buffer for 1 h at room temperature on a rocking platform shaker to block unspecific binding sites. Subsequently, the membrane was transferred to the primary antibody solution and incubated on the shaker over night at 4°C. The primary antibody was then removed and the membrane was washed with TBST five times for 10 min. Next, the membrane was incubated in horseradish peroxidase-conjugated secondary antibody solution for 1 h at room temperature. Subsequently, the membrane was washed five times with TBST/T for 10 min and once with TBS for 2 min to remove the detergent. The membrane was then placed into a film cassette and 0.5-1 ml freshly mixed detection reagent (Amersham ECL Western Blotting Detection Reagents or SuperSignal West Femto) was distributed on the membrane. The membrane was covered with a plastic foil

and, after the removal of bubbles and excess liquid, immediately exposed to an X-ray film in the darkroom. After a suitable exposure time, typically 1 min to 1 h, the film was developed using the Curix 60 film developer.

TBS	10 mM Tris/HCl, 0.9% (w/v) NaCl, pH 7.4
TBST	TBS, 0.1% (v/v) Tween 20
TBST/T	TBS, 0.1% (v/v) Tween 20, 0.2% (v/v) Triton X-100
Blocking buffer	5% (w/v) non-fat dry milk in TBST
Antibody solutions	antibodies were diluted in blocking buffer as indicated in section 2.1.7

2.5 Kinetic assays

2.5.1 Steady-state enzyme kinetic assays

Kinetic assays with recombinant *Pf*GR, *Pf*Grx$^{C32S/C88S}$ and *Pf*AOP wild-type enzyme and mutants (section 2.4.2) were carried out at 25°C in 1 ml total reaction volume using a thermostatted Jasco V-650 UV-visual spectrophotometer. The assays were performed in assay buffer equilibrated to 25°C. All enzymes were freshly diluted with elution buffer; all other reagents (NADPH, *t*-BOOH, GSH, GSSG, HEDS) were freshly prepared in assay buffer before each experiment. Enzyme activity was monitored by the consumption of NADPH at 340nm (ε_{340} = 6.22 $mM^{-1}cm^{-1}$) using the Spectra Analysis program (Spectra Manager, Jasco). For each assay a baseline representing background reactions was recorded and subtracted from the initial slope (typically the first 5 s) of the curve after the initiation of the assay yielding ΔAbs_{340}/min. According to Lambert-Beer´s law ($Abs = \varepsilon \cdot d \cdot C$) the concentration of NADPH consumed during the assay (ΔNADPH/min) was calculated. This value reflects the reaction velocity, which was plotted against the substrate concentration. The data were fitted according to Michaelis-Menten theory and using the linearization methods according to Lineweaver-Burk, Eadie-Hofstee and Hanes with the software SigmaPlot 13.

Assay buffer	0.1 M Tris/HCl, 1 mM EDTA, pH 8.0
Elution buffer	200 mM imidazole, 50 mM $Na_xH_yPO_4$, 300 mM NaCl, pH 8.0 at 4°C

2.5.1.1 Glutathione reductase assay

The volume activity of *Pf*GR was determined as described previously (Worthington and Rosemeyer, 1976) with slight modifications. The *Pf*GR eluate was diluted 1:50 with elution buffer. *Pf*GR, NADPH and assay buffer were mixed in a quartz cuvette and a baseline was recoded for 30 s. The assay was started by the addition of GSSG.

Reaction scheme of the *Pf*GR assay: $GSSG+NADPH+H^+ \rightarrow 2GSH+NADP^+$

The *Pf*GR activity was calculated in Units per milliliter (U/ml), whereby one Unit corresponds to the oxidation of 1 µmol substrate per minute.

$$Pf\text{GR activity } (\text{U/ml}) = \frac{V_T \cdot DF}{V_A} \cdot \frac{\Delta NADPH}{min};$$

V_T: total assay volume, DF: dilution factor, V_A: volume *Pf*GR used in the assay, ΔNADPH/min: concentration NADPH consumed in the assay ($\mu mol \cdot ml^{-1} min^{-1}$)

Composition *Pf*GR assay:

Table 2.16 Composition *Pf*GR assay

Reagent	*Stock solution*	*Final concentration*
NADPH	4 mM	100 µM
GSSG	20 mM	1 mM
*Pf*GR	The eluate was diluted 1:50 with elution buffer	n.d. (5 µl of the dilution)

2.5.1.2 2-Hydroxyethyl disulfide (HEDS) assay

The activity *Pf*Grx$^{C32S/C88S}$ was monitored with the HEDS assay as previously described (Nagai and Black, 1968, Begas et al., 2015). In this assay the protein reduces a mixed disulfide (GSSEtOH), which is formed by a non-enzymatic reaction between GSH and HEDS. NADPH, HEDS, GSH and assay buffer were mixed in a quartz cuvette and incubated for 2 min to allow the formation of the mixed disulfide GSSEtOH. *Pf*GR was added and a baseline was recoded for 30 s. The assay was started by the addition of *Pf*Grx$^{C32S/C88S}$.

Composition HEDS assay:

Table 2.17 Composition HEDS assay

Reagent	*Stock solution*	*Final concentration*
NADPH	4 mM	100 µM
HEDS	29.4 mM	740 µM
GSH	40 mM	1 mM
*Pf*GR	200 U/ml	1 U/ml
*Pf*Grx$^{C32S/C88S}$	2.5 µM	12.5 nM

2.5.1.3 *Pf*AOP peroxidase activity assay

The activity of *Pf*AOP wild-type enzyme and mutants was determined in a coupled spectrophotometric assay as described previously (Djuika et al., 2013, Staudacher et al., 2015). Briefly, NADPH, GSH and *Pf*GR were mixed in assay buffer and incubated for 30 s. Afterwards, *Pf*Grx$^{C32S/C88S}$ was added and a baseline was recorded for another 30 s. Then, the assay was started by the simultaneous addition of *t*-BOOH and *Pf*AOP. The kinetic parameters k_{cat} and K_m of *Pf*AOP were determined at fixed concentrations of *Pf*AOP (1.5 µM for wild-type enzyme, 3 µM for L109A mutant and 1 µM of L109M mutant) and *t*-BOOH (75 µM) and varying concentrations of the substrates of the reductive half-reaction *Pf*Grx$^{C32S/C88S}$ (0.1-1 µM) and GSH (0.01-2 mM).

Composition peroxidase assay:

Table 2.18 Composition peroxidase assay

Reagent	***Stock solution***	***Final concentration***	
		Substrate *Pf*Grx$^{C32S/C88S}$	**Substrate GSH**
NADPH	6 mM	150 µM	150 µM
GSH	40 or 0.4 mM	1 mM	variable
*Pf*GR	200 U/ml	1 U/ml	1 U/ml
*Pf*Grx$^{C32S/C88S}$	200 or 20 µM	variable	2 µM
t-BOOH	3 mM	75 µM	75 µM
*Pf*AOP$^{wt\ or\ mutants}$	100 µM	1.5, 3.0 or 1 µM	1.5, 3.0 or 1 µM

2.5.1.4 *Pf*AOP inactivation assay

The inactivation of *Pf*AOP wild-type enzyme and mutants was determined analogously to the peroxidase assay. The peroxide substrate used was H_2O_2 instead of *t*-BOOH. To exclude background reactions caused by direct reactions of H_2O_2 with the assay components, the activity of a reference cuvette containing all assay components except *Pf*AOP was subtracted. The assay was performed at fixed concentrations of *Pf*AOP (1.5 µM for wild-type enzyme, 3 µM for L109A mutant and 1 µM of L109M mutant), *Pf*Grx$^{C32S/C88S}$ (2 µM) and GSH (2 mM) and varying concentrations of H_2O_2 (5-100 µM).

Composition inactivation assay:

Table 2.19 Composition *Pf*AOP inactivation assay

Reagent	*Stock solution*	*Final concentration*
NADPH	6 mM	150 µM
GSH	80 mM	2 mM
*Pf*GR	200 U/ml	1 U/ml
*Pf*Grx$^{C32S/C88S}$	100 µM	2 µM
H_2O_2	2 mM	variable
*Pf*AOP$^{wt/L109A/L109M}$	100 µM	1.5, 3.0 or 1 µM

2.5.2 Stopped-flow kinetic assay

The oxidative half-reaction of reduced recombinant *Pf*AOP wild-type enzyme and mutants with different peroxides was analyzed at 25°C in assay buffer using a SX-20 stopped-flow spectrofluorometer. Protein eluates (section 2.4.2) were treated with 5 mM DTT for 30 min at 4°C to obtain the fully reduced protein. Remaining imidazole and DTT were removed by gel filtration using HiTrap desalting columns equilibrated with assay buffer and protein elution was monitored at 280 nm using an Äkta FPLC system. The protein concentration was subsequently determined spectrophotometrically using the molar extinction coefficient ε_{280nm} = 21.43 $mM^{-1}cm^{-1}$ as calculated for the primary sequence of the protein using the ProtParam ExPASy tool.

The concentration of H_2O_2 stock solutions was determined spectrophotometrically at 240 nm using the molar extinction coefficient ε_{240nm} = 43.6 $M^{-1}cm^{-1}$.

The concentrations of cumene hydroperoxide and the fatty acid hydroperoxide (12(S)HpETE) were calculated considering the manufacturer´s specifications.

Peroxynitrite was synthesized from H_2O_2 and nitrous acid by Madia Trujillo and coworkers* as described previously. Manganese dioxide was added to the stock solutions of peroxynitrite to eliminate H_2O_2 remaining from the synthesis. The concentration of peroxynitrite stock solutions was determined spectrophotometrically at 302 nm using the molar extinction coefficient ε_{302nm} = 1670 $M^{-1}cm^{-1}$ (Beckman et al., 1990, Radi et al., 1991). The peroxynitrite solution was prepared in NaOH pH ≈10 and the enzyme in assay buffer pH ≈7, which after mixing of the reactants in the stopped-flow spectrofluorometer revealed a final reaction pH of 7.4.

Assay buffer 100 mM $Na_xH_yPO_4$, 0.1 mM DTPA, pH 7.4

* Departamento de Bioquímica, Facultad de Medicina, and Center for Free Radical and Biomedical Research, Universidad de la República, Montevideo, Uruguay

2.5.2.1 Direct assay

*Pf*AOP wild-type enzyme or mutants (1 µM) were mixed with H_2O_2 (1-100 µM), peroxynitrite (1-20 µM), cumene hydroperoxide (1-20 µM) or the fatty acid hydroperoxide 12(S)-hydroperoxy-(5Z,8Z,10E,14Z)-eicosatetraenoic acid (12(S)HpETE) (1-13 µM) and the changes of the total intrinsic tryptophan fluorescence emission were followed at an excitation wavelength of λ_{ex} = 295 nm. *Pf*AOP^{C117S} showed no change in fluorescence and served as a negative control. Experimental curves of *Pf*AOP wild-type, C143S mutant and L109M mutant enzymes showed two main phases of fluorescence intensity change, which were fitted to exponential curves using the Applied Photophysics Pro-data SX software. The first phase was recorded from 2 ms (mixing time of the apparatus) to 20-100 ms depending on the peroxide concentration and showed a rapid decrease in fluorescence. The second phase was followed from 0.1-10 s and showed a slower increase in fluorescence. After 10 s, there was a further small increase in fluorescence particularly at the higher peroxide concentrations that was disregarded in the fitting. The values for k_{obs} were obtained by analyzing the average of several (5-6) runs. Rate constants were calculated by plotting the obtained k_{obs} values against the according peroxide concentrations, which were fitted to linear plots (Trujillo et al., 2007, Hugo et al., 2009, Parsonage et al., 2015). Rate constants k_1 and k_2 were obtained from the slopes of the plots for the first respectively the second phase of fluorescence change. Rate constant k_3 was obtained from the offset (y-axis intercept) of the second plot.

2.5.2.2 HRP-competition assay

Rate constants for the oxidation of the enzyme by hydrogen peroxide or peroxynitrite (k_1*) were determined in a competition assay using horseradish peroxidase (HRP) as an alternative peroxide target as described previously (Ogusucu et al., 2007, Trujillo et al., 2008). In this assay the oxidation of 2 or 5 µM HRP by 1 µM peroxide to 'compound I' was followed at 398 nm in the absence or presence of increasing *Pf*AOP concentrations.

The rate constants for the reaction of HRP with H_2O_2 or peroxynitrite were determined as follows: Increasing concentrations of HRP (5-15 µM) were mixed with H_2O_2 or peroxynitrite (0.8 µM) and the changes in absorbance were followed at 398 nm. By fitting these changes to exponential curves using the Applied Photophysics Pro-data SX software, k_{obs} values were determined and plotted against the according HRP concentration. Rate constants (k_{HRP}) were obtained from the slopes of these plots and revealed 1.4×10^7 $M^{-1}s^{-1}$ for H_2O_2 and 3.5×10^6 $M^{-1}s^{-1}$ for peroxynitrite.

To determine the rate constant for the reaction of *Pf*AOP with the peroxide (k_{AOP}) the following formula was used:

$$\frac{k_{HRP}}{k_{AOP}} = \frac{ln\frac{HRP_i}{HRP_i - CI}}{ln\frac{AOP_i}{AOP_i - AOP_{ox}}}$$

The final amounts of 'compound I' (CI) were calculated using its molar absorption coefficient (ε_{398nm} = 42000 $M^{-1}cm^{-1}$). The amount of oxidized *Pf*AOP (AOP_{ox}) was calculated by subtracting the calculated concentration of 'compound I' from the initial hydrogen peroxide concentration (1µM).

2.5.3 roGFP2-*Pf*AOP response assay

Redox sensitive GFP2 (roGFP2) has two cysteine residues and can adopt different redox states (reduced dithiol or the oxidized disulfide). The fluorescence emission of the different redox states at 510 nm can be measured for different excitation wavelengths, 405 nm (oxidized disulfide) and 476.5 nm (reduced dithiol), which reflect the degree of oxidation of the roGFP2 sensor.

The response of roGFP2-*Pf*AOP fusion constructs to H_2O_2 or *t*-BOOH in yeast cells was analyzed as previously described (Morgan et al., 2011, Morgan et al., 2016). Plasmids p416TEF, p416TEF/*roGFP2* and p416TEF/*roGFP2-PFAOP* wild-type and mutants were transformed into yeast strain BY4742 (section 2.3.2), several colonies of the strains were inoculated in 10 ml HC medium lacking uracil and incubated for 24 h at 30°C. Subsequently, the cultures were diluted 1:200 - 1:400 and incubated for approximately 16-18 h until they reached the late exponential phase (OD_{600} = 3-4). Then, the cells were harvested by centrifugation (800 x g, 3 min) and resuspended in measurement buffer to a final concentration of 7.5 OD_{600} units/ml. The cell suspension was distributed in a flat-bottom 96

well microplate (black, transparent bottom). For each construct a whole row (12 wells, 200 µl cell suspension per well) was used for the experimental treatment plus two additional wells for the controls. Another three wells were supplemented with 200 µl cells transformed with p416TEF (empty) for the blanks. The plates were centrifuged (30 x g, 5 min), diamide was added to one of the control wells of each construct to a final concentration of 20 mM (fully oxidized control) and DTT was added to the second control well of each construct to a final concentration of 100 mM (fully reduced control). The control wells served for the determination of the degree of oxidation (OxD). The plates were inserted into a CLARIOstar plate reader and measured for 5 cycles. Subsequently, the cells in the experimental wells were treated with twelve increasing concentrations of H_2O_2 or *t*-BOOH (10-500 µM) without disturbing the cell layer at the bottom of the wells and fluorescence emissions were followed for 100 min at 30°C (λ_{ex} = 405 and 476.5 nm, λ_{em} = 510 nm).

The emissions of the blank wells were subtracted from all sample and control wells and the corrected values were exported into Excel using the MARS data analysis software. The OxD for each time point was calculated according to the following equation using the fluorescence emission intensities of the sample (I405 and I476.5) and the controls ($I405_{ox}$ and $I476.5_{ox}$, $I405_{red}$ and $I476.5_{red}$) after excitation at both 405 and 476.5 nm:

$$OxD_{roGFP2} = \frac{I405 \cdot I476.5_{red} - I405_{red} \cdot I476.5}{I405 \cdot I476.5_{red} - I405 \cdot I476.5_{ox} + I405_{ox} \cdot I476.5 - I405_{red} \cdot I476.5}$$

For each peroxide concentration the OxD was plotted against the time. The area under the curve (AUC (OxD x min)) was subsequently calculated in Excel for a measurement time of 1 h and plotted against the according peroxide concentration in SigmaPlot 13. All data were averaged from triplicate (*t*-BOOH treatment) or quadruplicate (H_2O_2 treatment) measurements from independent yeast cultures. Statistical analyses were carried out in SigmaPlot 13 using the One-way ANOVA method.

Measurement buffer 100 mM NaCl, 100 mM sorbitol, 100 mM Tris/HCl, pH 7.4

2.6 Cell culture and genetic manipulation of *P. falciparum*

P. falciparum asexual blood stage parasites were cultivated and manipulated under sterile conditions in a laminar flow hood. All media and solutions were sterilized by autoclaving or filtration with 0.2 µm filters before use and stored at 4°C or -20°C. All disposables and other materials were disinfected with 70% ethanol before use.

2.6.1 Cryopreservation of *P. falciparum* blood stage parasites

Usually, *P. falciparum* infected erythrocytes (iRBCs) with predominantly 3-5% ring stage parasites (section 2.6.4) were cryopreserved. The iRBCs were resuspended in culture medium and transferred to a 15 ml falcon tube. After centrifugation (300 x g, 5 min), the pellet was mixed with the same volume of pre-warmed freezing solution, which was slowly added dropwise. The cells were subsequently transferred to cryovials and frozen as quick as possible in liquid nitrogen.

Freezing solution 28% (v/v) glycerol, 0.65% (w/v) NaCl, 3% (w/v) sorbitol

2.6.2 Thawing of *P. falciparum* blood stage parasites

All thawing solutions and cell culture medium were pre-warmed to 37°C. A cryovial with frozen iRBCs was removed from the liquid nitrogen and thawed at 37°C in a water bath. The content was transferred to a 15 ml falcon tube and 0.2 volumes (related to the cryovial content) of thawing solution I were added dropwise and slowly to the cells. After incubation for 2 min, 10 volumes of thawing solution II were added dropwise and slowly to the cell suspension. The cells were centrifuged (300 x g, 5 min), the cell pellet was resuspended stepwise in 10 volumes of thawing solution III and centrifuged again. The cell pellet was washed with 10 ml culture medium (300 x g, 5 min), mixed with the same amount of fresh A^+ human erythrocytes and transferred to a culture dish containing 13 ml culture medium. Parasites were incubated in an atmosphere of 3% CO_2, 5% O_2, 92% N_2 and 95% humidity at 37°C.

Thawing solution I 12% (w/v) NaCl

Thawing solution II 1.6% (w/v) NaCl

Thawing solution III	0.9% (w/v) NaCl, 0.2% (w/v) glucose
Complete medium	RPMI 1640 (25 mM HEPES, L-Glutamine), 4,5% albumax II, 200 µM hypoxanthine, 2.7 µg/ml

2.6.3 Maintenance of a continuous *P. falciparum* blood stage culture

All *P. falciparum* parasite strains used were grown according to the method of Trager and Jensen (Trager and Jensen, 1976) with slight modifications. Culture conditions consisted of an atmosphere of 3% CO_2, 5% O_2, 92% N_2 and 95% humidity at 37°C. Parasites were grown in cell culture flasks or petri dishes containing 0.5 or 1.25 ml packed A^+ human RBCs suspended in 14 or 35 ml cell culture medium respectively. The parasitemia (percentage of iRBCs in relation to the total number of RBCs) was kept between 0.5 and 10%. The culture medium was replaced every one to three days depending on the parasitemia. The parasite culture was split when the parasitemia exceeded 5-10% in order to maintain parasite viability and to avoid toxification of the medium by parasitic metabolites. For genetically manipulated parasites the medium was supplemented with 5 nM WR99210 or in case of the pUF1-Cas9 transfected 3D7 strain 100 nM atovaquone.

Complete medium	RPMI 1640 (25 mM HEPES, L-Glutamine), 4,5% albumax II, 200 µM hypoxanthine, 2.7 µg/ml gentamicin

2.6.4 Giemsa staining, estimation of the parasitemia and parasite viability

In order to assess parasitemia, parasite stages, viability and morphology of a parasite culture, Giemsa-stained blood smears were prepared and evaluated using a light microscope (100 x magnification, oil-immersion). A drop of the iRBC layer at the bottom of the culture dish or flask was transferred to a microscope slide, smeared using a second slide and air-dried. The slide was fixed in 100% methanol for 30 s, transferred to a freshly prepared 10% (v/v) Giemsa solution and stained for 15-30 min. The slide was rinsed thoroughly with deionized water and air-dried. A suitable amount of cells was counted and the parasitemia was calculated as follows:

$$\text{Parasitemia } (\%) = \frac{\text{iRBCs}}{\text{total number of RBCs}} \cdot 100$$

2.6.5 Synchronization of *P. falciparum* culture

To obtain a culture with tightly synchronic parasites, the culture was treated with D-sorbitol as previously described (Lambros and Vanderberg, 1979) with slight variations. By treating the iRBCs with D-sorbitol, parasites in the trophozoite and schizont stage are lysed meanwhile ring stage parasites remain intact.

The parasite culture to be synchronized was transferred to a 15 ml falcon tube, centrifuged (300 x g, 5 min) and the cell pellet was resuspendend in 10 volumes of pre-warmed 5% sorbitol solution. The suspension was mixed thoroughly and incubated for 5 min at room temperature. After centrifugation (300 x g, 5 min), the cells were washed with 10 ml culture medium, transferred to a new petri dish containing the appropriate amount of cell culture medium and returned to the incubator.

Sorbitol solution 5% (w/v) sorbitol in ddH_2O

2.6.6 Saponin lysis of *P. falciparum* iRBCs

In order to isolate *P. falciparum* parasites, the erythrocytes were removed by saponin lysis (Benting et al., 1994). Usually, synchronized cultures (14 ml or 35 ml) with mostly trophozoites were used. If 35 ml cultures were used, 20 ml of the culture medium were discarded, cells were resuspended and transferred to two 15 ml falcon tubes and centrifuged (755 x g, 5 min). If 14 ml cultures were used, cells were resuspended and transferred to a 15 ml falcon tube and centrifuged (755 x g, 5 min). For challenging experiments parasites were pulsed with 50-300 µM *t*-BOOH for 1-30 min prior to centrifugation. Optionally, the pellets were resuspended in 3 ml PBS containing 100 mM NEM, incubated for 5 min at room temperature in order to block free thiols and centrifuged again (755 x g, 5 min). The pellets were resuspended in 9 ml ice cold PBS (with or without 10 mM NEM) and 1 ml 0.5% saponin in PBS was added. Cell lysis was performed for 1 min on ice. Subsequently, samples were centrifuged (1800 x g, 10 min, 4°C), washed once with 10 ml PBS (with or without 10 mM NEM) and once with 1 ml PBS/1xPI. The cells were taken up in 5xLämmli buffer (with of without 10 mM NEM) to a concentration of 10^7 parasites/20 µl. Samples were boiled for 10 min at 95°C and further analyzed via SDS-PAGE and western blotting (section 2.4.5 and 2.4.7).

PBS	1.84 mM KH_2PO_4, 10 mM Na_2HPO_4, 137 mM NaCl, 2.7 mM KCl, pH 7.4
Saponin lysis buffer	PBS, 0.5% saponin
5x Lämmli buffer	50 mM Tris/HCl pH 6.8, 10% (w/v) SDS, 25% (v/v) glycerol, 0.1% (w/v) bromophonol blue

2.6.7 Isolation of *P. falciparum* genomic DNA

The isolation of *P. falciparum* total genomic DNA (gDNA) was conducted as described previously (Beck, 2002) with slight modifications. A synchronized (section 2.6.5) 14 ml standard culture with late schizont or early ring-stage parasites was resuspended, transferred to a 15 ml falcon tube and centrifuged (755 x g, 5 min). The supernatant was completely discarded, the cell pellet was resuspended in 10 ml ice-cold saponin lysis buffer and incubated for 10 min on ice. The lysed erythrocytes were removed by centrifugation (3345 x g, 15 min) and the parasites were resuspended in 1.5 ml modified Ringer solution. The suspension was transferred to a 1.5 ml reaction tube, centrifuged (4000 x g, 15 min) and washed again with 1.5 ml modified Ringer solution. Subsequently, the parasites were resuspended in 190 µL TE buffer, 2 µl Proteinase K solution was added to a final concentration of 20 µg/ml and 5 µl 20% SDS solution was added to a final concentration of 0.5% SDS. The tube was gently inverted and incubated over night on a heating block at 55°C to completely liberate the DNA and to inactivate and digest all parasite proteins. The next day, the digest was cooled to room temperature, 3 µl of DNAse-free RNase solution was added and the mixture was incubated for 1 h at 37°C. Afterwards, the sample was again cooled to room temperature, 400 µl of phenol/chloroform/isoamylalcohol were added and the tube was slowly rotated for 10 min in a multi-function rotator. The tube was centrifuged (14000 x g, 10 min), the upper (aqueous) layer was transferred to a new tube using a cut pipette tip and 400 µl phenol/chloroform/isoamylalcohol were added. The tube was slowly rotated for 10 min and centrifuged again, the upper (aqueous) layer was transferred to a new tube and 200 µl of chloroform were added. The tube was slowly rotated for 5 min and centrifuged. The upper (aqueous) layer was transferred without contamination to a new tube, 1/10 volume of ice-cold NaAc buffer and 2.5 volumes of ice-cold absolute ethanol were added. The tube was gently inverted several times and centrifuged (14000 x g, 10 min, 4°C). The DNA pellet was washed with 1 ml ice-cold 70 % ethanol, centrifuged and dried under red

light. The DNA was taken up in 50 µl 10 mM Tris buffer and incubated over night at 65°C in order to completely dissolve the pellet. The next day, the DNA was analyzed on a 0.5% agarose gel to see a broad band at approximately 20 kbp corresponding to genomic DNA.

Modified Ringer solution	115 mM NaCl, 10 mM KCl, 1.2 mM $CaCl_2$, 0.8 mM $MgCl_2$, 5.5 mM glucose, 1.0 mM NaH_2PO_4, 10 mM HEPES, pH 7.1
Saponin lysis buffer	modified Ringer solution, 0.05% (w/v) saponin
TE buffer	10 mM Tris/HCl, 1 mM EDTA, pH 7.6 at 25
Proteinase K solution	2 mg/ml proteinase K
RNase A solution	4 mg/ml DNase-free RNase A
NaAc buffer	3 M NaAc/HAc, pH 4.7
SDS solution	20% (w/v) SDS

2.6.8 Transfection of *P. falciparum*

Transfection of plasmid DNA into *P. falciparum* parasites was achieved by spontaneous uptake of DNA from pre-loaded non-infected RBCs as described previously (Deitsch et al., 2001). A culture was synchronized (section 2.6.5) 1.5 days prior to transfection to obtain a synchronous schizont culture. Before transfection, the parasitemia was estimated and the culture was diluted to 1% schizonts. A petri dish with 100 µl iRBCs and 8 ml culture medium was prepared and stored in the incubator. Non-infected RBCs (2 ml) were mixed with 6 ml cold incomplete cytomix and centrifuged (800 x g, 2 min). The RBCs were washed again with another 6 ml of cold incomplete cytomix and 400 µl of the RBC pellet were mixed with 400 µl cytomix containing 100 µg of plasmid DNA. The mixture was transferred 400 µl each to two pre-chilled electroporation cuvettes and incubated on ice for 5 min. The cells were subsequently electroporated at 0.3 kV voltage and 950 µF capacitance. The time constant usually ranged between 12 and 18 ms. The cuvettes were immediately transferred on ice for 5 min and, subsequently, the electroporated cells from both cuvettes were transferred to a 15 ml tube by rinsing the cuvettes with 4 ml culture medium. The cells were centrifuged (800 x g, 2 min), resuspended in 5 ml culture medium and added to the previously prepared schizont culture. On the following day (Day 1), the parasitemia was checked (expected were 1-2% rings) and the medium was changed. The electroporation was repeated after 48 h (Day

2) to increase the chance of the parasites to invade loaded RBCs. From the day after the second transfection (Day 3) a suitable selection marker was added (5 nM WR99210 for 3D7Δ*pfaop* or 100 nM atovaquone for 3D7pUF1-Cas9). In the first week the medium was renewed every day and afterwards three times a week. Once a week 50-100 µl fresh RBCs were added. Transfectants usually appeared 3-8 weeks post transfection.

Transgenic 3D7pUF1-Cas9 parasites were obtained by transfection of pUF1/Cas9 into 3D7 wild-type cells. Transgenic 3D7Δ*pfaop* parasites were obtained by transfection of pL7/*PFAOP* into transgenic 3D7pUF1-Cas9 cells.

Cytomix (incomplete) 120 mM KCl, 0.15 mM $CaCl_2$, 2 mM EGTA, 5 mM $MgCl_2$, 10 mM K_2HPO4, 10 mM KH_2PO4, 25 mM HEPES, pH 7.6

2.6.9 Limiting dilution assay

Clonal 3D7Δ*pfaop* parasites were obtained by limiting dilution. As soon as transgenic parasites came up after transfection (section 2.6.8), cells were synchronized (section 2.6.5) and the parasitemia was estimated on the following day. The concentration of parasites per milliliter resuspended culture was determined by counting the concentration of erythrocytes with a hemocytometer. The culture was diluted to a concentration of 2 parasites per ml, the hematocrit was adjusted to 2% and 5 nM WR99210 were added. The cells were inoculated in two rows of a 48 well plate (500 µl per well). In the two remaining rows the cells were further diluted 1:10 and 1:100 to increase the chance to get a clonal line. The medium was renewed three times a week and once a week 10 µl fresh RBCs were added to each well. After approximately two weeks, clonal parasites came up and were transferred to 14 ml cultures.

2.6.10 Growth curve determination

Growth curves were determined in triplicate for asynchronous parasites. The cultures were diluted to a parasitemia of 0.1%, the medium was renewed daily and from day four twice a day. Every day the parasitemia was estimated by counting at least 1000 erythrocytes per Giemsa-stained blood smear (section 2.6.4).

2.6.11 *In vitro* drug susceptibility assays

2.6.11.1 IC_{50} determination

The sensitivity of 3D7 wild-type and 3D7Δ*pfaop* parasites towards artemisinin, H_2O_2, *t*-BOOH and diamide was assessed using a SYBR Green I based fluorescence assay. The cyanine dye SYBR Green I binds to nucleic acids and specifically to double-stranded DNA. Hence, the parasite drug susceptibility is assessed indirectly by quantifying the amount of DNA in iRBCs that correlates with the parasite growth (Smilkstein et al., 2004, Wezena et al., 2017). The parasite cultures were synchronized (section 2.6.5) and returned to the incubator for at least 2 h to allow the cells to recover. The parasitemia was determined (section 2.6.4), the culture was centrifuged (300 x g) and 0.3 ml of packed synchronized cells were resuspended in 10 ml cell culture medium containing 2x AlbuMax. The parasitemia and the hematocrit were adjusted to 0.5% and 3%, respectively. The culture plate for the assay was prepared by dispensing 50 µl of culture medium without AlbuMax in a dark flat-bottomed 96-wells plate. The drug stock solution, prepared in culture medium without AlbuMax, was added to the first row of the plate (25 µl per well) and mixed thoroughly by pipetting up and down. Afterwards, 25 µl of this mixture from the first row was added to the following row. This step was repeated until the last row was reached. Thus, from the bottom to the top row, the plate contained a serial dilution of the drug. Subsequently, 50 µl of the parasitized suspension prepared as described above was distributed in each well, yielding a final volume of 100 µl, 0.5% starting parasitemia and 1.5% hematocrit per well. Two sets of negative controls were included in each assay: 6 drug free wells containing iRBCs (last row) and 36 drug free wells containing uninfected RBCs (outer wells). The plates were incubated at 37°C for 72 h and, subsequently, stored at -80°C. Prior to the analysis, the plates were thawed at room temperature for at least 30 min, covered with aluminium foil to avoid light exposure and 100 µl of complete IC_{50} lysis buffer were added to each well and mixed thoroughly. The plates were incubated in the dark for 1 h at room temperature and parasite growth was measured by determining the fluorescence intensity using a microplate reader at a gain set of 60 with 485 nm excitation and 535 nm emission wavelength. IC_{50} values were calculated by fitting the data to a sigmoidal dose-response curve using the four parameter Hill function of the SigmaPlot software to yield the drug concentration that inhibits the growth of 50% of the parasites relative to the drug free control wells.

IC_{50} lysis buffer	20 mM Tris/HCl, pH 7.5, 5 mM EDTA, 0.08% (v/v) Triton X-100, 0.008% (w/v) saponin in PBS 0,12 µl/ml SYBR Green I freshly added prior to use

Tested drugs

Table 2.20 Tested drugs in IC_{50} determination

Drug	*Stock solution*	*Final concentration*
Artemisinin	1.8 µM	300 nM – 0.046 nM
H_2O_2	60 mM	10 mM – 2 µM
t-BOOH	60 mM	10 mM – 2 µM
Diamide	60 mM	10 mM – 2 µM

2.6.11.2 Ring-stage survival assay (RSA)

To address the resistance of *P. falciparum* parasites to artemisinin, a ring-stage survival assay (RSA) was conducted. With this assay resistances can be discovered that are overlooked in classical IC_{50} determinations due to short artemisinin half-lives or drug induced parasite dormancy by treating the early ring-stages (0-3 h post invasion) with the drug (Tucker et al., 2012, Witkowski et al., 2013a, Witkowski et al., 2013b, Kite et al., 2016). The parasite culture was synchronized very tightly using three or more times sorbitol synchronization (section 2.6.5) with a time difference of 40 h. The culture containing only ring-stages 0-3 h post invasion was adjusted to 0.5-1% parasitemia and 2% hematocrit and distributed in a 6 well plate (2 ml per well). The initial parasitemia (INI) was determined with a Giemsa-stained blood smear (section 2.6.4) and parasites were treated with 700 nM artemisinin (ART) or DMSO as a control (NE) for exactly 6 h at 37°C in the incubator. Following treatment, the cultures from all wells were transferred to 15 ml falcon tubes, centrifuged (300 x g, 5 min) and resuspended in 5 ml cell culture medium to wash of the drug. This procedure was repeated four times. After the final wash, the cell pellets were taken up in 2 ml culture medium, dispensed in fresh wells and incubated for another 66 h (72 h total) at 37°C in the incubator. Giemsa-stained smears of all wells were prepared and at least 3000 cells per smear were counted to assess the final parasitemia. For each sample four independent measurements were conducted. The percentage survival (%RSA) was calculated according to the following formula: $\%\mathrm{RSA} = \frac{ART}{NE} \cdot 100$.

3 Results

3.1 Kinetic characterization of *Pf*AOP *in vitro*

Kinetic characterization of *Pf*AOP wild-type enzyme and mutants was based on the previous work of Carine F. Djuika, Joshua Koduka and Sarah Schlossarek (Djuika et al., 2013, Staudacher et al., 2015) (see also section 1.10).

3.1.1 Steady-state kinetics

3.1.1.1 Kinetic parameters of *Pf*AOP are influenced by residue Leu109

Based on the identification of *Pf*AOP^{L109M} as a gain-of-function mutant towards the oxidizing substrate *t*-BOOH (Djuika et al., 2013, Staudacher et al., 2015), I aimed to further investigate the role of the potential gatekeeper residue Leu109. Therefore, I analyzed the kinetic parameters of wild-type *Pf*AOP as well as the gain- and loss-of function mutants *Pf*AOP^{L109M} and *Pf*AOP^{L109A}, respectively, for the reducing substrates GSH and *Pf*Grx$^{C32S/C88S}$.

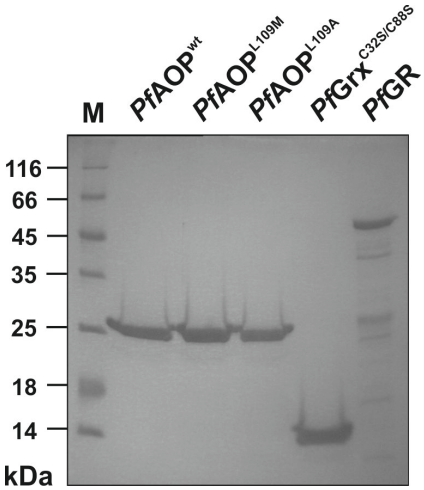

Figure 3.1 Affinity purification of *Pf*AOP.
Confirmation of the purity of the eluate fractions of recombinant *Pf*AOP wild-type enzyme and mutants, *Pf*Grx$^{C32S/C88S}$ and *Pf*GR by reducing SDS-PAGE. The gel was stained with Coomassie. M: Molecular weight marker.

The *Pf*Grx double mutant was previously shown to be functional in the assay and was chosen instead of wild-type enzyme in order to exclude Grx-dependent side reactions (Djuika et al., 2013). All recombinant proteins were expressed in *E. coli* and affinity-purified using Ni-NTA agarose (Figure 3.1).

The activities of *Pf*AOP^{L109M} (gain-of function mutant), *Pf*AOP^{L109A} (loss-of function mutant) and wild-type enzyme at variable GSH concentrations showed biphasic kinetics in the Michalis-Menten plots and the Hanes plots (Figure 3.2a,b) in accordance with previous observations (Djuika et al., 2013). In terms of the kinetic parameters, *Pf*AOP^{L109M} showed about 20- and 10-fold lower K_{m1}^{app} (low substrate concentrations) and K_{m2}^{app} (high substrate concentrations) values compared to the wild-type enzyme (Figure 3.2c, Table 3.1). Thus, the apparent affinity of the oxidized enzyme towards GSH is drastically improved if Leu109 is mutated to methionine. The constants k_{cat1}^{app} (low substrate concentrations) and k_{cat2}^{app} (high substrate concentrations) were only 40% and 20% increased compared to wild-type enzyme (Staudacher et al., 2015).

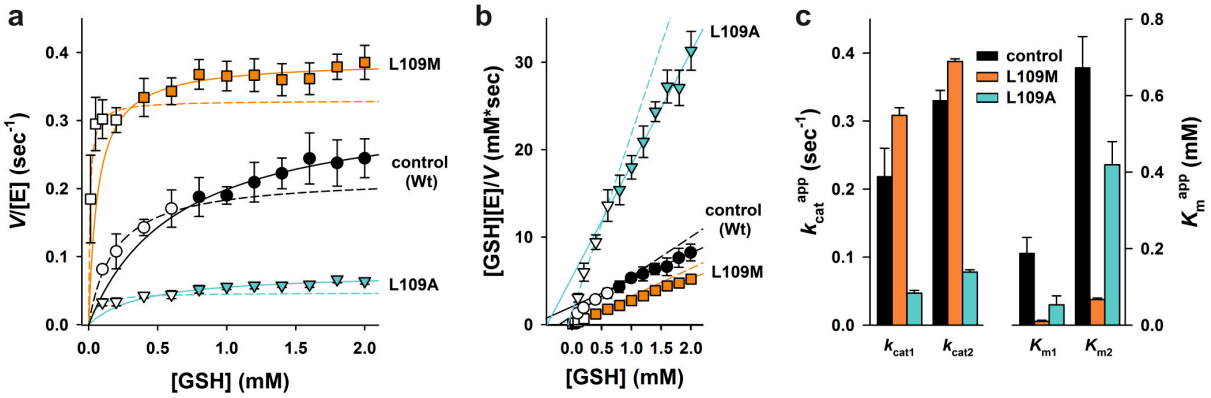

Figure 3.2 Steady-state kinetics of *Pf*AOP^{L109X} mutants with the substrate GSH.
(a) Michaelis-Menten plot of the biphasic GSH-dependent hydroperoxidase activities of *Pf*AOP^{L109M} and *Pf*AOP^{L109A} with *t*-BOOH. Wild-type *Pf*AOP served as a control. Closed and dashed lines indicate the hyperbolic fits for the values at high (closed symbols) and low (open symbols) GSH concentrations, respectively. (b) Hanes plot with negative K_m^{app} values for GSH as *x*-intercepts. Closed and dashed lines indicate the linear fits for the data at high (closed symbols) and low (open symbols) GSH concentrations, respectively. (c) Comparison of the kinetic parameters k_{cat}^{app} and K_m^{app} (see also Table 3.1). All values were determined with 75 µM *t*-BOOH, 2 µM *Pf*Grx$^{C32S/C88S}$ and variable GSH concentrations in the assay, all data are the mean ± SD of three to six replicate measurements of at least three independent enzyme purifications. Adapted from Staudacher et al., 2015.

Table 3.1 Kinetic parameters derived from the Michaelis-Menten plots (Figure 3.2a).

Protein	k_{cat}^{app} (s^{-1})	k_{cat}^{app} (%)	K_m^{app} (GSH) (mM)	K_m^{app} (GSH) (%)	k_{cat}^{app}/K_m^{app} ($M^{-1}s^{-1}$)	k_{cat}^{app}/K_m^{app} (%)
*Pf*AOP[a]	0.22±0.04	100	0.188±0.041	100	1.2×10^3	100
*Pf*AOP^{L109M} [a]	0.31±0.02	141	0.010±0.003	5	31×10^3	2710
*Pf*AOP^{L109A} [a]	0.05±0.00	22	0.053±0.023	28	0.9×10^3	76
*Pf*AOP[b]	0.33±0.02	100	0.673±0.081	100	0.5×10^3	100
*Pf*AOP^{L109M} [b]	0.39±0.00	117	0.066±0.004	10	5.8×10^3	1190
*Pf*AOP^{L109A} [b]	0.08±0.00	24	0.419±0.060	62	0.2×10^3	38

All values were determined with 75 µM *t*-BOOH, 2 µM *Pf*Grx$^{C32S/C88S}$ and variable concentrations of GSH in the assay.
[a] Apparent values at low GSH concentrations as indicated in Figure 3.2.
[b] Apparent values at high GSH concentrations as indicated in Figure 3.2.
Adapted from Staudacher et al., 2015.

The effect of the mutation of Leu109 to methionine was specific for GSH as a substrate of the reductive half-reaction because *Pf*AOP^{L109M} and wild-type enzyme had similar K_m^{app} values for the second substrate, *Pf*Grx$^{C32S/C88S}$ (Figure 3.3, Table 3.2). The k_{cat}^{app} value was about 2.3 times increased compared to wild-type enzyme at variable Grx concentrations (Staudacher et al., 2015).

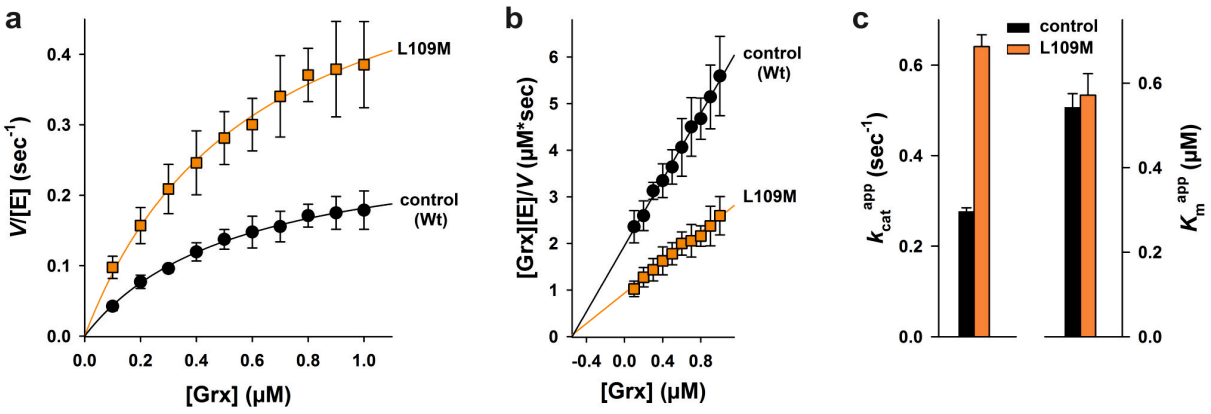

Figure 3.3 Steady-state kinetics of *Pf*AOP^{L109M} and wild-type enzyme with the substrate *Pf*Grx$^{C32S/C88S}$.
(a) Michaelis–Menten plot of the Grx-dependent hydroperoxidase activities with *t*-BOOH. (b) Hanes plot with -K_m^{app} values for Grx as *x*-intercepts. (c) Comparison of the kinetic parameters k_{cat}^{app} and K_m^{app} (see also Table 3.2). All values were determined with 75 µM *t*-BOOH, 1 mM GSH, and variable concentrations of *Pf*Grx$^{C32S/C88S}$ in the assay, and all data are the mean ± SD of three to six replicate measurements of at least three independent enzyme purifications. Adapted from Staudacher et al., 2015.

Table 3.2 Kinetic parameters derived from the Michaelis-Menten plots (Figure 3.3a).

Protein	k_{cat}^{app} (s^{-1})	k_{cat}^{app} (%)	K_m^{app} (Grx) (mM)	K_m^{app} (Grx) (%)	k_{cat}^{app}/K_m^{app} ($M^{-1}s^{-1}$)	k_{cat}^{app}/K_m^{app} (%)
*Pf*AOP	0.28±0.01	100	0.54±0.03	100	5.1×10^5	100
*Pf*AOP^{L109M}	0.64±0.03	232	0.57±0.05	105	11×10^5	220

All values were determined with 75 µM *t*-BOOH, 1 mM GSH and variable concentrations of *Pf*Grx$^{C32S/C88S}$ in the assay.
Adapted from Staudacher et al., 2015.

3.1.1.2 Residue Leu109 affects the susceptibility of the enzyme to inactivation

When I tried to analyze kinetic parameters with H_2O_2 as peroxide substrate I could not determine apparent Michaelis-Menten kinetics for *Pf*AOP wild-type enzyme or mutants as all enzymes were rapidly inactivated in a concentration-dependent manner. However, for *Pf*AOP^{L109M} I observed an initial increase in peroxidase activity at very low peroxide concentrations and, in contrast to wild-type enzyme and *Pf*AOP^{L109A}, a residual activity up to 100 µM H_2O_2 (Figure 3.4). *Pf*AOP^{L109A} was even more efficiently inactivated than the wild-type enzyme. Thus, residue Leu109 influences the susceptibility to inactivation, which can be partially compensated by the mutation to methionine (Staudacher et al., 2015).

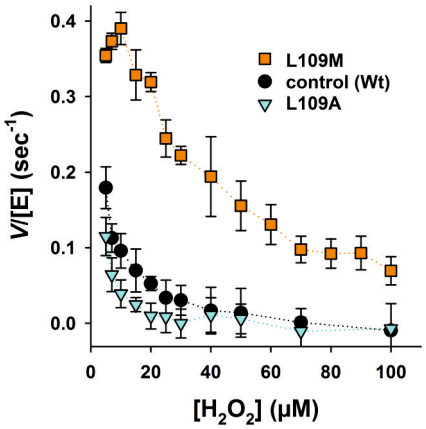

Figure 3.4 Inactivation of *Pf*AOP^{L109X} mutants by H_2O_2.
Michaelis–Menten plot of the hydroperoxidase activities of wild-type *Pf*AOP, *Pf*AOP^{L109A} and *Pf*AOP^{L109M} with H_2O_2. Initial reaction velocities were determined within 5 s after the addition of enzyme, revealing a concentration-dependent inactivation of mutant and wild-type enzyme by H_2O_2. All data are the mean ± SD of at least four replicate measurements of two independent enzyme purifications. Adapted from Staudacher et al., 2015.

3.1.2 Stopped-flow kinetics

To gain further insights into the kinetic properties of *Pf*AOP, the oxidative half-reaction of the catalytic cycle was analyzed using stopped-flow kinetic measurements. This was done particularly with regard to the roles of the potential gatekeeper residue Leu109 and the second cysteine residue Cys143. In the steady-state assay the enzyme activity was measured indirectly by monitoring a coupled enzymatic reaction. In contrast, using stopped-flow measurements the direct reaction between the enzyme and the peroxide substrate was monitored.

3.1.2.1 Kinetic constants for the direct reaction of *Pf*AOP with H_2O_2

Recombinant *Pf*AOP^{wt}, *Pf*AOP^{L109M} and *Pf*AOP^{C143S} were mixed with variable concentration of H_2O_2 in a stopped-flow spectrofluorometer. The reaction between the reduced enzymes and the peroxide was directly monitored following changes in the intrinsic tryptophan fluorescence of the enzyme.

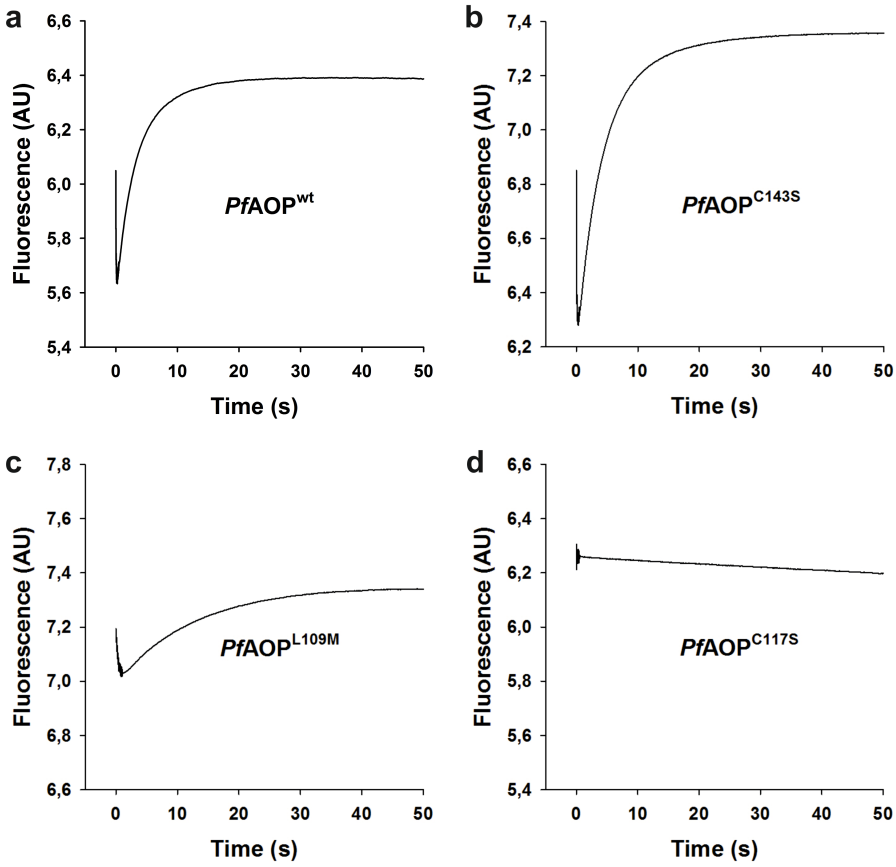

Figure 3.5 Stopped-flow kinetics of *Pf*AOP wild-type enzyme and mutants.
Stopped-flow kinetics of the oxidative half-reaction of reduced recombinant *Pf*AOP after mixing with H_2O_2 at pH 7.4 and 25°C. Representative traces are shown for 1 µM enzyme and 1 µM substrate. (a) Kinetics for wild-type *Pf*AOP. (b) Kinetics for *Pf*AOP^{C143S} lacking the non-catalytic second cysteine residue. (c) Kinetics for the gatekeeper mutant *Pf*AOP^{L109M}. d) *Pf*AOP^{C117S} without the peroxidatic cysteine residue served as a negative control. Adapted from Staudacher et al., 2018.

For all enzymes an initial biphasic change in fluorescence was observed that consisted of a fast decrease (typically the first 100 ms) followed by a slower increase in fluorescence (0.1 - 10 s) (Figure 3.5a-c). The mutant enzyme *Pf*AOP^{C117S}, which carries a mutation of the peroxidatic cysteine residue Cys117, showed no change in fluorescence and served as a negative control (Figure 3.5d).

The experimental data were fitted to exponential curves and the obtained k_{obs} values were plotted against the according peroxide concentrations and fitted linearly. The slope of the plot for the first phase of fluorescence change revealed the H_2O_2-dependent rate constant k_1. Rate constants k_2 (H_2O_2-dependent) and k_3 (H_2O_2-independent) were obtained from the slope and the y-axis intercept of the plot for the second phase, respectively (Figure 3.6) (Staudacher et al., 2018).

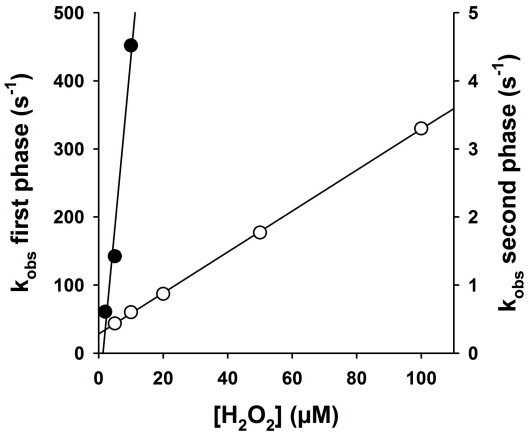

Figure 3.6. Determination of the rate constants k_1, k_2 and k_3.
The k_{obs} values obtained from the stopped-flow curves (Figure 3.5) were plotted against the corresponding peroxide concentrations. Rate constants k_1 and k_2 were obtained from the slope of the plot from the first and second phase, respectively. Rate constant k_3 was obtained from the y-axis intercept of the plot from the second phase. Representative plots of the k_{obs} values determined for one set of measurements. First phase: closed circles, second phase: open circles. Adapted from Staudacher et al., 2018.

The rate constants k_1 were similar for *Pf*AOP^{wt} and *Pf*AOP^{C143S} with values ≈ 3.5×10^7 $M^{-1}s^{-1}$ (Table 3.3) and seemed to reflect the sulfenic acid formation of the enzymes. This interpretation was further analyzed by a spectrophotometric competition assay with horseradish peroxidase (HRP). In this assay the enzyme competes with HRP for the reaction with the peroxide. As the rate constant for the reaction of HRP with the peroxide to 'HRP-compound I' is known, the constant for the reaction of *Pf*AOP with the peroxide can be calculated from the resulting amount of 'HRP-compound I' at different concentrations of *Pf*AOP (Figure 3.7). For *Pf*AOP^{wt}, *Pf*AOP^{C143S} and *Pf*AOP^{L109M} the HRP competition assay

revealed rate constants k_1*≈ 2.1 × 10^7 $M^{-1}s^{-1}$ (Table 3.3). As these values are very similar to the values obtained for k_1, this confirms that the first phase of fluorescence change reflects the direct reaction between the reduced enzyme and H_2O_2 to the sulfenic acid form of *Pf*AOP (Staudacher et al., 2018).

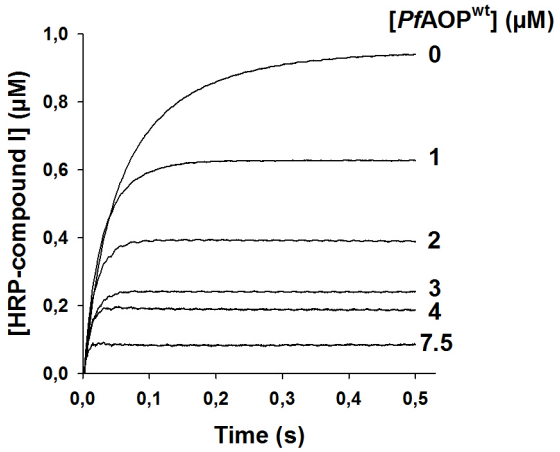

Figure 3.7 Stopped-flow peroxidase competition assay.
Stopped-flow peroxidase competition assay with 1 µM H_2O_2, 2 µM HRP and the indicated concentrations of recombinant reduced *Pf*AOP at pH 7.4 and 25°C. The formation of 'HRP-compound I' was determined spectrophotometrically at 398 nm. Adapted from Staudacher et al., 2018.

The rate constant k_2 of *Pf*AOP^{L109M} at around 1.4 × 10^3 $M^{-1}s^{-1}$ was more than one order of magnitude smaller than k_2 of *Pf*AOP^{wt} and *Pf*AOP^{C143S} (≈ 4.0 × 10^4 $M^{-1}s^{-1}$) (Table 3.3). As this constant depends on the H_2O_2 concentration, it probably reflects the reaction of the enzymes with a second peroxide molecule to form the over-oxidized sulfinic acid form. Steady-state kinetic measurements identified the *Pf*AOP^{L109M} mutant as less susceptible to H_2O_2-dependent inactivation (section 3.1.1.2). Thus, the stopped-flow results were in good agreement with our previous data.

The H_2O_2-independent rate constant k_3 presumably reflects a conformational change that occurs (once the enzyme is oxidized) in parallel to the over-oxidation of the enzyme. However, the meaning of k_3 cannot be interpreted confidently with the present data (Staudacher et al., 2018).

Table 3.3 Rate constants for the reaction of *Pf*AOP wild-type enzyme and mutants with H_2O_2.

Protein	k_1* [a] ($M^{-1}s^{-1}$)	k_1 ($M^{-1}s^{-1}$)	k_2 ($M^{-1}s^{-1}$)	k_3 (s^{-1})
*Pf*AOP^{wt}	2.1±0.8×10^7	3.2±0.5×10^7	3.6±0.6×10^4	0.28±0.02
*Pf*AOP^{C143S}	2.2±0.6×10^7	3.7±1.5×10^7	4.3±0.0×10^4	0.16±0.01
*Pf*AOP^{L109M}	2.0±0.8×10^7	n.d.	1.4±0.1×10^3	0.04±0.00

[a] Rate constant k_1* was determined in a peroxidase competition assay. Adapted from Staudacher et al., 2018.

3.1.2.2 *Pf*AOP reacts similar with different peroxide substrates

To further investigate the substrate preferences and specificity of *Pf*AOP, stopped-flow kinetic measurements with different peroxide substrates were conducted. As further substrates peroxynitrite, cumene hydroperoxide and a fatty acid hydroperoxide (12(S)-hydroperoxy-5Z,8Z,10E,14Z-eicosatetraenoic acid) were used. The experiments were performed analogously to the H_2O_2 measurements. For peroxynitrite k_2 and k_3 values could not be determined due to radical formation at higher peroxide concentrations that led to additional fluorescence changes. The HRP competition assay was only performed for peroxynitrite because the other peroxides do not react with HRP.

The rate constants k_1 for the oxidation of *Pf*AOP^{wt} to its sulfenic acid form by hydrogen peroxide, peroxynitrite and the fatty acid hydroperoxide revealed similar values around 2-4.5 × 10^7. For the reaction with cumene hydroperoxide the rate constant k_1 was about one order of magnitude smaller. This could be due to steric hindrance of this more bulky substrate. The determined rate constants for the second phase of fluorescence change revealed similar values for all used peroxides (Table 3.4). Thus, *Pf*AOP is able to react with a variety of different hydroperoxides in a similar manner (Staudacher et al., 2018).

Table 3.4 Rate constants for the reaction of *Pf*AOP wild-type enzyme with different peroxides.

Peroxide	k_1* [a] ($M^{-1}s^{-1}$)	k_1 ($M^{-1}s^{-1}$)	k_2 ($M^{-1}s^{-1}$)	k_3 (s^{-1})
peroxynitrite	2.6±1.9×10^7	1.5±0.5×10^7	n.d.	n.d.
hydrogen peroxide	2.1±0.8×10^7	3.2±0.5×10^7	3.6±0.6×10^4	0.28±0.02
cumene hydroperoxide	n.d.	4.8±0.5×10^6	4.5±2.7×10^4	0.27±0.17
fatty acid hydroperoxide (12(S)HpETE)	n.d.	1.9±0.6×10^7	5.6±1.2×10^4	0.45±0.05

[a] Rate constant *k*1* was determined in a peroxidase competition assay. Adapted from Staudacher et al., 2018.

3.2 *In vivo* kinetics of *Pf*AOP using redox sensitive GFP2

Fusion constructs between redox-sensitive green fluorescent protein 2 (roGFP2) and peroxiredoxins are used to monitor intracellular hydroperoxide concentrations (Schwarzlander et al., 2016, Morgan et al., 2016). The peroxiredoxin serves as the peroxide sensor moiety and transfers its redox state to the roGFP2. Here, I aimed to use this fusion constructs to investigate the peroxidase properties and kinetic mechanisms of *Pf*AOP wild-type enzyme and mutants *in vivo*.

Plasmids p416TEF encoding roGFP2, roGFP2-*Pf*AOP^{wt} (wt), roGFP2-*Pf*AOP^{L109M} (L109M), roGFP2-*Pf*AOP^{L109A} (L109A) or roGFP2-*Pf*AOP^{C143S} (C143S) were transformed into yeast strain BY4742 wild-type, which successfully expressed the constructs in the cytosol (Figure 3.8).

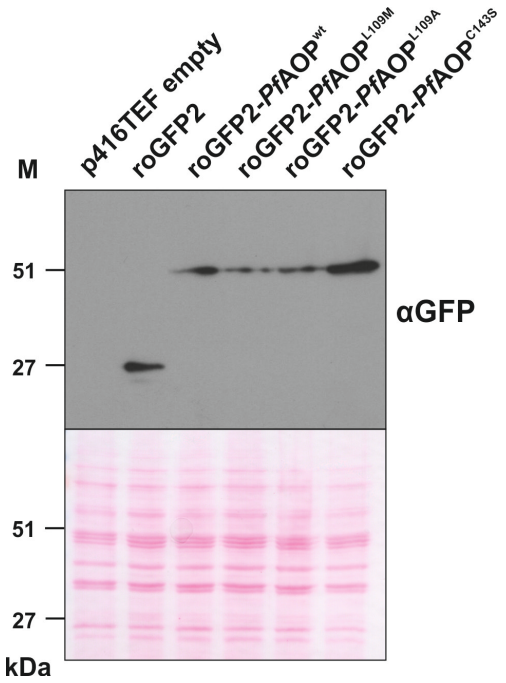

Figure 3.8 Expression of roGFP2-*Pf*AOP fusion constructs in yeast cells.
Confirmation of the presence of roGFP2 and fusion constructs in yeast cell lysates by western blot analysis. As loading control the membrane was stained with Ponceau S.

The cells were treated with increasing concentrations of H_2O_2 or *t*-BOOH (10-500 µM) and the ratiometric degree of oxidation (OxD) of roGFP2 was followed over time. As shown in Figure 3.9 the maximum change in roGFP2 oxidation (OxD_{max}) was higher for L109M compared to wt at most of the H_2O_2 and *t*-BOOH concentrations. At H_2O_2 concentrations higher than 200 µM the OxD_{max} decreased for both constructs, although the L109M mutant was more robust than the wt. For *t*-BOOH treatment no decrease in OxD_{max} was observed for L109M, while the wt reached a plateau at concentrations higher than 300 µM.

In order to make the differences between the single constructs more clearly and better comparable, the areas under the curves (AUC) were integrated between 0 and 60 min and plotted against the according peroxide concentrations for all analyzed constructs (Figure 3.10a,c) (Staudacher et al., 2018).

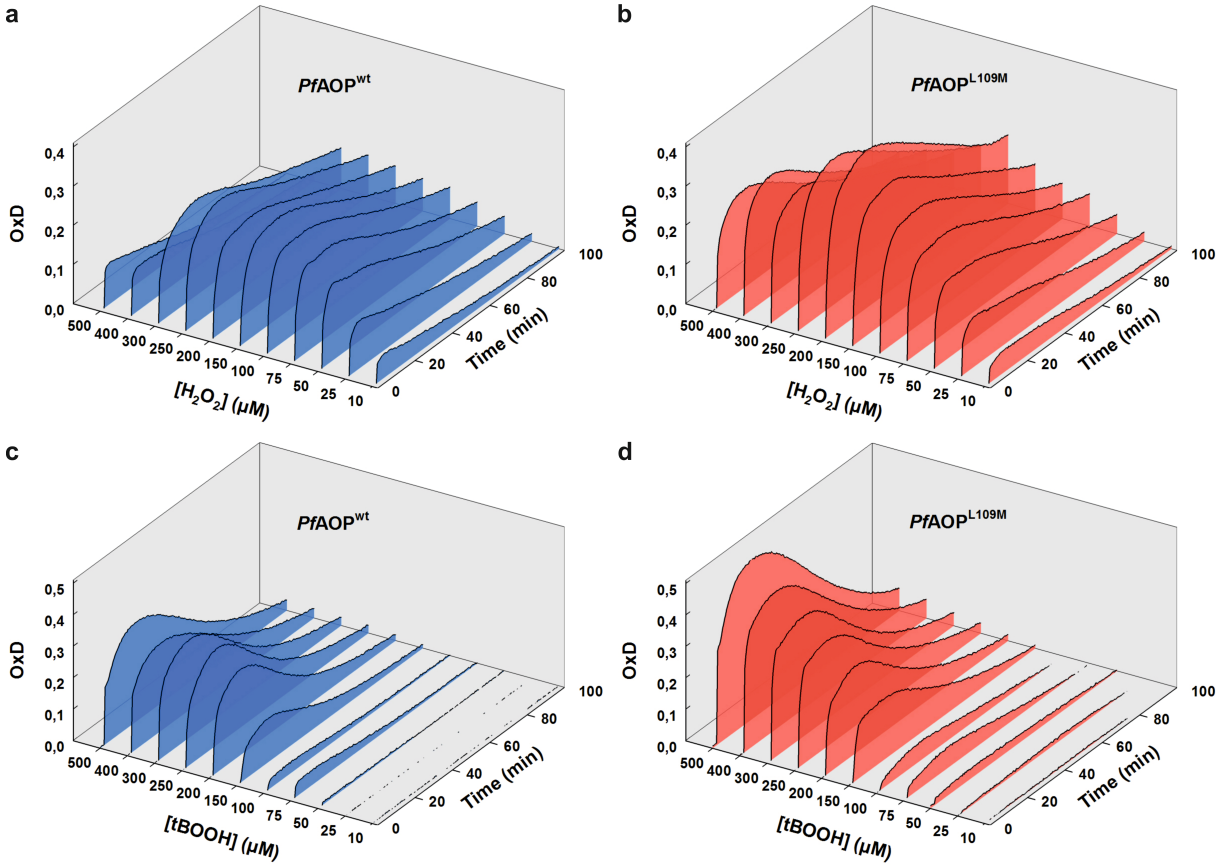

Figure 3.9 Response curves of roGFP2-*Pf*AOP measurements.
Dose-response curves for yeast cells with genetically encoded roGFP2-*Pf*AOP fusion constructs after bolus treatments with hydroperoxides at 30°C. (a) Time-course measurements of the ratiometric degree of oxidation (OxD) for the wild-type roGFP2-*Pf*AOP fusion construct (wt) at different initial H_2O_2 concentrations. (b) Time-course measurements of the OxD for the roGFP2-*Pf*AOP^{L109M} fusion construct (L109M) at different initial H_2O_2 concentrations. (c,d) Time-course measurements of the OxD for wt and L109M at different initial *t*-BOOH concentrations. Data were averaged from four (H_2O_2) or three (*t*-BOOH) independent biological replicates. Adapted from Staudacher et al., 2018.

As a negative control served roGFP2 alone, which only showed slight increases in the OxD with increasing peroxide concentrations and confirmed that the observed changes in OxD were *Pf*AOP-dependent for the fusion constructs. In contrast to L109M, L109A showed a decreased AUC for all H_2O_2 concentrations compared to wt. Mutation of the non-catalytic second cysteine residue also slightly decreased the AUC albeit not to the same extend. Similar observations were also made for the *t*-BOOH treatment.

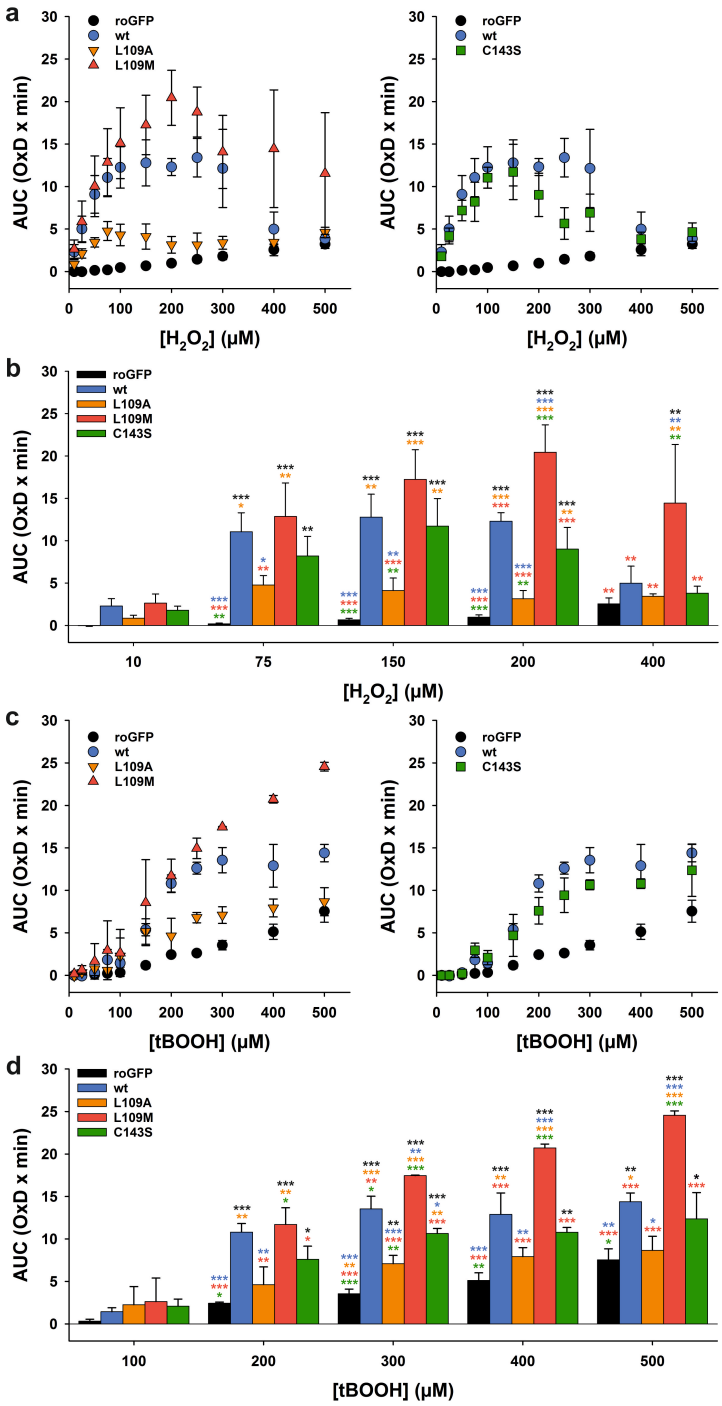

Figure 3.10 Integrated dose-response curves from Figure 3.9.
Integrated dose-response curves for yeast cells with genetically encoded roGFP2-*Pf*AOP fusion constructs after bolus treatments with hydroperoxides. Wild-type roGFP2-*Pf*AOP (wt) and roGFP2 alone (roGFP) served as positive and negative control, respectively, and confirmed that the OxD was *Pf*AOP-dependent. Constructs roGFP2-*Pf*AOP^{L109A} (L109A), roGFP2-*Pf*AOP^{L109M} (L109M) and roGFP2-*Pf*AOP^{C143S} (C143S) carry previously characterized single point mutations of *Pf*AOP (Staudacher et al., 2015). (a) The area under the OxD curves (AUC) from Figure 3.9 was determined between 0-60 min and plotted against the initial H_2O_2 concentration. All data were averaged from quadruplicate independent biological replicates. (b) Statistical analysis of the data from panel a. P-values were calculated using the One-way ANOVA method in SigmaPlot 13. (c) AUC from Figure 3.9 plotted against the initial *t*-BOOH concentration. All data were averaged from triplicate independent biological replicates. (d) Statistical analysis of the data from panel c. *, p<0.05; ** p<0.01; *** p<0.001. Adapted from Staudacher et al., 2018.

Figure 3.10b,d shows that most of the differences between the constructs were statistically significant (Staudacher et al., 2018).

These findings are in excellent agreement with the previously conducted *in vitro* studies. The differences in the AUC for L109M and L109A can be correlated with the k_{cat}^{app} values of the rate-limiting reductive half-reaction of the respective constructs. Likewise, the decreased AUC values for C143S correlate with the lower *in vitro* activity and k_{cat}^{app} value of this construct (Staudacher et al., 2018).

Another parameter that was analyzed was the H_2O_2 concentration at which the AUC reached its maximum. The AUC of L109A reached its maximum at a much lower concentration (75 µM) as wt or L109M (150-200 µM). Furthermore, the AUC of wt, L109A and C143S clearly decreased after the maximum value and showed no statistical difference to roGFP2 alone at 400 and 500 µM H_2O_2 indicating that the observed response was only due to direct roGFP2 oxidation. In contrast, the AUC of L109M was still statistically different to the negative control showing that this construct was much more robust at high H_2O_2 concentrations. For the *t*-BOOH treatment no decrease in the AUC values was observed at higher peroxide concentrations for all constructs, although all constructs apart from L109M seemed to reach a plateau above 300 µM *t*-BOOH (Staudacher et al., 2018).

These outcomes correlate quite well with the observed inactivation properties of the recombinant constructs. While H_2O_2 rapidly inactivates *Pf*AOP, much higher concentrations of *t*-BOOH are required for inactivation *in vitro*. The differences between the constructs also correlate with the *in vitro* data that identified *Pf*AOP^{L109M} and *Pf*AOP^{L109A} as less and more susceptible to H_2O_2-dependent inactivation, respectively (Staudacher et al., 2018).

3.3 Physiological relevance of *Pf*AOP

3.3.1 Generation and validation of 3D7Δ*pfaop* knockout parasites

In order to assess the relevance of *Pf*AOP for parasite survival and growth, the *PFAOP* gene was successfully knocked-out in *P. falciparum* strain 3D7 by double crossover using the CRISPR-Cas9 system (Figure 3.11a). After limiting dilution, three different clonal strains were obtained and further analyzed. All three clones had successfully integrated the selection marker by 5'- and 3'-crossover and lost the endogenous gene as confirmed by analytical PCR (Figure 3.11b).

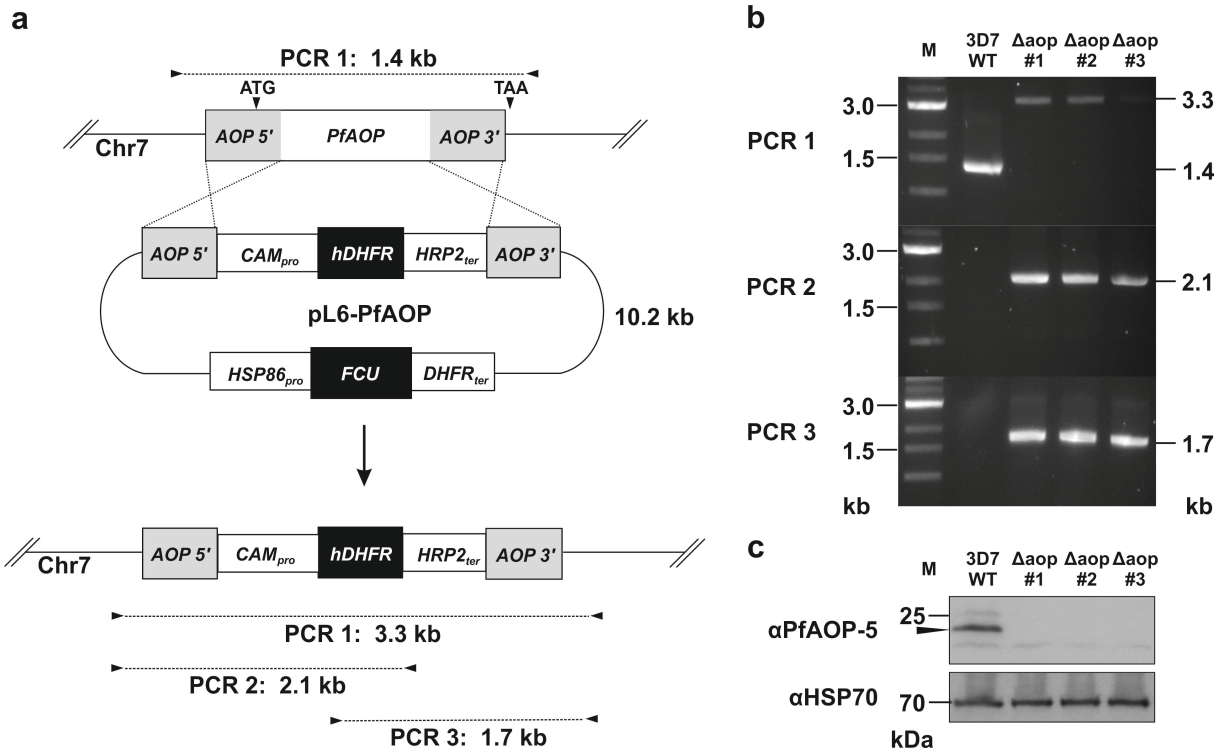

Figure 3.11 Generation and validation of Δ*pfaop* knockout parasites.
(a) Schematic summary of the knockout strategy by double crossover using the plasmid pL7-*PFAOP*. Expected product sizes from analytical PCR reactions 1–3 are highlighted. The two external primers should anneal to chromosome 7, whereas the two internal primers should anneal to the gene that encodes the selection marker human dihydrofolate reductase (hDHFR). (b) Following the genetic manipulation of the wild-type strain 3D7 (3D7 WT) and isolation of three clonal cell lines (Δaop#1-3), products from PCR reactions 1-3 were analyzed by agarose gel electrophoresis. Marker (M) and expected product sizes are indicated on the left and right side, respectively. (c) Western blot analysis of parasite cell lines Δaop#1-3. Protein extracts from 10^7 parasites were loaded per lane. Hsp70 was decorated as a control. Adapted from Djuika et al., 2017.

Furthermore, western blot analysis with a specific *Pf*AOP antibody (α*Pf*AOP-5) showed the loss of the enzyme in the prepared parasite extracts (Figure 3.11c) (Djuika et al., 2017).

The obtained 3D7Δ*pfaop* knockout parasites were subsequently analyzed regarding their growth phenotype and morphology. Giemsa-stained blood smears of the three knockout strains and 3D7 wild-type parasites as control were prepared and evaluated daily. The starting parasitemia was adjusted to 0.1%. Within a culture time of 6 days no suspicious morphologies were detected and the growth rates of all knockout strains did not differ significantly from the wild-type control (Figure 3.12). In conclusion, *PFAOP* is not essential and the loss of the gene causes no altered growth phenotype under standard culture conditions (Djuika et al., 2017).

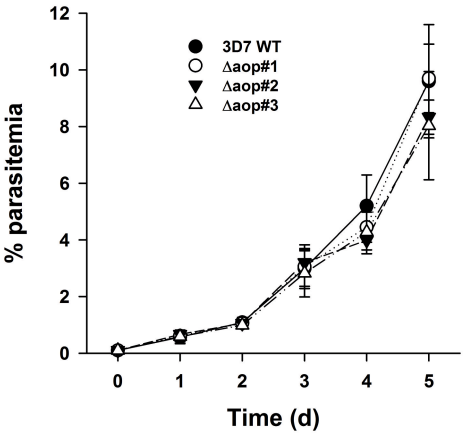

Figure 3.12 Growth curve analysis.
The parasitemia in standard asynchronous blood stage cultures of strains Δaop#1-3 from Figure 3.11 was determined by counting parasites from Giesma-stained blood smears. Wild-type strain 3D7 served as a control. All data are the mean ± standard deviation of triplicate measurements for each strain. None of the differences between the parasitemias was found to be significant ($p > 0.05$) based on statistical analyses in SigmaPlot 13 using the one way ANOVA method. Adapted from Djuika et al., 2017.

3.3.2 *Pf*AOP does not protect against artemisinin or external oxidants

A quantitative trait locus (QTL) analysis conducted by Cecilia P. Sanchez and Michael Lanzer identified *PF*AOP as one of 49 genes that correlate with altered artemisinin susceptibility (Djuika et al., 2017). Previous work of Carine F. Djuika revealed that over-expression of different *PFAOP* variants in 3D7 parasites has no impact on the artemisinin susceptibility and that artemisinins are neither substrates nor inhibitors of *Pf*AOP (Djuika et al., 2017) (see also section 1.10).

This study aimed to investigate the impact of the deletion of the *PF*AOP gene in 3D7 parasites on the susceptibility to artemisinin or other external oxidants. Therefore, IC_{50} values for artemisinin, *t*-BOOH and diamide were determined for three different knockout strains and 3D7 wild-type parasites as control in a SYBR Green based assay. The assay revealed IC_{50} values for artemisinin between 1.1±0.1 nM and 1.3±0.1 nM, for *t*-BOOH between 90±8 µM and 100±7 µM and for diamide between 75±4 µM and 84±11 µM. Deletion of the *PF*AOP gene affected none of the measured IC_{50} values compared to the wild-type strain (Figure 3.13). Attempts to test the susceptibility towards H_2O_2 failed, probably because the majority of the peroxide did not reach the parasites due to its removal by the erythrocytic peroxidases. Thus, *Pf*AOP does not alter the artemisinin susceptibility and is dispensable for the removal of external oxidants such as *t*-BOOH and diamide in the *P. falciparum* strain 3D7 (Djuika et al., 2017).

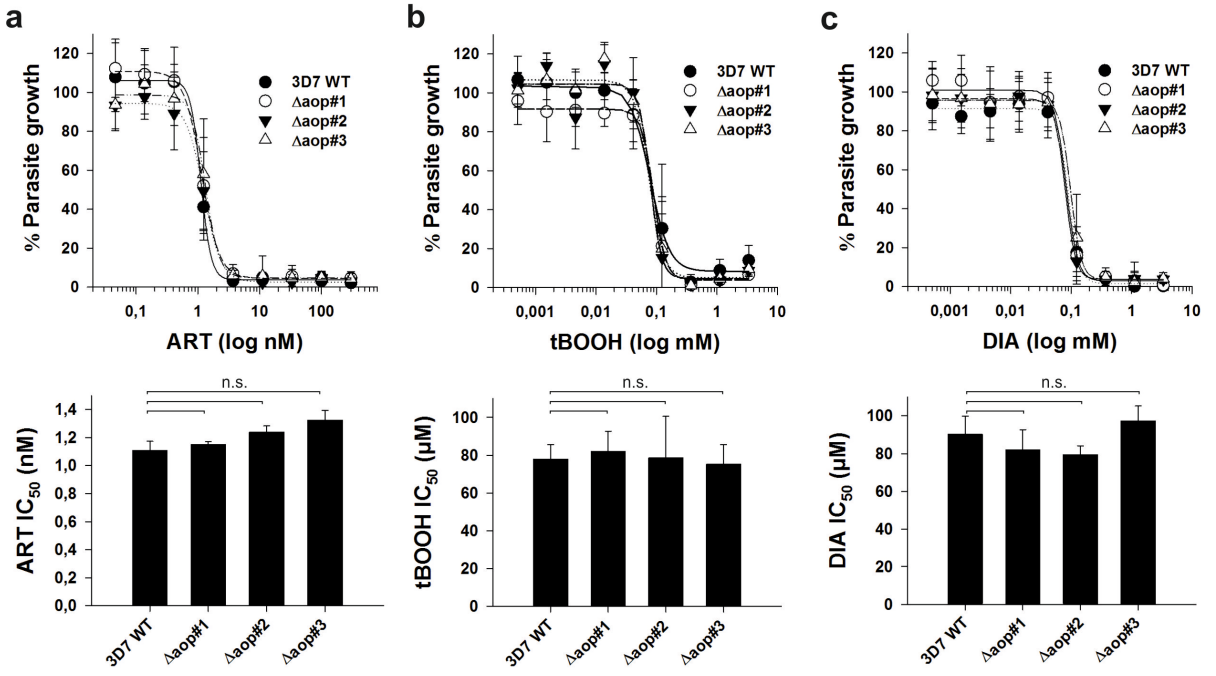

Figure 3.13 IC_{50} values for artemisinin and oxidants of Δ*pfaop* knockout parasites.
(a) Artemisinin dose response curves (upper panel) and IC_{50} values (lower panel) of blood stage cultures of strains Δaop#1-3 from Figure 3.11. (b,c) *t*-BOOH and diamide (DIA) dose-response curves (upper panel) and IC_{50} values (lower panel). All data are the mean ± standard deviation of at least three independent triplicate measurements. Wild-type strain 3D7 served as a control. None of the differences between the IC_{50} values was found to be significant ($p > 0.05$) based on statistical analyses in SigmaPlot 13 using the one way ANOVA method. Adapted from Djuika et al., 2017.

As shown by recent studies (Tucker et al., 2012, Witkowski et al., 2013a, Witkowski et al., 2013b, Kite et al., 2016), ring stage survival assays can be advantageous to detect potential artemisinin resistances, due to short artemisinin half-lives and drug-induced parasite dormancy. Therefore, the percentage of parasite survival of the 3D7Δ*pfaop* knockout strain as well as a strain over-expressing GFP-tagged full-length *PFAOP* (generated by Carine F. Djuika) was assessed after treatment of the parasites with 700 nM artemisinin in the early ring stage of the parasite life cycle. As controls *P. falciparum* 3D7 wild-type parasites (artemisinin susceptible) and the *P. falciparum* mutant strain NF54 encoding the resistance factor $K13^{C580Y}$ (artemisinin resistant) were analyzed. Only for the artemisinin resistant control ($NF54K13^{C580Y}$) significant differences in the ring-stage survival percentages in comparison to 3D7 wild-type parasites were detected (Figure 3.14). In summary, neither the deletion nor the over-expression of *PFAOP* alters the susceptibility towards artemisinin in the *P. falciparum* strain 3D7 (Djuika et al., 2017).

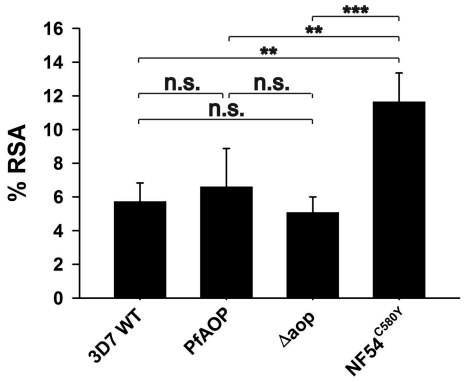

Figure 3.14 Ring-stage survival assays.
Highly synchronous ring stage parasites were treated with or without 700 nM artemisinin for 6 h, washed and further incubated for 66 h. The parasitemia was subsequently determined from Giemsa-stained blood smears. The parasite survival percentages were calculated for wild-type strain 3D7 (3D7 WT), a strain over-expressing GFP-tagged full length *PFAOP* (*Pf*AOP), a knockout strain from Figure 3.11 (Δaop#1) and a positive control that carries the mutation for $K13^{C580Y}$ ($NF54K13^{C580Y}$). All data are the mean ± standard deviation of four independent experiments. Statistical analyses were performed in SigmaPlot 13 using the one way ANOVA method. Results are summarized on top of the bar chart (n.s., not significant; **p < 0.01; ***p < 0.001). Adapted from Djuika et al., 2017.

3.3.3 Detection of potential interaction partners of *Pf*AOP *in vivo*

As the physiological relevance of *Pf*AOP could not be unraveled by the generation of knockout parasites, I tried to gain more insight into the function of the enzyme by identifying possible interaction partners of *Pf*AOP. Therefore, extracts from *P. falciparum* 3D7 wild-type parasites, 3D7Δ*pfaop* knockout parasites and 3D7 strains over-expressing *PFAOP* were prepared and analyzed by western blot analysis after non-reducing SDS-PAGE. The over-expressing strains were either GFP-tagged Fl-AOP (C-terminal fusion of full-length *Pf*AOP)(Djuika et al., 2015), which is targeted to the apicoplast of the parasite, or GFP-tagged Δ-Nterm-AOP (C-terminal fusion of shortened *Pf*AOP lacking the apicoplast targeting sequence)(Djuika et al., 2015), which is targeted to the cytosol of the parasite. To 'freeze' the redox state of the proteins, the parasites were treated with 100 mM *N*-ethylmaleimide (NEM) prior to saponin lysis and 10 mM NEM was present in all solutions used during the sample preparation. The prepared protein extracts were separated by non-reducing SDS-PAGE, the gels were blotted and either probed with α-*Pf*AOP (3D7 wild-type and Δ*pfaop*) or α-GFP (Fl-AOP and Δ-Nterm-AOP).

Non-reducing gels of 3D7 wild-type parasite extracts showed several higher molecular weight bands (>50 kDa), most of which disappeared under reducing conditions (Figure 3.15a). However, blots of 3D7Δ*pfaop* knockout parasite extracts, prepared and analyzed under the same conditions, revealed that all bands except the double-band at ≈25 kDa

representing monomeric unconjugated *Pf*AOP were unspecific (Figure 3.15a). Based on these results I decided to use GFP-tagged *PFAOP* over-expressing strains to analyze possible interaction partners. Protein extracts of Fl-AOP and Δ-Nterm-AOP parasites were prepared with and without NEM-blocking and analyzed under non-reducing conditions. The blots showed the *Pf*AOP-GFP specific bands at ≈50 kDa. No higher molecular weight bands, showing *Pf*AOP-GFP coupled to a possible interaction partner, could be detected under these conditions (Figure 3.15b).

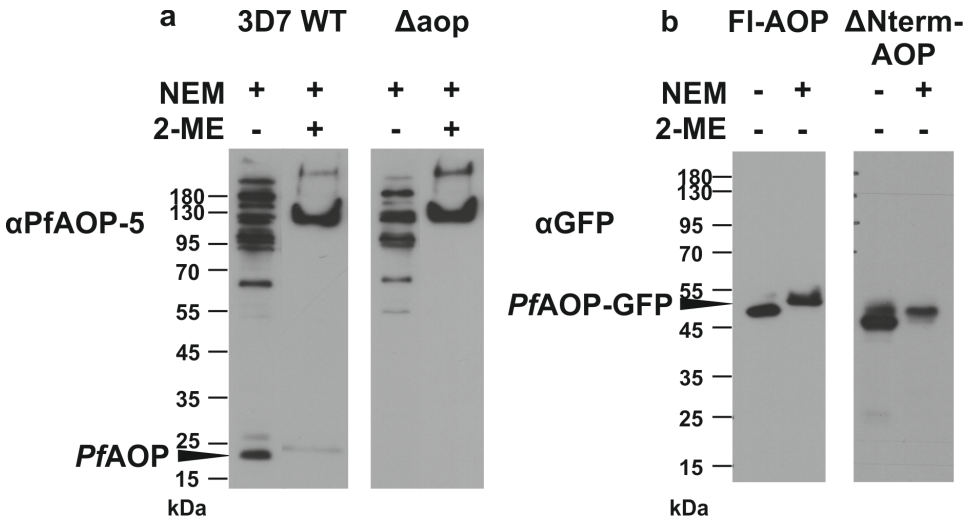

Figure 3.15 Western blot analysis of *P. falciparum* parasites.
(a) 3D7 wild-type or 3D7Δ*pfaop* knockout parasites were treated with 100 mM NEM, saponin-lysed and taken up in Lämmli buffer with or without 30% β-mercaptoethanol (2-ME). Protein extracts from 10^7 parasites were separated by 10% SDS-PAGE and analyzed by western blot analysis. Membranes were decorated with α-*Pf*AOP-5. (b) Fl-AOP or ΔNterm-AOP parasites were treated with or without 100 mM NEM, saponin-lysed and taken up in Lämmli buffer without β-mercaptoethanol. Protein extracts from 10^7 parasites were separated by 10% SDS-PAGE and analyzed by western blot analysis. Membranes were decorated with α-GFP.

To further look for possible interaction partners of *Pf*AOP, challenging experiments were performed. As peroxide substrate *t*-BOOH was chosen, because H_2O_2 is the substrate of several erythrocyte peroxidases and does not seem to reach the parasites at concentrations commonly used for these experiments (Wezena et al., 2017). Cultures of *P. falciparum* 3D7 over-expressing Fl-AOP-GFP or Δ-Nterm-AOP-GFP were challenged with 50 or 100 µM *t*-BOOH for 1, 5 or 30 min and, subsequently, treated with 100 mM NEM. Parasites were isolated by saponin lysis and protein extracts were prepared. Proteins were separated by non-reducing SDS-PAGE, the gels were blotted and probed with α-GFP.

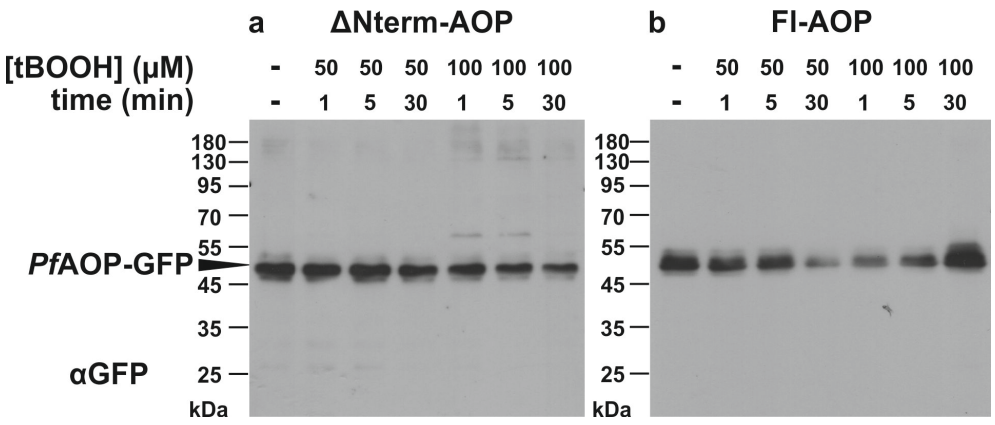

Figure 3.16 Time dependent *t*-BOOH challenge.
P. falciparum cultures over-expressing (a) ΔNterm-AOP-GFP or (b) Fl-AOP-GFP were treated with 50 or 100 µM *t*-BOOH for 1, 5 or 30 min and, subsequently, treated with 100 mM NEM. Cultures were saponin-lysed and isolated parasites were taken up in Lämmli buffer without β-mercaptoethanol. Protein extracts from 10^7 parasites were separated by 10% SDS-PAGE and analyzed by western blot analysis. Membranes were decorated with α-GFP.

For the Δ-Nterm-AOP strain one additional band at ≈60 kDa was detected after peroxide challenge with 100 µM *t*-BOOH for one and five minutes. For the longer challenge of 30 minutes this band disappeared again (Figure 3.16). For the Fl-AOP strain no additional band was visible for the chosen conditions.

To reproduce these findings and test weather the detected band is not only time- but also concentration-dependent, the experiment was repeated with *t*-BOOH treatments from 50 to 300 µM for 3 minutes.

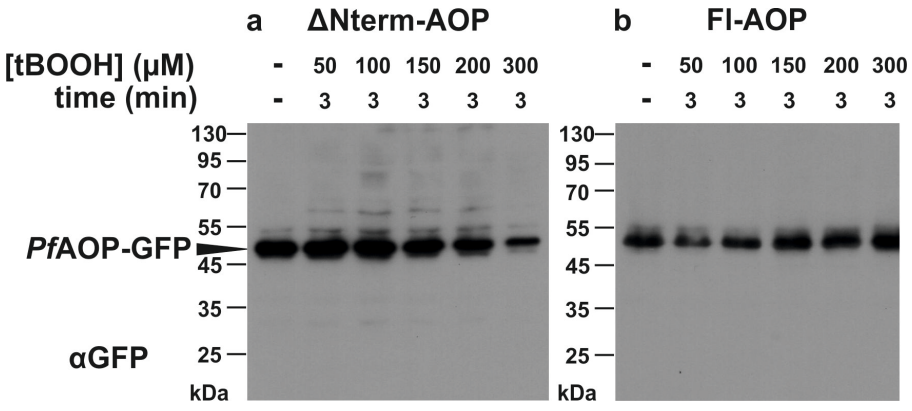

Figure 3.17 Concentration dependent *t*-BOOH challenge.
P. falciparum cultures over-expressing (a) ΔNterm-AOP-GFP or (b) Fl-AOP-GFP were treated with 50-300 µM *t*-BOOH for 3 min and, subsequently, treated with 100 mM NEM. Cultures were saponin-lysed and isolated parasites were taken up in Lämmli buffer without β-mercaptoethanol. Protein extracts from 10^7 parasites were separated by 10% SDS-PAGE and analyzed by western blot analysis. Membranes were decorated with α-GFP.

The appearance of the additional band could be reproduced for the Δ-Nterm-AOP strain at *t*-BOOH concentrations from 50 to 200 µM. For 100 µM *t*-BOOH the intensity of the additional band was the strongest (Figure 3.17). For Fl-AOP no additional band was detected.

In summary, one redox-depended band showing a possible interaction between cytosolic *Pf*AOP and a second protein with a size of aproxximately 10-15 kDa could be detected. The appearance of this band was dependent on the concentration of the peroxide and the time of peroxide challenge.

4 Discussion

4.1 Kinetic characterization of *Pf*AOP

4.1.1 Model of *Pf*AOP catalysis – a Grx/GSH-dependent peroxiredoxin

One main question of this work was to decipher the role of the potential gatekeeper residue Leu109 and the second cysteine residue Cys143. Furthermore, the significant gain-of-function of the mutant enzyme *Pf*AOP^{L109M} could not be explained yet.

Which is the rate-limiting step of the complex catalytic cycle of the peroxiredoxin *Pf*AOP? In this cycle, Prx adopt many different redox states such as E-SH, E-SOH and E-SSR (Figure 4.1a). Additionally, E-SH and E-SOH exist in two different conformations with a fully folded (E-SH_{fo} and E-SOH_{fo}) and a locally unfolded (E-SH_{lu} and E-SOH_{lu}) helix α2 (Wood et al., 2003a, Hall et al., 2011, Perkins et al., 2013). The peroxidatic cysteine is highly reactive and gets oxidized to a sulfenic acid as soon as the hydroperoxide is available for reaction (Trujillo et al., 2007, Parsonage et al., 2015). Hence, the rate-limiting step presumably represents the regeneration of the reduced enzyme. This includes conformational changes as well as the formation of E-SSR and E-SH_{lu} (Figure 4.1a) (Flohé et al., 2011, Deponte, 2013, Parsonage et al., 2015).

The previous study of our group revealed that *Pf*AOP is mechanistically a Grx/GSH-dependent 1-Cys Prx. However, the exact mechanism of the reductive half-reaction of the catalytic cycle could not be deciphered yet (Djuika et al., 2013). In this study, I could provide experimental evidence that the oxidized sulfenic acid form of the peroxidatic cysteine residue (Cys117, E-SOH) reacts first with GSH to form an intermolecular disulfide bond (E-SSG), which is then reduced by *Pf*Grx$^{C32S/C88S}$. This is supported by the kinetic data generated for the *Pf*AOP^{L109M} gain-of-function mutant (Figure 4.1b). The replacement of Leu109 with Met seems to destabilize the fully folded conformation of the enzyme and to change the equilibrium between the fully folded and the locally unfolded conformation as suggested by the comparison of the crystal structures of *Pf*AOP wild-type and *Pf*AOP^{L109M} mutant enzyme (Staudacher et al., 2015). Hence, *Pf*AOP^{L109M} probably has changed values for the rate constants k_3 and k_{-3} (Figure 4.1), the local unfolding of helix α2 may be accelerated and the steady-state concentration of E-SOH_{lu} may be increased.

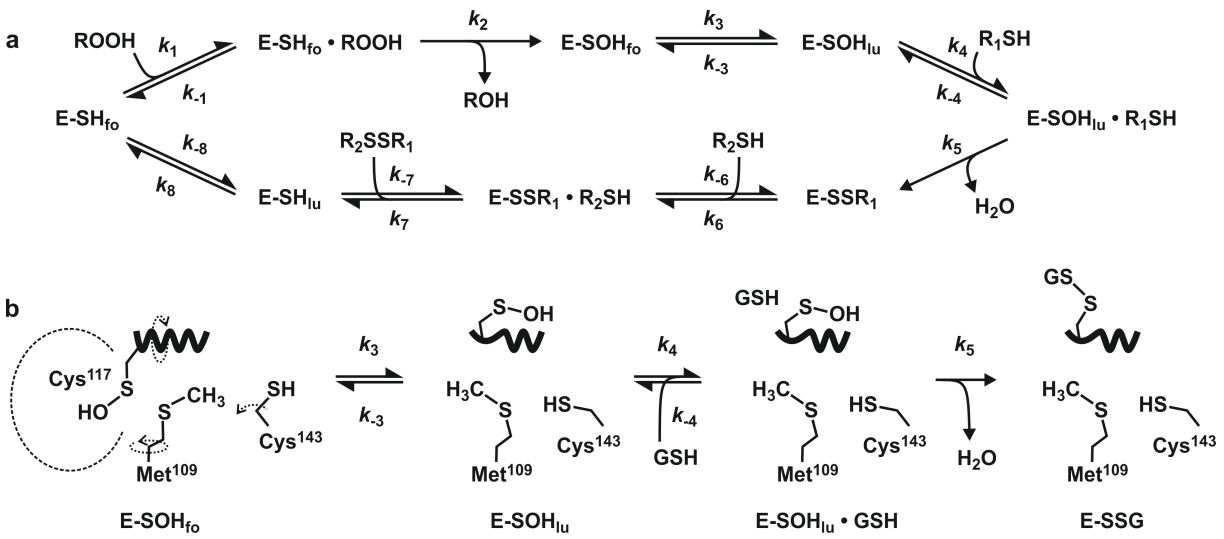

Figure 4.1 Mechanistic model for *Pf*AOP catalysis
(a) General model for Prx catalysis. (b) Potential effects of residue 109 and the second cysteine residue on *Pf*AOP^{L109M} catalysis. The active site pocket, where hydroperoxide reduction takes place, is indicated by a dashed line. Crucial protonation and deprotonation steps are omitted for simplicity. Adapted from Staudacher et al., 2015.

Our kinetic data revealed a drastically lower K_m^{app} value of *Pf*AOP^{L109M} for GSH compared to the wild-type enzyme. This implies that the mutant has a much higher apparent affinity for GSH and might reflect more successful encounters between the mutant enzyme and GSH. The K_m^{app} value of *Pf*AOP^{L109M} for the second substrate of the reductive half-reaction (*Pf*Grx$^{C32S/C88S}$) remains unchanged. A crucial first step for the reduction of the enzyme is the local unfolding of the enzyme, as represented by the constants k_3 and k_{-3}. If we suppose that especially these kinetic constants are affected by the mutation of residue 109, the first substrate of the reductive half-reaction is presumably GSH that forms a mixed disulfide with *Pf*AOP (E-SSG). This disulfide is trapped in the locally unfolded state and cannot isomerize into the folded state. E-SSG is then further reduced by *Pf*Grx$^{C32S/C88S}$. This step does not depend on k_3/k_{-3}, which therefore explains the unchanged K_m^{app} value for *Pf*Grx$^{C32S/C88S}$. The increased K_m^{app} value of *Pf*AOP^{L109M} for *t*-BOOH (Staudacher et al., 2015) also perfectly fits in this theory. If a higher proportion of the mutant enzyme adopts the locally unfolded conformation (E-SH$_{lu}$), the steady-state conformation of the fully folded enzyme (E-SH$_{fo}$) is decreased and the successful encounters of the enzyme and *t*-BOOH are less frequent.

How is the gatekeeper residue Leu109 influenced by the second cysteine residue Cys143? The observed gain-of-function of *Pf*AOP^{L109M} requires the presence of Cys143 as the double mutant *Pf*AOP$^{L109M/C143S}$ showed no increased activity compared to *Pf*AOP^{C143S}. However, *Pf*AOP^{C143S} is still catalytically active in the assay, therefore Cys143 is not mandatory for the

overall function of the enzyme (Staudacher et al., 2015). Thus, residue 109 and Cys143 have a combined influence on catalysis. This is probably reflected by a direct effect on the peroxidatic cysteine residue and an indirect effect on the reaction with GSH during the reductive half-reaction, caused by the impact of these residues on the equilibrium between the different conformations of helix α2. Direct experimental data on rate constants of the reductive half-reaction are still missing but might be determined by stopped-flow measurements in the future.

Why was the L109M mutant not selected in the course of evolution, which has a 20-fold decreased K_m^{app} value for a potential rate-limiting substrate and a threefold increased k_{cat}^{app} value compared to the existing wild-type enzyme? This points to the fact that *Pf*AOP may not only act as a hydroperoxide scavenger but might also execute an additional function that is lost in the mutant enzyme. This is further supported by the conservation of the gatekeeper residue Leu109 of *Pf*AOP among many Prx5 homologues of *Pf*AOP from other organisms (Staudacher et al., 2015). For many Prx, it has been suggested or even shown that they act not only as peroxidases but also as redox sensors (Rhee and Woo, 2011, O'Neill and Reddy, 2011, Edgar et al., 2012, Cho et al., 2014, Poynton and Hampton, 2014). How Prx execute their alternative functions is not fully understood, yet. According to the floodgate model, it was suggested that the Prx gets over-oxidized by elevated peroxide concentrations resulting in an inactive enzyme that has altered protein-protein interactions and that cannot prevent the accumulation of other oxidized proteins (Wood et al., 2003a, Sayed and Williams, 2004, Hall et al., 2011, Peskin et al., 2013). This theory is based on the fact that a common feature of many Prx is their susceptibility to over-oxidation. Another theory, the redox-relay model, proposes that the Prx is converted into a signal transducer that can form mixed disulfides with other molecules (Brigelius-Flohé and Flohé, 2011). Examples for such mixed disulfides are yeast Ahp1 and Cad1 (Iwai et al., 2010), mammalian Prx1/2 and Ask1 (Jarvis et al., 2012), yeast Prx1 and Trx3 (Greetham et al., 2013) and mammalian Prx2 and STAT3 (Sobotta et al., 2015). So far, it is unknown if *Pf*AOP can act as a redox sensor. However, its high susceptibility to inactivation by H_2O_2 might point to this direction. Moreover, the fact that the more active *Pf*AOP^{L109M} mutant is less efficiently inactivated supports the theory that the susceptibility to inactivation could be the evolutionary advantage of the wild-type enzyme against the mutant.

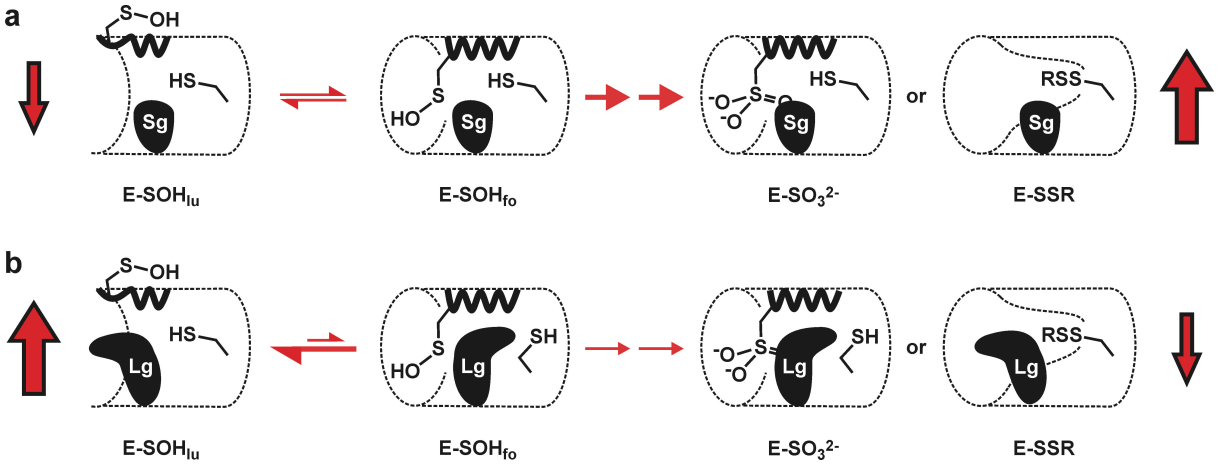

Figure 4.2 Mechanistic model for *Pf*AOP inactivation with implications for potential redox sensing.
Altered conformational dynamics and gatekeeper-dependent shielding of the second cysteine residue could affect the formation of the previously detected E-SSR species (Djuika et al., 2013) or the formation of the sulfinic and sulfonic acid species as detected in the crystal structure (Sarma et al., 2005) and by mass spectrometry (Djuika et al., 2013). (a) Short gatekeeper mutants (Sg) have a delayed unfolding of helix α2 and a less shielded second cysteine residue. As a result, turnover decreases, and the enzyme is more susceptible to inactivation. (b) Long gatekeeper constructs (Lg) have a promoted unfolding of helix α2 and a highly shielded second cysteine. As a result, turnover increases, and the enzyme has an increased durability. Adapted from Staudacher et al., 2015.

In this study I assessed the influence of the gatekeeper residue and the second cysteine residue on the inactivation properties of *Pf*AOP. Short gatekeeper residues (e.g. alanine) and the presence of Cys143 make *Pf*AOP more susceptible to inactivation, whereas long gatekeeper residues (e.g. methionine) and the absence of Cys143 make *Pf*AOP less susceptible to inactivation. How do these two residues contribute to inactivation? The exact species of the inactivated *Pf*AOP could not be assessed experimentally so far, but two possibilities why the peroxidatic cysteine cannot contribute to catalysis anymore are supposable (Figure 4.2): (i) the enzyme is inactivated by over-oxidation or (ii) the inactivation is the result of a disulfide bridge formation between the two cysteine residues. (i) The crystal structure of *Pf*AOP reveals that it is prone to over-oxidation as the active site pocket of the fully folded conformation is able to accommodate not only the sulfenic acid form of the peroxidatic cysteine residue but also its sulfinic and sulfonic acid forms including the peroxide molecules necessary for each oxidation step (Sarma et al., 2005). Furthermore, it was suggested that over-oxidation exclusively takes place in the fully folded conformation (Wood et al., 2003a). As outlined above, the mutations of the gatekeeper residue probably affect the equilibrium between the fully folded and the locally unfolded conformation of helix α2. The mutation to a long gatekeeper residue (methionine) shifts the equilibrium to the locally unfolded conformation, thus making the mutant enzyme less susceptible to over-

oxidation (Figure 4.2a). The mutation to a short gatekeeper residue (alanine) shifts the equilibrium to the fully folded conformation resulting in a mutant enzyme that is more susceptible to over-oxidation (Figure 4.2b). (ii) A Cys143 disulfide species could be detected previously (Djuika et al., 2013) and the long gatekeeper residue may decrease the accessibility of Cys143 making *Pf*AOP^{L109M} less susceptible to inactivation caused by the formation of an intramolecular disulfide between Cys117 and Cys143.

In summary, the reductive half-reaction of *Pf*AOP consists of the formation of a mixed disulfide of the peroxidatic cysteine residue and GSH (E-SSG) that is subsequently reduced by *Pf*Grx$^{C32S/C88S}$. Furthermore, the gatekeeper residue 109 probably regulates the accessibility of Cys143 and the unfolding balance of helix α2, thus making *Pf*AOP^{L109M} a mutant enzyme with a higher hydroperoxidase activity and a higher durability regarding peroxide-dependent inactivation. Nevertheless, this may be coupled with a loss of function for redox sensing *in vivo*.

4.1.2 Determination of rate constants for the (over-)oxidation of *Pf*AOP

How do the gatekeeper residue Leu109 and the second cysteine residue Cys143 influence the oxidation and over-oxidation of *Pf*AOP exactly? To address these questions, stopped-flow kinetic measurements were conducted taking advantage of the intrinsic tryptophan fluorescence of *Pf*AOP (Staudacher et al., 2018). The measurements revealed three different constants for the direct reaction of *Pf*AOP wild-type enzyme and mutants with H_2O_2. The kinetic data indicate that the first rate constant $k_1 \approx 3.5 \times 10^7\ M^{-1}s^{-1}$ reflects the sulfenic acid formation of the peroxidatic cysteine residue. This could be confirmed by the determination of this constant with an alternative method, the HRP-competition assay, which revealed similar values $k_1^* \approx 2.1 \times 10^7\ M^{-1}s^{-1}$. This is in good accordance with previously reported values for the rate constant of the sulfenic acid formation of other Prx (Cox et al., 2009, Nagy et al., 2011, Peskin et al., 2013). Interestingly, the determined values for constant k_1 are very similar for *Pf*AOP^{wt}, *Pf*AOP^{L109M} and *Pf*AOP^{C143S} indicating that the mutation of the gatekeeper residue or the second cysteine has no influence on the sulfenic acid formation. However, the total initial change in fluorescence was different for the *Pf*AOP^{L109M} mutant compared to the wild-type enzyme, which can be explained with the shifted equilibrium between fully folded and locally unfolded conformation of this mutant (see section 4.1.1). As

confirmed by the results of the HRP-competition assay, the rate constant for the sulfenic acid formation is unaffected by this special steady-state conformation of *Pf*AOP^{L109M}.

In addition, rate constant k_1 is very similar not only for the reaction of the different mutant enzymes with H_2O_2 but also for the reaction of *Pf*AOP wild-type enzyme with different peroxides. Only k_1 for the reaction with aromatic cumene hydroperoxide was about one order of magnitude smaller. This is not really surprising as cumene hydroperoxide is a quite bulky molecule that may take longer to adopt the right position in the active site pocket that is necessary for the reaction with the peroxidatic cysteine residue due to its steric hindrance.

In addition to the rate constant k_1 representing the sulfenic acid formation of *Pf*AOP, two other rate constants (k_2 and k_3) were determined. These two constants represent two subsequent reactions that occur in parallel and are in one case peroxide-dependent (k_2) and in the other case peroxide-independent (k_3) (Figure 4.3).

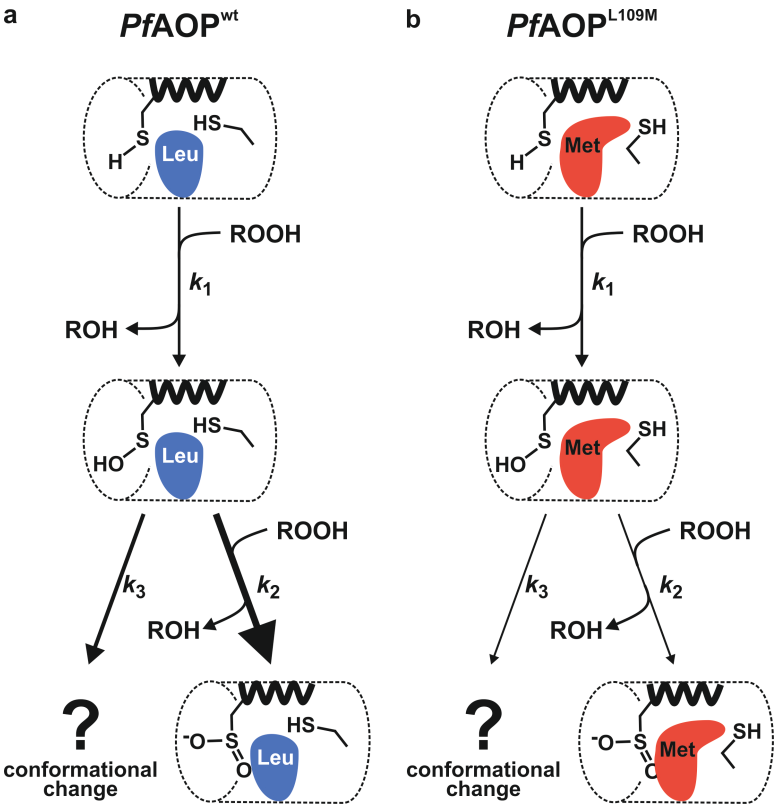

Figure 4.3 Model for the relevance of the different kinetic constants of *Pf*AOP determined by stopped-flow kinetic measurements.

The peroxidatic cysteine is oxidized by a hydroperoxide to the sulfenic acid represented by rate constant k_1. Rate constants k_2 and k_3 represent two subsequent reactions that occur in parallel: the potential over-oxidation of the peroxidatic cysteine to the sulfinic acid (k_2) and probably a conformational change of the enzyme (k_3). (a) Model for *Pf*AOP^{wt} that is susceptible to over-oxidation. (b) Model for *Pf*AOP^{L109M} that is less susceptible to over-oxidation.

As constant k_2 represents a subsequent peroxide-dependent reaction, it seems likely that k_2 is the constant for the further oxidation of the peroxidatic cysteine residue from the sulfenic acid form (E-SOH) to the sulfinic acid form (E-SO_2H). The determined rate constant $k_2 \approx 4.0 \times 10^4$ $M^{-1}s^{-1}$ for *Pf*AOP^{wt} and *Pf*AOP^{C143S} is similar to the values reported for the sulfinic acid formaton of Prx2 and Prx3 (Peskin et al., 2013). Furthermore, the gatekeeper mutant *Pf*AOP^{L109M} showed a rate constant k_2 that is more than ten times smaller as the constant determined for the wild-type enzyme. This is in good accordance with its decreased susceptibility to inactivation (probably caused by over-oxidation) determined by stead-state kinetic measurements (see section 4.1.1).

The significance of constant k_3 remains quite difficult to interpret. As it is independent on the peroxide concentration and takes place in parallel to the presumable over-oxidation of the enzyme, it may reflect a slow conformational change that happens during the reaction of the enzyme with the second peroxide molecule. The values of this third constant k_3 for *Pf*AOP^{L109M} were again about one order of magnitude smaller compared to wild-type enzyme. This could indicate that this conformational change is somehow coupled to the over-oxidation, which happens also slower in the *Pf*AOP^{L109M} mutant enzyme.

In summary, stopped-flow kinetic measurements revealed that the formation of the sulfenic acid form of *Pf*AOP is independent on the mutant form of the enzyme or the nature of the peroxide and happens with a rate constant in the range of 10^7 $M^{-1}s^{-1}$. The over-oxidation of *Pf*AOP presumably happens with a rate constant in the range of 10^4 $M^{-1}s^{-1}$ and is about one order of magnitude slower in the *Pf*AOP^{L109M} mutant. Overall, the results from the stopped-flow kinetic measurements are in good accordance with the previously conducted steady-state kinetic measurements on *Pf*AOP wild-type enzyme and mutants.

To complete the kinetic characterization of *Pf*AOP, it would be interesting to determine rate constants for the rate-limiting reductive half-reaction of the catalytic cycle of *Pf*AOP with its substrates *Pf*Grx and GSH using stopped-flow kinetic measurements. Furthermore, stopped-flow experiments with *t*-BOOH could strengthen the model proposing that k_2 reflects the over-oxidation of the enzymes to their sulfinic acid form. As the susceptibility to *t*-BOOH-dependent inactivation was much lower in the steady-state experiments, the reaction of *Pf*AOP and *t*-BOOH should yield smaller values for k_2 in stopped-flow experiments.

Another interesting experiment would be to engineer *P. falciparum* parasites bearing the *in vitro* characterized mutations of Leu109 and Cys143 in the gene encoding *Pf*AOP. The

characterization of these parasites could unravel the impact of these amino acids on the enzyme function of *Pf*AOP *in vivo*.

4.1.3 roGFP2-*Pf*AOP fusion constructs for monitoring the catalytic mechanism and inactivation of peroxiredoxins inside living cells

How are the readouts of the fusion constructs between roGFP2 and *Pf*AOP affected by the kinetic properties of *Pf*AOP? Is it possible to transfer our *in vitro* results to an *in vivo* system and can roGFP2 fusion constructs be used to characterize peroxidases *in vivo*?

The first parameter that can be derived from the roGFP2 readout is the AUC. The AUC values of the fusion constructs at the single *t*-BOOH concentrations, L109M > wt > L109A, correlate quite well with the k_{cat}^{app} values of the corresponding recombinant proteins determined by steady-state kinetic measurements. These k_{cat}^{app} values represent the rate-limiting reductive half-reaction with GSH *in vitro*. Equally the slightly smaller AUC values of C143S compared to wt correlate with the *in vitro* results where recombinant *Pf*AOP^{C143S} was shown to have a 25% lower enzyme activity (Djuika et al., 2013). Hence, the enzyme activity is reflected by the AUC of the roGFP2 readout.

The second parameter that can be derived from the roGFP2 readouts is the peroxide concentration at which the OxD curves reach their maximum amplitude. Recombinant *Pf*AOP wild-type enzyme and mutants were shown to be rapidly inactivated by H_2O_2 in the steady-state kinetic measurements whereas much higher *t*-BOOH concentrations were needed for the inactivation *in vitro*. This correlates with the observation that for the roGFP2 fusion constructs the highest AUCs were reached at much higher *t*-BOOH concentrations compared to H_2O_2. Furthermore, the recombinant enzymes showed different susceptibilities to H_2O_2-dependent inactivation, *Pf*AOP^{L109A} > *Pf*AOP^{wt} > *Pf*AOP^{L109M}, and *Pf*AOP^{L109M} showed a more than ten times smaller rate constant k_2 in the stopped-flow measurements compared to the other enzymes. This correlates perfectly with the increasing robustness of the roGFP2 responses of the according fusion constructs (L109M > wt > L109A). From these results I can conclude that the inactivation of the Prx is reflected by the roGFP2 readout.

How can we now describe these findings in a comprehensive model (Figure 4.4)? The oxidation of the peroxidatic cysteine residue of *Pf*AOP to its sulfenic acid form probably does not affect the different roGFP2 readouts (step i). This is supported by the fact that for the different mutants no differences for k_1 were measured in stopped-flow kinetic

measurements. In the next step, the oxidized *Pf*AOP is reduced by the roGFP2 reporter moiety yielding oxidized roGFP2 (step ii). Therefore, the local unfolding of the active site helix α2 is mandatory (step iia). This step depends on residue Leu109 and Cys143 (section 4.1.1 and 4.1.2) and explains the different AUC values measured for the different fusion constructs. Next, the oxidized roGFP2 is reduced (step iii) to complete the catalytic cycle. This step is also not responsible for the different readouts as the roGFP2 reporter moiety and the genetic background did not differ among the analyzed fusion constructs.

What could further happen to the fusion constructs? The oxidized *Pf*AOP sensor moiety could be reduced directly by alternative reducing agents present in the cell (step iv). Although this step cannot be excluded, it probably does not represent a major factor affecting the roGFP2 readouts, as all roGFP2-*Pf*AOP fusion constructs were sensitive and responded quite well to the peroxide challenges. The last parameter to be analyzed was the over-oxidation of the peroxidatic cysteine residue of *Pf*AOP to its sulfinic acid form resulting in an inactivated *Pf*AOP sensor moiety (step v). This step depends again on residue Leu109 (section 4.1.1 and 4.1.2) and explains the varying robustness of the roGFP2 readouts for the different fusion constructs.

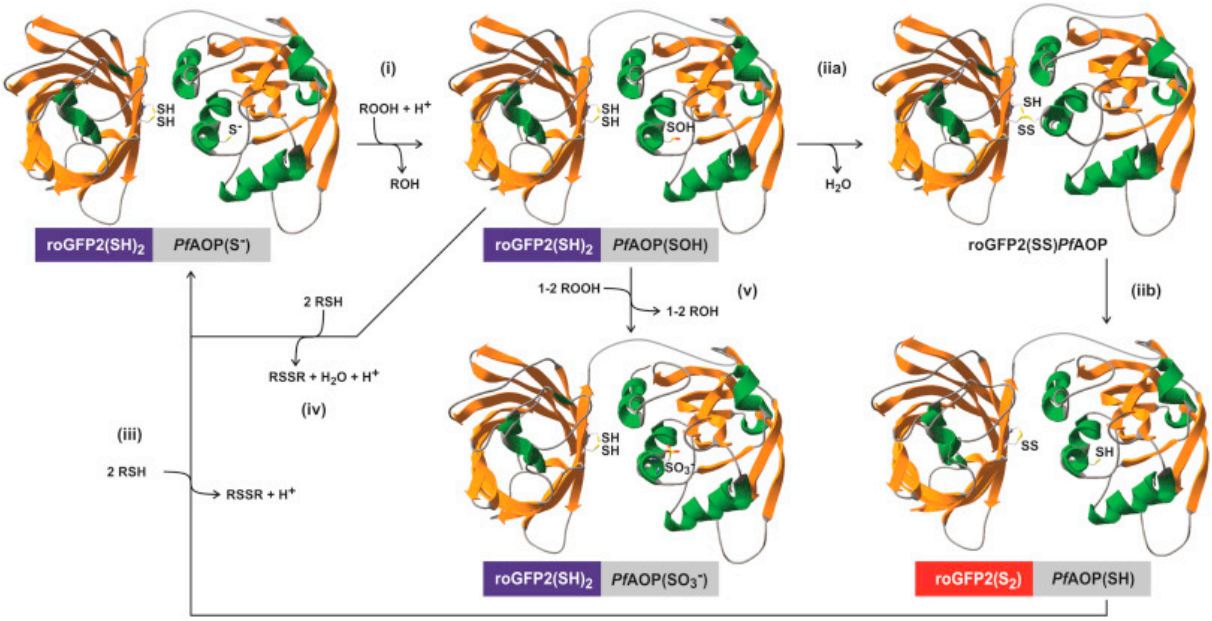

Figure 4.4 Model for the intracellular roGFP2-dependent assessment of *Pf*AOP catalysis.
The metabolic flux monitored by roGFP2 comprises (i) the peroxide-dependent oxidation of the *Pf*AOP sensor moiety, (ii) the two-step reduction of the sensor moiety yielding the oxidized roGFP2 reporter moiety, (iii) the reduction of the reporter moiety, (iv) a potential roGFP2-independent bypass reaction between oxidized *Pf*AOP and alternative reducing agents, and (v) the inactivation of the sensor moiety because of over-oxidation. Adapted from Staudacher et al., 2018.

To further strengthen the proposed model for the intracellular roGFP2-dependent assessment of *Pf*AOP catalysis, it would be interesting to analyze the single steps directly. Using stopped-flow kinetic measurements the direct reaction of the fusion constructs with its oxidizing and reducing substrates could be assessed and compared to the direct reaction of roGFP2 and *Pf*AOP with these substrates.

Which further findings can be derived from this study? We can try to estimate the cytosolic H_2O_2 concentration inside the yeast cells and the ratio between the extra- and intracellular H_2O_2 concentration after bolus treatments. The latter is of particular interest for the evaluation of experiments with bolus treatments with H_2O_2 as there are, to the best of my knowledge, no data available so far. The physiological H_2O_2 concentrations in a variety of organisms are estimated around 1 nM under steady-state conditions. Peak levels are estimated to reach 0.5 – 0.7 µM (Stone and Yang, 2006). In the steady-state kinetic measurements I observed that the activity of recombinant *Pf*AOP^{L109M} peaked at a H_2O_2 concentration of 10 µM. With higher concentrations the activity decreased due to inactivation of the enzyme (see section 3.1.1.2). For the fusion construct between roGFP2 and *Pf*AOP^{L109M} the OxD curves reach their maximum amplitude when the cells were treated with a H_2O_2 concentration of 200 µM. Therefore, it seems likely that the intracellular H_2O_2 concentration is about 20-fold lower then than the extracellular concentration. For yeast cells it was shown that the permeability of the plasma membranes is variable for H_2O_2 and adapting to the concentration (Branco et al., 2004, Folmer et al., 2008). Despite this, our findings are in good agreement with reports for *E. coli* or mammalian cells for which 7- to 10-fold differences between intra- and extracellular H_2O_2 concentrations following bolus treatment were reported (Antunes and Cadenas, 2000, Seaver and Imlay, 2001, Makino et al., 2004). Assuming a 20-fold difference in intra- and extracellular H_2O_2 concentration, the intracellular concentrations in our experiments probably ranged between 0.5 and 25 µM, which significantly exceeds physiological peek levels around 0.7 µM.

Thus, by estimating the intracellular H_2O_2 concentration using inactivation properties of *Pf*AOP^{L109M}, our experiments could provide valuable information about the physiological relevance of common H_2O_2-bolus treatments in yeast research.

4.2 Physiological relevance of *Pf*AOP

4.2.1 Knockout of *PFAOP*

What could be the physiological function of *Pf*AOP? The enzyme is constitutively expressed during blood stage development of the parasite as shown by immunofluorescence microscopy and transcriptome analyses (Deponte et al., 2007, Djuika et al., 2015). From the five *P. falciparum* peroxiredoxins, *Pf*AOP is the only one that localizes to the apicoplast of the parasite. It was shown that the apicoplast is essential for parasite survival because of the biosynthesis of the isoprenoid precursor isopentenyl pyrophosphate (Jomaa et al., 1999, Yeh and DeRisi, 2011). Two enzymes of this biosynthetic pathway rely on iron-sulfur-cluster cofactors (Gisselberg et al., 2013, Ralph et al., 2004) and, thus, are quite redox-sensitive. Hence, it is surprising that the loss of the hydroperoxidase *Pf*AOP did not impair parasite survival.

Among the *P. falciparum* peroxiredoxins, *Pf*PrxQ, which locates to the nucleus, is the only one that seems to be essential (Richard et al., 2011). Thus, it seems likely that the other peroxidases in the cytosol and the apicoplast can compensate for the loss of *Pf*AOP. In the cytosol possible candidate enzymes are the peroxiredoxins *Pf*Prx1a, *Pf*Prx6 and the imported human Prx2 (Kawazu et al., 2003, Kawazu et al., 2005, Yano et al., 2005, Koncarevic et al., 2009). The apicoplast harbors no further peroxiredoxins but a glutathione peroxidase-like thioredoxin peroxidase *Pf*TPx$_{Gl}$ that could compensate the loss of *Pf*AOP (Kehr et al., 2010, Chaudhari et al., 2012).

Another explanation for the absent phenotype could be the potential absence of major sources of $O_2^{\bullet-}$ and H_2O_2 in the apicoplast. Contradictory to this assumption is the presence of further antioxidant enzymes in the apicoplast such as the superoxide dismutase *Pf*SOD2 (Pino et al., 2007) and *Pf*TPx$_{Gl}$ that would not be necessary without major sources of $O_2^{\bullet-}$ and H_2O_2 in the apicoplast.

A third explanation is that the main function of *Pf*AOP is not exerted by its hydroperoxidase activity but by a non-essential function, e.g. redox-sensing for transducing redox signals (Brigelius-Flohé and Flohé, 2011).

In summary, the physiological function of *Pf*AOP could not be identified by the generation of 3D7Δ*pfaop* knockout parasites and the encoding gene is fully dispensable for blood stage development of *P. falciparum* under the experimental cell culture conditions.

To further assess the physiological relevance of *Pf*AOP, it would be interesting to characterize the knockout parasites in the complete life-cycle of *P. falciparum*. The parasites may show a phenotype in liver or mosquito stages or regarding gametocyte development. As the analysis of *P. falciparum* liver and mosquito stages is quite challenging the relevance of the gene for these stages could also be assessed using a mouse model and the rodent malaria parasite *P. berghei*. Furthermore, the generation and evaluation of parasites bearing the *in vitro* characterized L109M mutation in the gene encoding *Pf*AOP could unravel the potential addition function of the enzyme for blood, liver and mosquito stages of the live-cycle.

4.2.2 *Pf*AOP and artemisinin

Resistance to artemisinins, especially in Southeast Asia, is becoming a severe problem for the treatment of malaria. Mutational changes in the gene encoding the *P. falciparium* kelch protein K13 were associated to altered artemisinin susceptibility but cannot account alone for all resistance cases (Dondorp et al., 2009, Mbengue et al., 2015, Fairhurst and Dondorp, 2016, Tilley et al., 2016). In a recently conducted QTL analysis a genetic locus on chromosome 7 was identified that is associated with an altered artemisinin susceptibility in a genetic cross between the *P. falciparum* strains 7G8 (Latin America) x GB4 (Africa). This genetic locus encodes 49 genes including *PFAOP* (Djuika et al., 2017). As artemisinins are endoperoxides it seemed likely that *Pf*AOP, a peroxidase, would be associated with resistance to artemisinins. A study conducted by Carine Djuika in our group revealed that artemisinins are neither substrates nor inhibitors of *Pf*AOP. Furthermore, no altered artemisinin susceptibility could be detected for different *PFAOP* over-expressing strains in traditional growth inhibition assays (IC_{50} measurements) (Djuika et al., 2017). In this study, I showed that also the 3D7Δ*pfaop* knockout strains have no altered susceptibility towards artemisinin. It was recently shown that ring stage survival assays (RSA) can be advantageous to address a potential artemisinin resistance due to short artemisinin half-lives or drug induced parasite dormancy (Witkowski et al., 2013a, Witkowski et al., 2013b, Kite et al., 2016). However, neither with this alternative growth inhibition assay (RSA) nor with the classical method (IC_{50} measurements) altered artemisinin susceptibilities for *PFAOP* over-expressing and 3D7Δ*pfaop* knockout parasite strains were detected.

Thus, *Pf*AOP alone is not associated with the resistance to artemisinins and the effects from the QTL analysis are either caused by a polygenetic trait or by one of the other 48 identified genes within the detected locus on chromosome 7.

Among these 48 genes identified in our QTL analysis are three genes that were also detected by other studies on artemisinin susceptibility of *P. falciparum* and, thus, are potential candidates. A study using chemogenetic profiling identified PF3D7_0727100 as a potential artemisinin susceptibility factor (Pradhan et al., 2015). The gene encodes a conserved *Plasmodium* protein of unknown function and could be the crucial factor within the identified artemisinin susceptibility locus on chromosome 7. Two other studies using modified artemisinin probes and click chemistry identified two more candidates that were also detected in our QTL analysis. The first one is PF3D7_0729900, which encodes a putative dynein heavy chain (Ismail et al., 2016). The second one is PF3D7_0727400, which encodes a putative proteasome subunit alpha type-5 (Wang et al., 2015). The latter one might be of particular interest as in recent studies artemisinin susceptibility was linked to the ubiquitine-proteasome pathway (Mok et al., 2015, Dogovski et al., 2015, Mbengue et al., 2015, Tilley et al., 2016). Nevertheless, future studies are necessary to evaluate the relevance of these three candidates for altered artemisinin susceptibility. For instance, the generation of parasite strains either lacking or over-expressing the respective genes would be interesting.

4.2.3 Interaction partners of *Pf*AOP

The findings from the kinetic characterization as well as the analysis of the 3D7Δ*pfaop* knockout parasites suggest that *Pf*AOP is not only involved in the detoxification of hydroperoxides but may also exert an additional function as a redox sensor involved in signal transduction (Brigelius-Flohé and Flohé, 2011). To further test this hypothesis I sought to identify interaction partners of *Pf*AOP by analyzing parasite extracts by western blot analysis after non-reducing SDS-PAGE. Western blots of parasite extracts of 3D7 wild-type and 3D7Δ*pfaop* knockout parasites revealed that the α*Pf*AOP antibody is not suited for this purpose as several higher molecular weight bands were detected, which also appeared in the blots with the 3D7Δ*pfaop* knockout parasite extracts and therefore were identified as unspecific bands. Thus, I decided to use parasite strains over-expressing fusion constructs between different parts of *PFAOP* and GFP. These constructs could be detected with a αGFP antibody and, furthermore, their different localization properties could be taken into

account. Using the αGFP antibody and different *PFAOP* over-expressing parasite strains, one specific *Pf*AOP-GFP band was detected but no bands corresponding to possible interaction partners. After peroxide challenge with *t*-BOOH, a faint band above the *Pf*AOP-GFP band was detected in the strain localizing to the cytosol (Δ-Nterm-AOP) but not in the one that localizes to the apicoplast (Fl-AOP). This band appeared and disappeared depending on the concentration and time of the *t*-BOOH challenge. Hence, this band represents *Pf*AOP-GFP disulfide-bonded to a protein with a size of approximately 15-20 kDa. Furthermore, the interaction with this protein is induced by oxidative challenge. Therefore, the protein could be involved in the catalytic cycle of *Pf*AOP or in peroxide-induced *Pf*AOP-dependent signal transduction. For other Prx it was shown that they interact with transcription factors, kinases or other redox proteins (Iwai et al., 2010, Jarvis et al., 2012, Greetham et al., 2013, Sobotta et al., 2015). If the interaction partner is part of the catalytic cycle it could be *Pf*Grx that is involved in the reductive half-reaction. If the interaction partner is part of a redox relay involved in redox sensing many other proteins are possible. For the identification of the interaction partner further experiments such as pull-down assays in combination with proteomic analyses are necessary.

5 Conclusion and Outlook

Based on different mutants of *Pf*AOP I could identify a modularly effect of Leu109 and Cys143 on *Pf*AOP catalysis and inactivation. Although the formation of the sulfenic acid form of the peroxidatic cysteine residue was unaffected by the mutation of these residues, I could show that both residues most likely alter the equilibrium between the fully folded conformation and the locally unfolded conformation of helix α2. This affects the overall reactivity of the enzymes and their susceptibility to inactivation (Staudacher et al., 2015). Furthermore, GSH could be identified as the first substrate of the rate limiting reductive half-reaction. The identification of *Pf*AOP^{L109M} as a more active and more durable enzyme regarding inactivation *in vitro* suggests that the wild-type enzyme may exert an additional function *in vivo*, e.g. as a possible signal transducer in redox signaling.

Next, based on our *in vitro* enzyme kinetic measurements, I generated genetically encoded roGFP2 fusion constructs with the identified gain- and loss-of-function mutants of *Pf*AOP. With these constructs, I could show that *in vitro* k_{cat}^{app} values and inactivation properties correlate with the roGFP2 readout inside living cells. Hence, fusion constructs between roGFP2 and Prx can be used to asses kinetic properties of Prx *in vivo* (Staudacher et al., 2018). Furthermore, these results might be useful for the evaluation of the relevance of post-translational protein modifications on enzyme catalysis, the optimization of redox sensors and the estimation of absolute intracellular hydroperoxide concentrations in future studies.

P. falciparum 3D7Δ*pfaop* knockout parasites did not reveal the physiological relevance of *Pf*AOP. The enzyme is dispensable for the growth of asexual blood stage parasites in cell culture and the parasite´s ability to remove external oxidants was also unaffected by the loss of *Pf*AOP. Furthermore, I could rebut the hypothesis that *Pf*AOP might contribute to artemisinin resistance because IC_{50} values and ring stage survival rates were identical in wild-type and knockout parasites (Djuika et al., 2017). This hypothesis was based on a quantitative trait locus analysis in which a locus encoding *PFAOP* together with 48 other genes was identified. It remains to be shown if one of the other identified genes is associated with altered artemisinin susceptibility.

To further assess the physiological relevance of *Pf*AOP, the analysis of the complete life-cycle of the 3D7Δ*pfaop* strain or a *P. falciparum* strain, encoding *Pf*AOP^{L109M}, would be interesting.

With these experiments, an additional function of *Pf*AOP as a potential redox sensor could also be investigated.

Western-blot analyses of *P. falciparum* 3D7 strains with up-regulated *Pf*AOP-GFP revealed an additional band, corresponding to *Pf*AOP coupled to another cytosolic protein. The interaction was observed after peroxide challenge and is, thus, redox-dependent. The interaction partner could be a protein involved in the catalytic cycle of *Pf*AOP or a protein that is part of a redox relay involved in redox sensing and signal transduction. The identification of this protein would be quite interesting but requires further experiments such as pull-down assays and proteomic analyses.

6 References

AKERMAN, S. E. & MÜLLER, S. 2003. 2-Cys peroxiredoxin PfTrx-Px1 is involved in the antioxidant defence of Plasmodium falciparum. *Mol Biochem Parasitol,* 130**,** 75-81.

ANTONY, H. A. & PARIJA, S. C. 2016. Antimalarial drug resistance: An overview. *Trop Parasitol,* 6**,** 30-41.

ANTUNES, F. & CADENAS, E. 2000. Estimation of H2O2 gradients across biomembranes. *FEBS Lett,* 475**,** 121-126.

ARIEY, F., WITKOWSKI, B., AMARATUNGA, C., BEGHAIN, J., LANGLOIS, A.-C., KHIM, N., KIM, S., DURU, V., BOUCHIER, C., MA, L., LIM, P., LEANG, R., DUONG, S., SRENG, S., SUON, S., CHUOR, C. M., BOUT, D. M., MENARD, S., ROGERS, W. O., GENTON, B., FANDEUR, T., MIOTTO, O., RINGWALD, P., LE BRAS, J., BERRY, A., BARALE, J.-C., FAIRHURST, R. M., BENOIT-VICAL, F., MERCEREAU-PUIJALON, O. & MENARD, D. 2014. A molecular marker of artemisinin-resistant Plasmodium falciparum malaria. *Nature,* 505**,** 50-55.

ARISUE, N. & HASHIMOTO, T. 2015. Phylogeny and evolution of apicoplasts and apicomplexan parasites. *Parasitol Int,* 64**,** 254-259.

ASHLEY , E. A., DHORDA , M., FAIRHURST , R. M., AMARATUNGA , C., LIM , P., SUON , S., SRENG , S., ANDERSON , J. M., MAO , S., SAM , B., SOPHA , C., CHUOR , C. M., NGUON , C., SOVANNAROTH , S., PUKRITTAYAKAMEE , S., JITTAMALA , P., CHOTIVANICH , K., CHUTASMIT , K., SUCHATSOONTHORN , C., RUNCHAROEN , R., HIEN , T. T., THUY-NHIEN , N. T., THANH , N. V., PHU , N. H., HTUT , Y., HAN , K.-T., AYE , K. H., MOKUOLU , O. A., OLAOSEBIKAN , R. R., FOLARANMI , O. O., MAYXAY , M., KHANTHAVONG , M., HONGVANTHONG , B., NEWTON , P. N., ONYAMBOKO , M. A., FANELLO , C. I., TSHEFU , A. K., MISHRA , N., VALECHA , N., PHYO , A. P., NOSTEN , F., YI , P., TRIPURA , R., BORRMANN , S., BASHRAHEIL , M., PESHU , J., FAIZ , M. A., GHOSE , A., HOSSAIN , M. A., SAMAD , R., RAHMAN , M. R., HASAN , M. M., ISLAM , A., MIOTTO , O., AMATO , R., MACINNIS , B., STALKER , J., KWIATKOWSKI , D. P., BOZDECH , Z., JEEYAPANT , A., CHEAH , P. Y., SAKULTHAEW , T., CHALK , J., INTHARABUT , B., SILAMUT , K., LEE , S. J., VIHOKHERN , B., KUNASOL , C., IMWONG , M., TARNING , J., TAYLOR , W. J., YEUNG , S., WOODROW , C. J., FLEGG , J. A., DAS , D., SMITH , J., VENKATESAN , M., PLOWE , C. V., STEPNIEWSKA , K., GUERIN , P. J., DONDORP , A. M., DAY , N. P. & WHITE , N. J. 2014. Spread of Artemisinin Resistance in Plasmodium falciparum Malaria. *N Engl J Med,* 371**,** 411-423.

ATAMNA, H. & GINSBURG, H. 1997. The Malaria Parasite Supplies Glutathione to its Host Cell — Investigation of Glutathione Transport and Metabolism in Human Erythrocytes Infected with Plasmodium Falciparum. *Eur J Biochem,* 250**,** 670-679.

BANNISTER, L. & MITCHELL, G. 2003. The ins, outs and roundabouts of malaria. *Trends Parasitol,* 19**,** 209-213.

BANNISTER, L. H., HOPKINS, J. M., FOWLER, R. E., KRISHNA, S. & MITCHELL, G. H. 2000. A Brief Illustrated Guide to the Ultrastructure of Plasmodium falciparum Asexual Blood Stages. *Parasitol Today,* 16**,** 427-433.

BARNES, D. A., FOOTE, S. J., GALATIS, D., KEMP, D. J. & COWMAN, A. F. 1992. Selection for high-level chloroquine resistance results in deamplification of the

pfmdr1 gene and increased sensitivity to mefloquine in Plasmodium falciparum. *EMBO J,* 11**,** 3067-3075.
BECK, H.-P. 2002. Extraction and Purification of Plasmodium Parasite DNA. *In:* DOOLAN, D. L. (ed.) *Malaria Methods and Protocols: Methods and Protocols.* Totowa, NJ: Humana Press.
BECKER, K., RAHLFS, S., NICKEL, C. & SCHIRMER, R. H. 2003. Glutathione – Functions and Metabolism in the Malarial Parasite Plasmodium falciparum. *Biol Chem,* 384**,** 551-566.
BECKER, K., TILLEY, L., VENNERSTROM, J. L., ROBERTS, D., ROGERSON, S. & GINSBURG, H. 2004. Oxidative stress in malaria parasite-infected erythrocytes: host–parasite interactions. *Int J Parasitol,* 34**,** 163-189.
BECKMAN, J. S., BECKMAN, T. W., CHEN, J., MARSHALL, P. A. & FREEMAN, B. A. 1990. Apparent hydroxyl radical production by peroxynitrite: implications for endothelial injury from nitric oxide and superoxide. *Proc Natl Acad Sci,* 87**,** 1620-1624.
BEGAS, P., STAUDACHER, V. & DEPONTE, M. 2015. Systematic re-evaluation of the bis(2-hydroxyethyl)disulfide (HEDS) assay reveals an alternative mechanism and activity of glutaredoxins. *Chem Sci,* 6**,** 3788-3796.
BELOUSOV, V. V., FRADKOV, A. F., LUKYANOV, K. A., STAROVEROV, D. B., SHAKHBAZOV, K. S., TERSKIKH, A. V. & LUKYANOV, S. 2006. Genetically encoded fluorescent indicator for intracellular hydrogen peroxide. *Nat Meth,* 3**,** 281-286.
BENTING, J., MATTEI, D. & LINGELBACH, K. 1994. Brefeldin A inhibits transport of the glycophorin-binding protein from Plasmodium falciparum into the host erythrocyte. *Biochem J,* 300**,** 821-826.
BIAGINI, G. A., BRAY, P. G., SPILLER, D. G., WHITE, M. R. H. & WARD, S. A. 2003. The Digestive Food Vacuole of the Malaria Parasite Is a Dynamic Intracellular Ca2+ Store. *J Biol Chem,* 278**,** 27910-27915.
BIRBEN, E., SAHINER, U. M., SACKESEN, C., ERZURUM, S. & KALAYCI, O. 2012. Oxidative Stress and Antioxidant Defense. *World Allergy Organ J,* 5**,** 9-19.
BIRNBOIM, H. C. & DOLY, J. 1979. A rapid alkaline extraction procedure for screening recombinant plasmid DNA. *Nucleic Acids Res,* 7**,** 1513-1523.
BLACKMAN, M. J. & BANNISTER, L. H. 2001. Apical organelles of Apicomplexa: biology and isolation by subcellular fractionation. *Mol Biochem Parasitol,* 117**,** 11-25.
BOUCHER, I. W., MCMILLAN, P. J., GABRIELSEN, M., AKERMAN, S. E., BRANNIGAN, J. A., SCHNICK, C., BRZOZOWSKI, A. M., WILKINSON, A. J. & MÜLLER, S. 2006. Structural and biochemical characterization of a mitochondrial peroxiredoxin from Plasmodium falciparum. *Mol Microbiol,* 61**,** 948-959.
BRADFORD, M. M. 1976. A rapid and sensitive method for the quantitation of microgram quantities of protein utilizing the principle of protein-dye binding. *Anal Biochem,* 72**,** 248-254.
BRANCO, M. R., MARINHO, H. S., CYRNE, L. & ANTUNES, F. 2004. Decrease of H2O2 Plasma Membrane Permeability during Adaptation to H2O2 in Saccharomyces cerevisiae. *J Biol Chem,* 279**,** 6501-6506.
BRIGELIUS-FLOHÉ, R. & FLOHÉ, L. 2011. Basic Principles and Emerging Concepts in the Redox Control of Transcription Factors. *Antioxid Redox Signal,* 15**,** 2335-2381.

CHAUDHARI, R., NARAYAN, A. & PATANKAR, S. 2012. A novel trafficking pathway in Plasmodium falciparum for the organellar localization of glutathione peroxidase-like thioredoxin peroxidase. *FEBS J,* 279**,** 3872-3888.

CHAUDHARI, R., SHARMA, S. & PATANKAR, S. 2017. Glutathione and thioredoxin systems of the malaria parasite Plasmodium falciparum: Partners in crime? *Biochem Biophys Res Commun,* 488**,** 95-100.

CHO, C.-S., YOON, H. J., KIM, J. Y., WOO, H. A. & RHEE, S. G. 2014. Circadian rhythm of hyperoxidized peroxiredoxin II is determined by hemoglobin autoxidation and the 20S proteasome in red blood cells. *Proc Nat Acad Sci U S A,* 111**,** 12043-12048.

CHUANG, M.-H., WU, M.-S., LO, W.-L., LIN, J.-T., WONG, C.-H. & CHIOU, S.-H. 2006. The antioxidant protein alkylhydroperoxide reductase of Helicobacter pylori switches from a peroxide reductase to a molecular chaperone function. *Proc Natl Acad Sci U S A,* 103**,** 2552-2557.

COWMAN, A. F., HEALER, J., MARAPANA, D. & MARSH, K. 2016. Malaria: Biology and Disease. *Cell,* 167**,** 610-624.

COX, A. G., PESKIN, A. V., PATON, L. N., WINTERBOURN, C. C. & HAMPTON, M. B. 2009. Redox Potential and Peroxide Reactivity of Human Peroxiredoxin 3. *Biochemistry,* 48**,** 6495-6501.

DAHL, E. L., SHOCK, J. L., SHENAI, B. R., GUT, J., DERISI, J. L. & ROSENTHAL, P. J. 2006. Tetracyclines Specifically Target the Apicoplast of the Malaria Parasite Plasmodium falciparum. *Antimicrob Agents Chemother,* 50**,** 3124-3131.

DEITSCH, K. W., DRISKILL, C. L. & WELLEMS, T. E. 2001. Transformation of malaria parasites by the spontaneous uptake and expression of DNA from human erythrocytes. *Nucleic Acids Res,* 29**,** 850-853.

DELAUNAY, A., PFLIEGER, D., BARRAULT, M.-B., VINH, J. & TOLEDANO, M. B. 2002. A Thiol Peroxidase Is an H2O2 Receptor and Redox-Transducer in Gene Activation. *Cell,* 111**,** 471-481.

DEPONTE, M. 2013. Glutathione catalysis and the reaction mechanisms of glutathione-dependent enzymes. *Biochim Biophys Acta,* 1830**,** 3217-3266.

DEPONTE, M. 2017. The Incomplete Glutathione Puzzle: Just Guessing at Numbers and Figures? *Antioxid Redox Signal,* 27**,** 1130-1161.

DEPONTE, M. & LILLIG, C. H. 2015. Enzymatic control of cysteinyl thiol switches in proteins. *Biol Chem,* 396**,** 401-413.

DEPONTE, M., RAHLFS, S. & BECKER, K. 2007. Peroxiredoxin Systems of Protozoal Parasites. *Subcell Biochem,* 44**,** 219-229.

DJUIKA, C. F., FIEDLER, S., SCHNOLZER, M., SANCHEZ, C., LANZER, M. & DEPONTE, M. 2013. Plasmodium falciparum antioxidant protein as a model enzyme for a special class of glutaredoxin/glutathione-dependent peroxiredoxins. *Biochim Biophys Acta,* 1830**,** 4073-4090.

DJUIKA, C. F., HUERTA-CEPAS, J., PRZYBORSKI, J. M., DEIL, S., SANCHEZ, C. P., DOERKS, T., BORK, P., LANZER, M. & DEPONTE, M. 2015. Prokaryotic ancestry and gene fusion of a dual localized peroxiredoxin in malaria parasites. *Microb Cell,* 2**,** 5-13.

DJUIKA, C. F., STAUDACHER, V., SANCHEZ, C. P., LANZER, M. & DEPONTE, M. 2017. Knockout of the peroxiredoxin 5 homologue PFAOP does not affect the artemisinin susceptibility of Plasmodium falciparum. *Sci Rep,* 7**,** 4410.

DOGOVSKI, C., XIE, S. C., BURGIO, G., BRIDGFORD, J., MOK, S., MCCAW, J. M., CHOTIVANICH, K., KENNY, S., GNÄDIG, N., STRAIMER, J., BOZDECH, Z., FIDOCK, D. A., SIMPSON, J. A., DONDORP, A. M., FOOTE, S., KLONIS, N.

& TILLEY, L. 2015. Targeting the Cell Stress Response of Plasmodium falciparum to Overcome Artemisinin Resistance. *PLOS Biol,* 13**,** e1002132.
DONDORP , A. M., NOSTEN , F., YI , P., DAS , D., PHYO , A. P., TARNING , J., LWIN , K. M., ARIEY , F., HANPITHAKPONG , W., LEE , S. J., RINGWALD , P., SILAMUT , K., IMWONG , M., CHOTIVANICH , K., LIM , P., HERDMAN , T., AN , S. S., YEUNG , S., SINGHASIVANON , P., DAY , N. P. J., LINDEGARDH , N., SOCHEAT , D. & WHITE , N. J. 2009. Artemisinin Resistance in Plasmodium falciparum Malaria. *N Engl J Med,* 361**,** 455-467.
DOUGLAS, R. G., AMINO, R., SINNIS, P. & FRISCHKNECHT, F. 2015. Active migration and passive transport of malaria parasites. *Trends Parasitol,* 31**,** 357-362.
EDGAR, R. S., GREEN, E. W., ZHAO, Y., VAN OOIJEN, G., OLMEDO, M., QIN, X., XU, Y., PAN, M., VALEKUNJA, U. K., FEENEY, K. A., MAYWOOD, E. S., HASTINGS, M. H., BALIGA, N. S., MERROW, M., MILLAR, A. J., JOHNSON, C. H., KYRIACOU, C. P., O'NEILL, J. S. & REDDY, A. B. 2012. Peroxiredoxins are conserved markers of circadian rhythms. *Nature,* 485**,** 459-464.
ESPINOSA-DIEZ, C., MIGUEL, V., MENNERICH, D., KIETZMANN, T., SÁNCHEZ-PÉREZ, P., CADENAS, S. & LAMAS, S. 2015. Antioxidant responses and cellular adjustments to oxidative stress. *Redox Biol,* 6**,** 183-197.
FAIRHURST, R. M. & DONDORP, A. M. 2016. Artemisinin-Resistant Plasmodium falciparum Malaria. *Microbiol Spectr,* 4**,** EI10-0013-2016.
FAST, N. M., KISSINGER, J. C., ROOS, D. S. & KEELING, P. J. 2001. Nuclear-encoded, plastid-targeted genes suggest a single common origin for apicomplexan and dinoflagellate plastids. *Mol Biol Evol,* 18**,** 418-426.
FLOHÉ, L., TOPPO, S., COZZA, G. & URSINI, F. 2011. A Comparison of Thiol Peroxidase Mechanisms. *Antioxid Redox Signal,* 15**,** 763-780.
FOLMER, V., PEDROSO, N., MATIAS, A. C., LOPES, S. C. D. N., ANTUNES, F., CYRNE, L. & MARINHO, H. S. 2008. H2O2 induces rapid biophysical and permeability changes in the plasma membrane of Saccharomyces cerevisiae. *Biochim Biophys Acta,* 1778**,** 1141-1147.
FOTH, B. J. & MCFADDEN, G. I. 2003. The apicoplast: A plastid in Plasmodium falciparum and other apicomplexan parasites. *Int Rev Cytol,* 224**,** 57-110.
FRISCHKNECHT, F., BALDACCI, P., MARTIN, B., ZIMMER, C., THIBERGE, S., OLIVO-MARIN, J.-C., SHORTE, S. L. & MÉNARD, R. 2004. Imaging movement of malaria parasites during transmission by Anopheles mosquitoes. *Cell Microbiol,* 6**,** 687-694.
GISSELBERG, J. E., DELLIBOVI-RAGHEB, T. A., MATTHEWS, K. A., BOSCH, G. & PRIGGE, S. T. 2013. The Suf Iron-Sulfur Cluster Synthesis Pathway Is Required for Apicoplast Maintenance in Malaria Parasites. *PLoS Pathog,* 9**,** e1003655.
GREETHAM, D., KRITSILIGKOU, P., WATKINS, R. H., CARTER, Z., PARKIN, J. & GRANT, C. M. 2013. Oxidation of the Yeast Mitochondrial Thioredoxin Promotes Cell Death. *Antioxid Redox Signal,* 18**,** 376-385.
GREGSON, A. & PLOWE, C. V. 2005. Mechanisms of Resistance of Malaria Parasites to Antifolates. *Pharmacol Rev,* 57**,** 117-145.
GRETES, M. C. P., LESLIE B.; KARPLUS, P. ANDREW 2012. Peroxiredoxins in Parasites. *Antioxid Redox Signal,* 17**,** 608-633.
GRIESBECK, O. 2004. Fluorescent proteins as sensors for cellular functions. *Curr Opin Neurobiol,* 14**,** 636-641.

GUPTA, P., MEHROTRA, S., SHARMA, A., CHUGH, M., PANDEY, R., KAUSHIK, A., KHURANA, S., SRIVASTAVA, N., SRIVASTAVA, T., DESHMUKH, A., PANDA, A., AGGARWAL, P., BHAVESH, N. S., BHATNAGAR, R. K., MOHMMED, A., GUPTA, D. & MALHOTRA, P. 2017. Exploring Heme and Hemoglobin Binding Regions of Plasmodium Heme Detoxification Protein for New Antimalarial Discovery. *J Med Chem,* 60**,** 8298-8308.

GUTSCHER, M., PAULEAU, A.-L., MARTY, L., BRACH, T., WABNITZ, G. H., SAMSTAG, Y., MEYER, A. J. & DICK, T. P. 2008. Real-time imaging of the intracellular glutathione redox potential. *Nat Meth,* 5**,** 553-559.

GUTSCHER, M., SOBOTTA, M. C., WABNITZ, G. H., BALLIKAYA, S., MEYER, A. J., SAMSTAG, Y. & DICK, T. P. 2009. Proximity-based Protein Thiol Oxidation by H2O2-scavenging Peroxidases. *J Biol Chem,* 284**,** 31532-31540.

HALL, A., KARPLUS, P. A. & POOLE, L. B. 2009. Typical 2-Cys Peroxiredoxins: Structures, mechanisms and functions. *FEBS J,* 276**,** 2469-2477.

HALL, A., NELSON, K., POOLE, L. B. & KARPLUS, P. A. 2011. Structure-based Insights into the Catalytic Power and Conformational Dexterity of Peroxiredoxins. *Antioxid Redox Signal,* 15**,** 795-815.

HUGO, M., TURELL, L., MANTA, B., BOTTI, H., MONTEIRO, G., NETTO, L. E., ALVAREZ, B., RADI, R. & TRUJILLO, M. 2009. Thiol and sulfenic acid oxidation of AhpE, the one-cysteine peroxiredoxin from Mycobacterium tuberculosis: kinetics, acidity constants, and conformational dynamics. *Biochemistry,* 48**,** 9416-9426.

IMLAY, J. A. 2003. Pathways of Oxidative Damage. *Annu Rev Microbiol,* 57**,** 395-418.

IMLAY, J. A. 2013. The molecular mechanisms and physiological consequences of oxidative stress: lessons from a model bacterium. *Nat Rev Microbiol,* 11**,** 443-454.

ISMAIL, H. M., BARTON, V., PHANCHANA, M., CHAROENSUTTHIVARAKUL, S., WONG, M. H. L., HEMINGWAY, J., BIAGINI, G. A., O'NEILL, P. M. & WARD, S. A. 2016. Artemisinin activity-based probes identify multiple molecular targets within the asexual stage of the malaria parasites Plasmodium falciparum 3D7. *Proc Nat Acad Sci U S A,* 113**,** 2080-2085.

IWAI, K., NAGANUMA, A. & KUGE, S. 2010. Peroxiredoxin Ahp1 Acts as a Receptor for Alkylhydroperoxides to Induce Disulfide Bond Formation in the Cad1 Transcription Factor. *J Biol Chem,* 285**,** 10597-10604.

JANG, H. H., LEE, K. O., CHI, Y. H., JUNG, B. G., PARK, S. K., PARK, J. H., LEE, J. R., LEE, S. S., MOON, J. C., YUN, J. W., CHOI, Y. O., KIM, W. Y., KANG, J. S., CHEONG, G.-W., YUN, D.-J., RHEE, S. G., CHO, M. J. & LEE, S. Y. 2004. Two Enzymes in One. *Cell,* 117**,** 625-635.

JANOUŠKOVEC, J., HORÁK, A., OBORNÍK, M., LUKEŠ, J. & KEELING, P. J. 2010. A common red algal origin of the apicomplexan, dinoflagellate, and heterokont plastids. *Proc Nat Acad Sciences U S A,* 107**,** 10949-10954.

JARVIS, R. M., HUGHES, S. M. & LEDGERWOOD, E. C. 2012. Peroxiredoxin 1 functions as a signal peroxidase to receive, transduce, and transmit peroxide signals in mammalian cells. *Free Radic Biol Med,* 53**,** 1522-1530.

JOMAA, H., WIESNER, J., SANDERBRAND, S., ALTINCICEK, B., WEIDEMEYER, C., HINTZ, M., TÜRBACHOVA, I., EBERL, M., ZEIDLER, J., LICHTENTHALER, H. K., SOLDATI, D. & BECK, E. 1999. Inhibitors of the Nonmevalonate Pathway of Isoprenoid Biosynthesis as Antimalarial Drugs. *Science,* 285**,** 1573-1576.

JÖNSSON, T. J. & LOWTHER, W. T. 2007. The Peroxiredoxin Repair Proteins. *Subcell Biochem,* 44**,** 115-141.
JORTZIK, E. & BECKER, K. 2012. Thioredoxin and glutathione systems in Plasmodium falciparum. *Int J Med Microbiol,* 302**,** 187-194.
JOSLING, G. A. & LLINÁS, M. 2015. Sexual development in Plasmodium parasites: knowing when it´s time to commit. *Nat Rev Microbiol,* 13**,** 573-587.
KALANON, M. & MCFADDEN, GEOFFREY I. 2010. Malaria, *Plasmodium falciparum* and its apicoplast. *Biochem Soc Transactions,* 38**,** 775-782.
KARPLUS, P. A. & POOLE, L. B. 2012. Peroxiredoxins as Molecular Triage Agents, Sacrificing Themselves to Enhance Cell Survival During a Peroxide Attack. *Mol Cell,* 45**,** 275-278.
KASOZI, D., MOHRING, F., RAHLFS, S., MEYER, A. J. & BECKER, K. 2013. Real-Time Imaging of the Intracellular Glutathione Redox Potential in the Malaria Parasite *Plasmodium falciparum*. *PLoS Pathog,* 9**,** e1003782.
KAWAZU, S.-I., IKENOUE, N., TAKEMAE, H., KOMAKI-YASUDA, K. & KANO, S. 2005. Roles of 1-Cys peroxiredoxin in haem detoxification in the human malaria parasite Plasmodium falciparum. *FEBS J,* 272**,** 1784-1791.
KAWAZU, S.-I., KOMAKI-YASUDA, K., OKU, H. & KANO, S. 2008. Peroxiredoxins in malaria parasites: Parasitologic aspects. *Parasitol Int,* 57**,** 1-7.
KAWAZU, S.-I., NOZAKI, T., TSUBOI, T., NAKANO, Y., KOMAKI-YASUDA, K., IKENOUE, N., TORII, M. & KANO, S. 2003. Expression profiles of peroxiredoxin proteins of the rodent malaria parasite Plasmodium yoelii. *Int J Parasitol,* 33**,** 1455-1461.
KAWAZU, S.-I., TSUJI, N., HATABU, T., KAWAI, S., MATSUMOTO, Y. & KANO, S. 2000. Molecular cloning and characterization of a peroxiredoxin from the human malaria parasite Plasmodium falciparum. *Mol Biochem Parasitol,* 109**,** 165-169.
KEHR, S., STURM, N., RAHLFS, S., PRZYBORSKI, J. M. & BECKER, K. 2010. Compartmentation of Redox Metabolism in Malaria Parasites. *PLoS Pathog,* 6**,** e1001242.
KITE, W. A., MELENDEZ-MUNIZ, V. A., MORAES BARROS, R. R., WELLEMS, T. E. & SÁ, J. M. 2016. Alternative methods for the Plasmodium falciparum artemisinin ring-stage survival assay with increased simplicity and parasite stage-specificity. *Malar J,* 15**,** 94.
KLUG, D. & FRISCHKNECHT, F. 2017. Motility precedes egress of malaria parasites from oocysts. *Elife,* 6**,** e19157.
KOMAKI-YASUDA, K., KAWAZU, S.-I. & KANO, S. 2003. Disruption of the Plasmodium falciparum 2-Cys peroxiredoxin gene renders parasites hypersensitive to reactive oxygen and nitrogen species. *FEBS Lett,* 547**,** 140-144.
KONCAREVIC, S., ROHRBACH, P., DEPONTE, M., KROHNE, G., PRIETO, J. H., YATES, J., RAHLFS, S. & BECKER, K. 2009. The malarial parasite Plasmodium falciparum imports the human protein peroxiredoxin 2 for peroxide detoxification. *Proc Natl Acad Sci,* 106**,** 13323-13328.
KORSINCZKY, M., CHEN, N., KOTECKA, B., SAUL, A., RIECKMANN, K. & CHENG, Q. 2000. Mutations in Plasmodium falciparum Cytochrome b That Are Associated with Atovaquone Resistance Are Located at a Putative Drug-Binding Site. *Antimicrob Agents Chemother,* 44**,** 2100-2108.
KRAUTH-SIEGEL, R. L., BAUER, H. & SCHIRMER, R. H. 2005. Dithiol Proteins as Guardians of the Intracellular Redox Milieu in Parasites: Old and New Drug

Targets in Trypanosomes and Malaria-Causing Plasmodia. *Angew Chem Int Ed,* 44**,** 690-715.
KRNAJSKI, Z., WALTER, R. D. & MÜLLER, S. 2001. Isolation and functional analysis of two thioredoxin peroxidases (peroxiredoxins) from Plasmodium falciparum. *Mol Biochem Parasitol,* 113**,** 303-308.
LAEMMLI, U. K. 1970. Cleavage of Structural Proteins during the Assembly of the Head of Bacteriophage T4. *Nature,* 227**,** 680-685.
LAMBROS, C. & VANDERBERG, J. P. 1979. Synchronization of Plasmodium falciparum Erythrocytic Stages in Culture. *J Parasitol,* 65**,** 418-420.
LEMGRUBER, L., KUDRYASHEV, M., DEKIWADIA, C., RIGLAR, D. T., BAUM, J., STAHLBERG, H., RALPH, S. A. & FRISCHKNECHT, F. 2013. Cryo-electron tomography reveals four-membrane architecture of the Plasmodium apicoplast. *Malar J,* 12**,** 25.
LIM, L. & MCFADDEN, G. I. 2010. The evolution, metabolism and functions of the apicoplast. *Philos Trans R Soc B Biol Sci,* 365**,** 749-763.
MAKINO, N., SASAKI, K., HASHIDA, K. & SAKAKURA, Y. 2004. A metabolic model describing the H2O2 elimination by mammalian cells including H2O2 permeation through cytoplasmic and peroxisomal membranes: comparison with experimental data. *Biochim Biophys Acta,* 1673**,** 149-159.
MARSH , K., FORSTER , D., WARUIRU , C., MWANGI , I., WINSTANLEY , M., MARSH , V., NEWTON , C., WINSTANLEY , P., WARN , P., PESHU , N., PASVOL , G. & SNOW , R. 1995. Indicators of Life-Threatening Malaria in African Children. *N Engl J Med,* 332**,** 1399-1404.
MASUDA-SUGANUMA, H., USUI, M., FUKUMOTO, S., INOUE, N. & KAWAZU, S.-I. 2012. Mitochondrial peroxidase TPx-2 is not essential in the blood and insect stages of Plasmodium berghei. *Parasit Vectors,* 5**,** 252.
MBENGUE, A., BHATTACHARJEE, S., PANDHARKAR, T., LIU, H., ESTIU, G., STAHELIN, R. V., RIZK, S. S., NJIMOH, D. L., RYAN, Y., CHOTIVANICH, K., NGUON, C., GHORBAL, M., LOPEZ-RUBIO, J.-J., PFRENDER, M., EMRICH, S., MOHANDAS, N., DONDORP, A. M., WIEST, O. & HALDAR, K. 2015. A molecular mechanism of artemisinin resistance in Plasmodium falciparum malaria. *Nature,* 520**,** 683-687.
MOK, S., ASHLEY, E. A., FERREIRA, P. E., ZHU, L., LIN, Z., YEO, T., CHOTIVANICH, K., IMWONG, M., PUKRITTAYAKAMEE, S., DHORDA, M., NGUON, C., LIM, P., AMARATUNGA, C., SUON, S., HIEN, T. T., HTUT, Y., FAIZ, M. A., ONYAMBOKO, M. A., MAYXAY, M., NEWTON, P. N., TRIPURA, R., WOODROW, C. J., MIOTTO, O., KWIATKOWSKI, D. P., NOSTEN, F., DAY, N. P. J., PREISER, P. R., WHITE, N. J., DONDORP, A. M., FAIRHURST, R. M. & BOZDECH, Z. 2015. Population transcriptomics of human malaria parasites reveals the mechanism of artemisinin resistance. *Science,* 347**,** 431-435.
MOORE, R. B., OBORNÍK, M., JANOUŠKOVEC, J., CHRUDIMSKÝ, T., VANCOVÁ, M., GREEN, D. H., WRIGHT, S. W., DAVIES, N. W., BOLCH, C. J. S., HEIMANN, K., ŠLAPETA, J., HOEGH-GULDBERG, O., LOGSDON, J. M. & CARTER, D. A. 2008. A photosynthetic alveolate closely related to apicomplexan parasites. *Nature,* 451**,** 959-963.
MORGAN, B., EZERINA, D., AMOAKO, T. N., RIEMER, J., SEEDORF, M. & DICK, T. P. 2013. Multiple glutathione disulfide removal pathways mediate cytosolic redox homeostasis. *Nat Chem Biol,* 9**,** 119-125.
MORGAN, B., SOBOTTA, M. C. & DICK, T. P. 2011. Measuring E(GSH) and H2O2 with roGFP2-based redox probes. *Free Radic Biol Med,* 51**,** 1943-1951.

MORGAN, B., VAN LAER, K., OWUSU, T. N., EZERINA, D., PASTOR-FLORES, D., AMPONSAH, P. S., TURSCH, A. & DICK, T. P. 2016. Real-time monitoring of basal H2O2 levels with peroxiredoxin-based probes. *Nat Chem Biol,* 12**,** 437-443.

MORRISON, D. A. 2009. Evolution of the Apicomplexa: where are we now? *Trends Parasitol,* 25**,** 375-382.

MOTA, M. M. & RODRIGUEZ, A. 2004. Migration through host cells: the first steps of Plasmodium sporozoites in the mammalian host. *Cell Microbiol,* 6**,** 1113-1118.

MÜLLER, S. 2004. Redox and antioxidant systems of the malaria parasite Plasmodium falciparum. *Mol Microbiol,* 53**,** 1291-1305.

NAGAI, S. & BLACK, S. 1968. A Thiol-Disulfide Transhydrogenase from Yeast. *J Biol Chem,* 243**,** 1942-1947.

NAGY, P., KARTON, A., BETZ, A., PESKIN, A. V., PACE, P., O'REILLY, R. J., HAMPTON, M. B., RADOM, L. & WINTERBOURN, C. C. 2011. Model for the exceptional reactivity of peroxiredoxins 2 and 3 with hydrogen peroxide: a kinetic and computational study. *J Biol Chem,* 286**,** 18048-18055.

NELSON, K. J., KNUTSON, S. T., SOITO, L., KLOMSIRI, C., POOLE, L. B. & FETROW, J. S. 2011. Analysis of the peroxiredoxin family: using active site structure and sequence information for global classification and residue analysis. *Proteins,* 79**,** 947-964.

NICKEL, C., RAHLFS, S., DEPONTE, M., KONCAREVIC, S. & BECKER, K. 2006. Thioredoxin networks in the malarial parasite Plasmodium falciparum. *Antioxid Redox Signal,* 8**,** 1227-1239.

NICKEL, C., TRUJILLO, M., RAHLFS, S., DEPONTE, M., RADI, R. & BECKER, K. 2005. Plasmodium falciparum 2-Cys peroxiredoxin reacts with plasmoredoxin and peroxynitrite. *Biol Chem,* 386**,** 1129-1136.

O'NEILL, J. S. & REDDY, A. B. 2011. Circadian clocks in human red blood cells. *Nature,* 469**,** 498-503.

OBORNÍK, M., MODRÝ, D., LUKEŠ, M., ČERNOTÍKOVÁ-STŘÍBRNÁ, E., CIHLÁŘ, J., TESAŘOVÁ, M., KOTABOVÁ, E., VANCOVÁ, M., PRÁŠIL, O. & LUKEŠ, J. 2012. Morphology, Ultrastructure and Life Cycle of Vitrella brassicaformis n. sp., n. gen., a Novel Chromerid from the Great Barrier Reef. *Protist,* 163**,** 306-323.

OGUSUCU, R., RETTORI, D., MUNHOZ, D. C., NETTO, L. E. & AUGUSTO, O. 2007. Reactions of yeast thioredoxin peroxidases I and II with hydrogen peroxide and peroxynitrite: rate constants by competitive kinetics. *Free Radic Biol Med,* 42**,** 326-334.

ØSTERGAARD, H., HENRIKSEN, A., HANSEN, F. G. & WINTHER, J. R. 2001. Shedding light on disulfide bond formation: engineering a redox switch in green fluorescent protein. *EMBO J,* 20**,** 5853-5862.

PARSONAGE, D., NELSON, K. J., FERRER-SUETA, G., ALLEY, S., KARPLUS, P. A., FURDUI, C. M. & POOLE, L. B. 2015. Dissecting peroxiredoxin catalysis: separating binding, peroxidation, and resolution for a bacterial AhpC. *Biochemistry,* 54**,** 1567-1575.

PERKINS, A., NELSON, K. J., WILLIAMS, J. R., PARSONAGE, D., POOLE, L. B. & KARPLUS, P. A. 2013. The Sensitive Balance Between the Fully Folded and Locally Unfolded Conformations of a Model Peroxiredoxin(). *Biochemistry,* 52**,** 8708-8721.

PERKINS, A., PARSONAGE, D., NELSON, KIMBERLY J., OGBA, O. M., CHEONG, PAUL H.-Y., POOLE, LESLIE B. & KARPLUS, P. A. 2016. Peroxiredoxin Catalysis at Atomic Resolution. *Structure,* 24**,** 1668-1678.

PERKINS, A., POOLE, L. B. & KARPLUS, P. A. 2014. Tuning of Peroxiredoxin Catalysis for Various Physiological Roles. *Biochemistry,* 53**,** 7693-7705.
PESKIN, A. V., DICKERHOF, N., POYNTON, R. A., PATON, L. N., PACE, P. E., HAMPTON, M. B. & WINTERBOURN, C. C. 2013. Hyperoxidation of peroxiredoxins 2 and 3: rate constants for the reactions of the sulfenic acid of the peroxidatic cysteine. *J Biol Chem,* 288**,** 14170-14177.
PETERSEN, I., EASTMAN, R. & LANZER, M. 2011. Drug-resistant malaria: Molecular mechanisms and implications for public health. *FEBS Lett,* 585**,** 1551-1562.
PETERSEN, I., GABRYSZEWSKI, S. J., JOHNSTON, G. L., DHINGRA, S. K., ECKER, A., LEWIS, R. E., DE ALMEIDA, M. J., STRAIMER, J., HENRICH, P. H., PALATULAN, E., JOHNSON, D. J., COBURN-FLYNN, O., SANCHEZ, C., LEHANE, A. M., LANZER, M. & FIDOCK, D. A. 2015. Balancing drug resistance and growth rates via compensatory mutations in the Plasmodium falciparum chloroquine resistance transporter. *Mol Microbiol,* 97**,** 381-395.
PINO, P., FOTH, B. J., KWOK, L.-Y., SHEINER, L., SCHEPERS, R., SOLDATI, T. & SOLDATI-FAVRE, D. 2007. Dual Targeting of Antioxidant and Metabolic Enzymes to the Mitochondrion and the Apicoplast of Toxoplasma gondii. *PLoS Pathog,* 3**,** e115.
POOLE, L. B., HALL, A. & NELSON, K. J. 2011. Overview of Peroxiredoxins in oxidant defense and redox regulation. *Curr Protoc Toxicol,* CHAPTER**,** Unit7.9-Unit7.9.
POYNTON, R. A. & HAMPTON, M. B. 2014. Peroxiredoxins as biomarkers of oxidative stress. *Biochim Biophys Acta,* 1840**,** 906-912.
PRADHAN, A., SIWO, G. H., SINGH, N., MARTENS, B., BALU, B., BUTTON-SIMONS, K. A., TAN, A., ZHANG, M., UDENZE, K. O., JIANG, R. H. Y., FERDIG, M. T., ADAMS, J. H. & KYLE, D. E. 2015. Chemogenomic profiling of Plasmodium falciparum as a tool to aid antimalarial drug discovery. *Sci Rep,* 5**,** 15930.
PREISER, P., KAVIRATNE, M., KHAN, S., BANNISTER, L. & JARRA, W. 2000. The apical organelles of malaria merozoites: host cell selection, invasion, host immunity and immune evasion. *Microbes Infect,* 2**,** 1461-1477.
RADI, R., BECKMAN, J. S., BUSH, K. M. & FREEMAN, B. A. 1991. Peroxynitrite oxidation of sulfhydryls. The cytotoxic potential of superoxide and nitric oxide. *J Biol Chem,* 266**,** 4244-4250.
RALPH, S. A., VAN DOOREN, G. G., WALLER, R. F., CRAWFORD, M. J., FRAUNHOLZ, M. J., FOTH, B. J., TONKIN, C. J., ROOS, D. S. & MCFADDEN, G. I. 2004. Tropical infectious diseases: Metabolic maps and functions of the Plasmodium falciparum apicoplast. *Nat Rev Microbiol,* 2**,** 203-216.
RAMYA, T. N. C., MISHRA, S., KARMODIYA, K., SUROLIA, N. & SUROLIA, A. 2007. Inhibitors of Nonhousekeeping Functions of the Apicoplast Defy Delayed Death in Plasmodium falciparum. *Antimicrob Agents Chemother,* 51**,** 307-316.
RHEE, S. G. 2016. Overview on Peroxiredoxin. *Mol Cells,* 39**,** 1-5.
RHEE, S. G., KANG, S. W., CHANG, T.-S., JEONG, W. & KIM, K. 2001. Peroxiredoxin, a Novel Family of Peroxidases. *IUBMB Life,* 52**,** 35-41.
RHEE, S. G. & WOO, H. A. 2011. Multiple Functions of Peroxiredoxins: Peroxidases, Sensors and Regulators of the Intracellular Messenger H2O2, and Protein Chaperones. *Antioxid Redox Signal,* 15**,** 781-794.

RICHARD, D., BARTFAI, R., VOLZ, J., RALPH, S. A., MULLER, S., STUNNENBERG, H. G. & COWMAN, A. F. 2011. A Genome-wide Chromatin-associated Nuclear Peroxiredoxin from the Malaria Parasite Plasmodium falciparum. *J Biol Chem,* 286**,** 11746-11755.

SARMA, G. N., NICKEL, C., RAHLFS, S., FISCHER, M., BECKER, K. & KARPLUS, P. A. 2005. Crystal Structure of a Novel Plasmodium falciparum 1-Cys Peroxiredoxin. *J Mol Biol,* 346**,** 1021-1034.

SAYED, A. A. & WILLIAMS, D. L. 2004. Biochemical Characterization of 2-Cys Peroxiredoxins from Schistosoma mansoni. *J Biol Chem,* 279**,** 26159-26166.

SCHANTZ-DUNN, J. & NOUR, N. M. 2009. Malaria and Pregnancy: A Global Health Perspective. *Rev Obstet Gynecol,* 2**,** 186-192.

SCHWARTZ, E. 2012. Prophylaxis of Malaria. *Mediterr J Hematol Infect Dis,* 4**,** e2012045.

SCHWARZLANDER, M., DICK, T. P., MEYER, A. J. & MORGAN, B. 2016. Dissecting Redox Biology Using Fluorescent Protein Sensors. *Antioxid Redox Signal,* 24**,** 680-712.

SEAVER, L. C. & IMLAY, J. A. 2001. Hydrogen Peroxide Fluxes and Compartmentalization inside Growing Escherichia coli. *J Bacteriol,* 183**,** 7182-7189.

SIDHU, A. B. S., VERDIER-PINARD, D. & FIDOCK, D. A. 2002. Chloroquine Resistance in Plasmodium falciparum Malaria Parasites Conferred by pfcrt Mutations. *Science,* 298**,** 210-213.

SIENKIEWICZ, N., DAHER, W., DIVE, D., WRENGER, C., VISCOGLIOSI, E., WINTJENS, R., JOUIN, H., CAPRON, M., MÜLLER, S. & KHALIFE, J. 2004. Identification of a mitochondrial superoxide dismutase with an unusual targeting sequence in Plasmodium falciparum. *Mol Biochem Parasitol,* 137**,** 121-132.

SIES, H. 1986. Biochemistry of Oxidative Stress. *Angew Chem Int Ed,* 25**,** 1058-1071.

SIES, H. 1993. Strategies of antioxidant defense. *Eur J Biochem,* 215**,** 213-219.

SINDEN, R. E. & BILLINGSLEY, P. F. 2001. Plasmodium invasion of mosquito cells: hawk or dove? *Trends Parasitol,* 17**,** 209-211.

SINKA, M. E., BANGS, M. J., MANGUIN, S., RUBIO-PALIS, Y., CHAREONVIRIYAPHAP, T., COETZEE, M., MBOGO, C. M., HEMINGWAY, J., PATIL, A. P., TEMPERLEY, W. H., GETHING, P. W., KABARIA, C. W., BURKOT, T. R., HARBACH, R. E. & HAY, S. I. 2012. A global map of dominant malaria vectors. *Parasit Vectors,* 5**,** 69.

SMILKSTEIN, M., SRIWILAIJAROEN, N., KELLY, J. X., WILAIRAT, P. & RISCOE, M. 2004. Simple and Inexpensive Fluorescence-Based Technique for High-Throughput Antimalarial Drug Screening. *Antimicrob Agents Chemother,* 48**,** 1803-1806.

SOBOTTA, M. C., LIOU, W., STÖCKER, S., TALWAR, D., OEHLER, M., RUPPERT, T., SCHARF, A. N. D. & DICK, T. P. 2015. Peroxiredoxin-2 and STAT3 form a redox relay for H2O2 signaling. *Nat Chem Biol,* 11**,** 64-70.

SOITO, L., WILLIAMSON, C., KNUTSON, S. T., FETROW, J. S., POOLE, L. B. & NELSON, K. J. 2011. PREX: PeroxiRedoxin classification indEX, a database of subfamily assignments across the diverse peroxiredoxin family. *Nucleic Acids Research,* 39**,** D332-D337.

STAUDACHER, V., DJUIKA, C. F., KODUKA, J., SCHLOSSAREK, S., KOPP, J., BUCHLER, M., LANZER, M. & DEPONTE, M. 2015. Plasmodium falciparum

antioxidant protein reveals a novel mechanism for balancing turnover and inactivation of peroxiredoxins. *Free Radic Biol Med,* 85**,** 228-236.
STAUDACHER, V., TRUJILLO, M., DIEDERICHS, T., DICK, T. P., RADI, R., MORGAN, B. & DEPONTE, M. 2018. Redox-sensitive GFP fusions for monitoring the catalytic mechanism and inactivation of peroxiredoxins in living cells. *Redox Biol,* 14**,** 549-556.
STONE, J. R. & YANG, S. 2006. Hydrogen Peroxide: A Signaling Messenger. *Antioxid Redox Signal,* 8**,** 243-270.
STRAIMER, J., GNÄDIG, N. F., WITKOWSKI, B., AMARATUNGA, C., DURU, V., RAMADANI, A. P., DACHEUX, M., KHIM, N., ZHANG, L., LAM, S., GREGORY, P. D., URNOV, F. D., MERCEREAU-PUIJALON, O., BENOIT-VICAL, F., FAIRHURST, R. M., MÉNARD, D. & FIDOCK, D. A. 2015. K13-propeller mutations confer artemisinin resistance in Plasmodium falciparum clinical isolates. *Science,* 347**,** 428-431.
STURM, A., AMINO, R., VAN DE SAND, C., REGEN, T., RETZLAFF, S., RENNENBERG, A., KRUEGER, A., POLLOK, J.-M., MENARD, R. & HEUSSLER, V. T. 2006. Manipulation of Host Hepatocytes by the Malaria Parasite for Delivery into Liver Sinusoids. *Science,* 313**,** 1287-1290.
TILLEY, L., STRAIMER, J., GNÄDIG, N. F., RALPH, S. A. & FIDOCK, D. A. 2016. Artemisinin Action and Resistance in Plasmodium falciparum. *Trends Parasitol,* 32**,** 682-696.
TRAGER, W. & JENSEN, J. 1976. Human malaria parasites in continuous culture. *Science,* 193**,** 673-675.
TRUJILLO, M., CLIPPE, A., MANTA, B., FERRER-SUETA, G., SMEETS, A., DECLERCQ, J. P., KNOOPS, B. & RADI, R. 2007. Pre-steady state kinetic characterization of human peroxiredoxin 5: taking advantage of Trp84 fluorescence increase upon oxidation. *Arch Biochem Biophys,* 467**,** 95-106.
TRUJILLO, M., FERRER-SUETA, G. & RADI, R. 2008. Kinetic studies on peroxynitrite reduction by peroxiredoxins. *Methods Enzymol,* 441**,** 173-96.
TSUJI, M., MATTEI, D., NUSSENZWEIG, R. S., EICHINGER, D. & ZAVALA, F. 1994. Demonstration of heat-shock protein 70 in the sporozoite stage of malaria parasites. *Parasitol Res,* 80**,** 16-21.
TUCKER, M. S., MUTKA, T., SPARKS, K., PATEL, J. & KYLE, D. E. 2012. Phenotypic and Genotypic Analysis of In Vitro-Selected Artemisinin-Resistant Progeny of Plasmodium falciparum. *Antimicrob Agents Chemother,* 56**,** 302-314.
TUTEJA, R. 2007. Malaria − an overview. *FEBS J,* 274**,** 4670-4679.
URSCHER, M., MORE, S. S., ALISCH, R., VINCE, R. & DEPONTE, M. 2012. Tight-binding inhibitors efficiently inactivate both reaction centers of monomeric Plasmodium falciparum glyoxalase 1. *FEBS J,* 279**,** 2568-2578.
VAN DOOREN, G. G. & STRIEPEN, B. 2013. The Algal Past and Parasite Present of the Apicoplast. *Annu Rev Microbiol,* 67**,** 271-289.
VAN DOOREN, G. G., SU, V., D'OMBRAIN, M. C. & MCFADDEN, G. I. 2002. Processing of an apicoplast leader sequence in Plasmodium falciparum and the identification of a putative leader cleavage enzyme. *J Biol Chem,* 277**,** 23612-23619.
VAN LAER, K. & DICK, T. P. 2016. Utilizing Natural and Engineered Peroxiredoxins As Intracellular Peroxide Reporters. *Mol Cells,* 39**,** 46-52.
WALLER, R. F., KEELING, P. J., DONALD, R. G. K., STRIEPEN, B., HANDMAN, E., LANG-UNNASCH, N., COWMAN, A. F., BESRA, G. S., ROOS, D. S. & MCFADDEN, G. I. 1998. Nuclear-encoded proteins target to the plastid in

Toxoplasma gondii and Plasmodium falciparum. *Proc Natl Acad Sci U S A,* 95**,** 12352-12357.

WALLER, R. F., REED, M. B., COWMAN, A. F. & MCFADDEN, G. I. 2000. Protein trafficking to the plastid of Plasmodium falciparum is via the secretory pathway. *EMBO J,* 19**,** 1794-1802.

WANG, J., ZHANG, C.-J., CHIA, W. N., LOH, C. C. Y., LI, Z., LEE, Y. M., HE, Y., YUAN, L.-X., LIM, T. K., LIU, M., LIEW, C. X., LEE, Y. Q., ZHANG, J., LU, N., LIM, C. T., HUA, Z.-C., LIU, B., SHEN, H.-M., TAN, K. S. W. & LIN, Q. 2015. Haem-activated promiscuous targeting of artemisinin in Plasmodium falciparum. *Nat Commun,* 6**,** 10111.

WEZENA, C. A., KRAFCZYK, J., STAUDACHER, V. & DEPONTE, M. 2017. Growth inhibitory effects of standard pro- and antioxidants on the human malaria parasite Plasmodium falciparum. *Exp Parasitol,* 180**,** 64-70.

WHO 2015. Guidelines for the treatment of malaria. Third edition April 2015.

WHO 2016. World Malaria Report 2016.

WILSON, R. J. M., DENNY, P. W., PREISER, P. R., RANGACHARI, K., ROBERTS, K., ROY, A., WHYTE, A., STRATH, M., MOORE, D. J., MOORE, P. W. & WILLIAMSON, D. H. 1996. Complete Gene Map of the Plastid-like DNA of the Malaria Parasite Plasmodium falciparum. *J Mol Biol,* 261**,** 155-172.

WINTERBOURN, C. C. 2008. Reconciling the chemistry and biology of reactive oxygen species. *Nat Chem Biol,* 4**,** 278-286.

WINTERBOURN, C. C. & HAMPTON, M. B. 2008. Thiol chemistry and specificity in redox signaling. *Free Radic Biol Med,* 45**,** 549-561.

WITKOWSKI, B., AMARATUNGA, C., KHIM, N., SRENG, S., CHIM, P., KIM, S., LIM, P., MAO, S., SOPHA, C., SAM, B., ANDERSON, J. M., DUONG, S., CHUOR, C. M., TAYLOR, W. R. J., SUON, S., MERCEREAU-PUIJALON, O., FAIRHURST, R. M. & MENARD, D. 2013a. Novel phenotypic assays for the detection of artemisinin-resistant Plasmodium falciparum malaria in Cambodia: in-vitro and ex-vivo drug-response studies. *Lancet Infect Dis,* 13**,** 1043-1049.

WITKOWSKI, B., KHIM, N., CHIM, P., KIM, S., KE, S., KLOEUNG, N., CHY, S., DUONG, S., LEANG, R., RINGWALD, P., DONDORP, A. M., TRIPURA, R., BENOIT-VICAL, F., BERRY, A., GORGETTE, O., ARIEY, F., BARALE, J. C., MERCEREAU-PUIJALON, O. & MENARD, D. 2013b. Reduced artemisinin susceptibility of Plasmodium falciparum ring stages in western Cambodia. *Antimicrob Agents Chemother,* 57**,** 914-923.

WOOD, Z. A., POOLE, L. B. & KARPLUS, P. A. 2003a. Peroxiredoxin Evolution and the Regulation of Hydrogen Peroxide Signaling. *Science,* 300**,** 650-653.

WOOD, Z. A., SCHRÖDER, E., ROBIN HARRIS, J. & POOLE, L. B. 2003b. Structure, mechanism and regulation of peroxiredoxins. *Trends Biochem Sci,* 28**,** 32-40.

WORTHINGTON, D. J. & ROSEMEYER, M. A. 1976. Glutathione Reductase from Human Erythrocytes. *Eur J Biochem,* 67**,** 231-238.

YAMAUCHI, L. M., COPPI, A., SNOUNOU, G. & SINNIS, P. 2007. Plasmodium sporozoites trickle out of the injection site. *Cell Microbiol,* 9**,** 1215-1222.

YANO, K., KOMAKI-YASUDA, K., KOBAYASHI, T., TAKEMAE, H., KITA, K., KANO, S. & KAWAZU, S. 2005. Expression of mRNAs and proteins for peroxiredoxins in Plasmodium falciparum erythrocytic stage. *Parasitol Int,* 54**,** 35-41.

YEH, E. & DERISI, J. L. 2011. Chemical Rescue of Malaria Parasites Lacking an Apicoplast Defines Organelle Function in Blood-Stage Plasmodium falciparum. *PLoS Biol,* 9**,** e1001138.

ZHANG, J., CAMPBELL, R. E., TING, A. Y. & TSIEN, R. Y. 2002. Creating new fluorescent probes for cell biology. *Nat Rev Mol Cell Biol,* 3**,** 906-918.